52

IRAS OXYGEN- AND CARBON-RICH MIRAS CLOSE TO THE GALACTIC PLANE

BY

LEROTHODI LA PULA LEEUW

THESIS PROJECT

Submitted in Partial Fulfilment

for the Degree of

MASTER of SCIENCE

in the Faculty of Science

UNIVERSITY OF CAPE TOWN

DECEMBER 1996

Abstract

Observations are presented for 101 *IRAS* sources that were expected to be Mira Variables and that lie close to the galactic plane: $-7.^\circ3 < b < +1^\circ$ and $282.^\circ5 < l < 285.^\circ5$. Over 1090 $JHKL$ photometry modules were obtained for the sources. From the photometry the sample was shown to comprise 85 Miras, 12 of which had published periods. New periods were determined for all the Miras. Of the 85 Miras in the sample, 21 had previous published spectra and the rest were tentatively classified as oxygen or carbon-rich Miras using infrared two-colour diagrams. The oxygen and carbon-rich Miras, respectively, have mean periods and K half-amplitudes of 386 days and 0.36 mag and 442 days and 0.46 mag. Statistical tests showed that the probability that the period distribution functions of the oxygen and carbon-rich stars came from the same population was very small: 0.00055. The period as well as the $K-L$ and $K-[12\mu m]$ colours were shown to be functions of amplitude. For the carbon-rich Miras the $[12\mu m]-[25\mu m]$ colour was shown to be correlated with amplitude. Bolometric magnitudes were determined by integrating under a spline curve fitted to the $JHKL12, 25\mu m$ fluxes of the Miras. Distances to the stars have been calculated using absolute mag-

nitude $P-L$ relations from oxygen-rich and carbon-rich Miras in the LMC, where the LMC distance modulus of 18.57 was adopted.

In addition, a search of Miras in the Galactic Bulge using APM-scanned I-plate data are presented. A total of 116 Mira candidates were identified, 43 of which were classified as strong candidates.

The presented work will contribute to the study of Galactic structure.

Contents

Acknowledgements

I thank Prof. M.W. Feast (MWF) of the University of Cape Town (UCT) and Dr. P.A. Whitelock (PAW) of the South African Astronomical Observatory (SAAO) for suggesting this thesis project and guiding me up to its completion. Thank you for making your near-infrared observations available to initiate my post-graduate research in astronomy. Your support in my academic and non-academic matters, here in South Africa and beyond, is greatly appreciated. During the last two years I have enjoyed warm support and friendship from the members of SAAO and the Department of Astronomy at UCT; my regards to all who will be missed and the respective heads of these research centres, Dr. R. Stobie and Prof. B. Warner. I thank the Foundation for Research and Development and the Mellon Foundation at UCT for their financial support.

In April and May I spend two months at the Royal Greenwich Observatory in Cambridge; my thanks to Dr. S. Hughes for hosting me there and to PAW & MWF for arranging my visit. Here I need to acknowledge Mr. S. Vine for generously arranging a large chunk of the wonderful social life I got to experience during my stay there. I thank the RGO for their two-months studentship and the UCT research office for a return air-ticket that made my visit at Cambridge possible.

For my academic inspiration, I acknowledge my alma matters Columbia U., MIT, Andover and MHS. I am grateful to my family for my health and my friends for their love. *Ka boikobo.*

DEDICATION

To P.M.S. LEEUW,

the aspirations of

our parents

will be realized.

Chapter 1

Introduction

1.1 Infrared Astronomy

In 1800 Sir William Herschel noted that a thermometer placed beyond the red end of the Sun's optical spectrum registered an increase in temperature due to the presence of invisible radiation. He called the radiation *caloric rays* and went on to demonstrate that the rays were reflected and refracted like ordinary light. Thus began **infrared astronomy** , 65 years before the discovery of James Clerk Maxwell's theory of the existence of the electromagnetic spectrum (McLean 1993).

For modern astronomy, the infrared spectral region extends from the limit of sensitivity of the visible-wavelength detectors, at about $1.1\mu m$ (the limits for CCDs), to the region where radio wavelength techniques become more efficient, at about $1000\mu m$ (Elias 1992). In general, the interval from 1 to $5\mu m$ is called the **near**-infrared, 5 to $20\mu m$ the **mid**-infrared, and 20 to $200\mu m$ the **far**-infrared; the wavelengths longer than $350\mu m$ are called

sub-millimetre and are observed using techniques of infrared and radio astronomy (McLean 1993).

Water vapour and carbon dioxide in the Earth's atmosphere limit the wavelengths that can be observed from the ground in the infrared to a number of *windows* between atmospheric absorption bands. Water vapour absorption is especially severe for the longer wavelengths. A simplified atmospheric transmission spectrum from $1\mu m$ to $1mm$ is shown in Figure 1.1, and the related standard wavelength bands or the atmospheric *windows* of transparency in the near- and mid-infrared are listed below (McLean 1993):

Standard Infrared Windows and Passbands

Wavelength (μm)	Symbol	Width (μm)
1.25	J	0.3
1.65	H	0.3
2.2	K	0.4
3.5	L	1.0
3.8	L'	0.6
4.8	M	0.6
11	N	2.0
20	Q	5.0

Besides limited atmospheric transparency, a further difficulty in infrared astronomy is provided by background radiation from warm objects on Earth, even the air and the telescope, (whose emissions peak between 3 and $10\mu m$) and solar-induced photochemical reactions in the Earth's atmosphere (which emit at 1 to $2.5\mu m$).

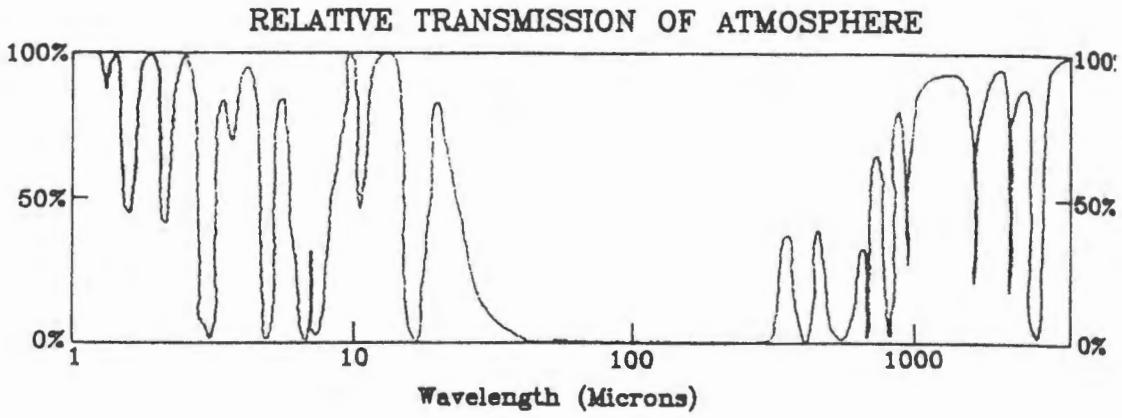

Figure 1.1: Relative atmospheric transmission in the infrared. (Reproduced from McLean, 1993.)

To take advantage of the available *windows* of transparency, interference filters have been built to match and observe through selected infrared bands. Cooled detectors and specialised telescopes have also been designed to avoid the background radiation. In addition cryogenically cooled infrared telescopes have been flown on aircraft, balloons, rockets, and spacecraft to completely avoid the atmosphere. Further details of infrared observing techniques, detectors, telescopes and space missions are listed elsewhere in literature, and those relevant to the present paper are described in subsequent sections.

1.1.1 The Infrared Astronomical Satellite

The *Infrared Astronomical Satellite (IRAS)* was launched in 1983 by the USA, Britain and the Netherlands. The mission mapped 98% of the sky at wavelengths of 12, 25, 60 and 100 μm until its on-board supply of liquid

helium was exhausted and the telescope and the detectors warmed-up and lost sensitivity. *IRAS* was in operation for about 10 months.

The telescope system, which included a 60 cm primary mirror telescope and the survey instruments, were mounted in a toroidal liquid helium tank providing a 1.8K thermal environment for detectors and optics. Three instruments were on board: (1) 62 detectors for the 12, 25, 60, 100 μm survey, (2) a Chopped Photometric Channel (CPC) photometer which operated at 50 and 100μm and (3) a low resolution spectrometer (LRS). The CPC was designed to make high spatial (1′) resolution observations in a 9′x9′ field. The LRS is a slitless prism spectrometer. *IRAS* was used in two modes: the survey mode to observe the whole sky several times and in the additional observations mode where a region of about 1°x1° was scanned several times (De Graauw 1993). The mission obtained data from nearly 250,000 point sources which are listed in the *IRAS Point Source Catalogue (IRAS PSC).* LRS spectra of some 5400 PSC sources and other data are also available in various *IRAS* catalogues. CPC high resolution maps and catalogue are also available.

This MSc thesis uses *near*-infrared (1.2, 1.6, 2.2, 3.5μm) photometry observations obtained from the 1.9m SAAO telescope, *mid* -infrared (12 and 25μm) data from *IRAS*, and limited data from literature to conduct an in-depth study of 101 Galactic infrared sources that were selected from the *IRAS* catalogue and expected to be Mira variables. The properties of the Miras have been analysed and the stars will be used as galactic-structure probes of a low-mass population. In addition a search of Miras in

the Galactic Bulge has been conducted using I-plate data and is discussed.

1.2 Miras, the Wonderful Red Giant Stars

Mira variables are mass-losing, pulsating red giant stars that can vary in brightness by a factor of 10 to 2000 times from minimum to maximum in visual light. Excluding supernovae and novae, o Ceti, the typical Mira representative, was the first star found to vary in brightness. Mira Ceti was discovered as a previously unlisted star in 1556, but it was not until 1638 that its variable nature was found, and not until 1662 that the star was shown to vary from second to tenth visual magnitude in a period of 330 days. Being the only known variable, the star was called Mira, the wonderful or the magical (Vardya 1992).

According to the *General Catalogue of Variable Stars* (GCVS), Mira variables have the following three defining characteristics:

(i) the spectral type is Me, Se, or Ce;

(ii) the visual light amplitude is from 2.5 to 11 magnitude;

(iii) the periods range from 80 to 1000 days.

The M, S, C spectral types indicate that Mira atmospheres contain strong molecular features and are therefore cool. The elemental abundance ratios of carbon to oxygen in the Mira atmospheres are less than 1 in M stars, close to unity in S stars, and greater than 1 in C stars. In other words, Miras may be oxygen-rich (Me), carbon-rich (Ce [sometimes listed as R or N]), or intermediate (Se). The e in Me etc. signifies the presence

of emission lines in the spectrum. These Hydrogen emission lines are especially bright on the declining branch, though the mechanism behind their excitation is uncertain. They are perhaps caused by shock or hydromagnetic waves (Merrill 1960).

In the cool atmospheres of Miras, carbon monoxide (CO) is a stable compound because CO has an exceptionally high dissociation energy. All carbon is tied up as CO in M and S stars and the excess oxygen is available for the formation of molecular oxides, whereas in C stars, all oxygen is tied up as CO and excess carbon is available for formation of carbon compounds. This means that the dichotomy of oxygen-rich and carbon-rich Miras is important and the compositions of the two types of atmospheres are significantly different.

The M-spectral type Miras are characterised by absorption bands of titanium and vanadium oxides (TiO, VO), S Miras by zirconium oxide (ZrO), and C Miras by molecular carbon, cyanogen, and silicon carbide (C_2, CN, SiC_2) bands. In addition, some M stars show broad silicate grain emission at 9.7 and 18 microns, and some C stars show a silicon carbide (SiC) grain-emission at 11.3 microns (Vardya 1992). An absorption line of technetium (Tc), the unstable radioactive element with a half-life of only 200,000 years for the most likely isotope, has also been found in S Miras, as well as in some of the M and C types. This was one of the first indications that some elements must be manufactured in the stellar interior by nuclear processes and then convected to the surface.

Though the amplitudes of Miras are very large in visual light, they are

much less in the infrared or in the total light output (bolometric magnitude). The large range in the visual amplitude is caused primarily by the change in the star's photospheric temperatures and the strength of the molecular bands. For the optically selected sample described by Vardya (1992), the mean visual amplitude is 5.4 mag for M spectral-type stars, 6.4 mag for S stars, and 4.6 mag for C stars. The bolometric magnitude range is large, over a magnitude for the stars with longer periods (Whitelock 1995). In general, the amplitude increases with period.

It can be shown theoretically that for a star of a given structure, the period (P) and the mean density (ρ) are related by an equation of the form $P\sqrt{\rho} = Q$, where Q is a constant which in general is of the value 0.04 to 0.06 days if ρ is measured in solar units and P in days. From this relation written in the form $P = Q/\sqrt{\rho} = Q_0/\sqrt{M/R^3}$, it can be inferred that the Miras' long periods imply that the stars have very large radii. For a centrally condensed star, the typical $Q = 0.04$ (similar to the values predicted by Fox & Wood (1982) for Miras pulsating in the first-overtone mode). The mean mass of a Mira is about $1M_{\odot}$. [The galactic kinematics of Miras (Feast 1963) show that Miras are evolved low mass stars]. Therefore for a centrally condensed star of $P = 400$ days, R would be about $500R_{\odot}$ for first-overtone pulsation. This has been confirmed by direct angular diameter measurements using lunar occultation or interferometry. Using these angular measurements and a $P - L$ relation, Feast (1996) derived linear radii of $542R_{\odot}$ for S Psc with a period of 405 days, and about $431R_{\odot}$ for o Cet with a period of 332 days.

The GCVS three distinguishing characteristics of Miras are not always

useful as stars with physical properties similar to Miras are often classified as *non-Miras* because their amplitudes or periods fall outside the ranges specified by the GCVS. Examples of such cases include those stars that get classified as Semi-Regular variables (SRs) merely because their amplitudes fall short of the visual or infrared respective 2.5 or 0.6 mag cut-offs (Whitelock 1996). Then there are a subset of the OH/IR sources which have no visible counterpart as they are surrounded by thick circumstellar dust shells. These stars are in a comparable evolutionary state to Miras, but they are often not classified as such because their periods are in the 1000 to 2000 day range (Whitelock 1996).

Miras are of great interest astrophysically for various reasons. In stellar evolution and the HR diagram they represent a short-lived ($\simeq 2 * 10^5$ years) mass-losing, pulsation phase at the tip of the asymptotic giant branch (AGB). The next evolutionary phase in the HR diagram is the transitional phase, at the top of the diagram, to becoming a planetary nebulae. This transitional phase is the least-understood phase in the HR diagram; and perhaps Miras hold the key to understanding its evolutionary theory. These AGB's mass-losing pulsators exhibit interesting physical phenomenon of *thermal pulses* and core-material *dredge-up* that permit the theoretical calculation of carbon star surface abundances that can be compared with abundance distributions determined from observations. Furthermore, the matter lost by the AGB stars, which contains *s*-processes products that have been *dredged-up* from the stellar interiors, permits the computation of the contribution of the AGB stars to the galactic nucleosynthesis of ^4He, ^{12}C, ^{13}C,

^{14}N and ^{22}Ne and neutron-rich isotopes (Iben & Renzini 1983).

These mass-losing stars are at the maximum luminosity they will ever achieve, and as such they can be detected relatively easily over large distances. They also obey period-luminosity relationships that can be expressed both in terms of total (bolometric) luminosity and the near-infrared magnitude, and are thus useful distance indicators (Feast et al. 1989). Additionally, various correlations suggest that Miras are good indicators of the population to which they belong. Stars with periods of around 200 days belong to the same, old population as do metal-rich globular clusters (Menzies & Whitelock et al. 1985). Miras can therefore serve as good Galactic-structure probes for low-mass populations (Whitelock et al. 1994). Consistent with this picture – but contrary to popular belief – there is no evidence that Miras systematically evolve to longer periods as they age (Whitelock 1996).

Additional Mira properties of interest include their pulsation mode. Although it is generally agreed that Miras pulsate radially, there has been uncertainty as to whether they are in the fundamental or first-overtone modes. Observations of the ratios of diameters to masses indicate the overtone. However the shockwave models which have been proposed for the excitation of emission lines in the spectrum require the star to be smaller and hotter and thus to pulsate in the fundamental. Another notable property of these stars is the variation of the shape of their light curves, period and amplitude from cycle to cycle, and perhaps this variation's statistical correlation to the Mira mass-loss and spectral types.

1.2.1 Evolution on the Asymptotic Giant Branch

The Asymptotic Giant Branch (AGB), the stage in which Mira Variables occur, is an evolutionary phase when low-to-intermediate-mass stars develop an electron-degenerate carbon-oxygen (C-O) core following the exhaustion of helium at the centre. Iben & Renzini (1983) define low-mass stars as those that develop an electron degenerate helium core following the main sequence (hydrogen burning core) phase; this puts a lower limit of about 0.8 to 1.0 $M_{\odot}$ and an upper limit of 2 to 2.3 $M_{\odot}$ on the initial main sequence mass of such stars. Intermediate-mass stars are those that ignite helium *non-degenerately*; this places an upper limit of about 8 to 9 $M_{\odot}$ on the initial mass of such stars (Iben & Renzini 1983), and in general on AGB stars.

When helium in the core of a low-to-intermediate-mass star is exhausted from burning into carbon and oxygen, the core contracts. This marks the end of the star's life on the horizontal branch and a move onto the asymptotic giant branch. As the core contracts, the pressure and temperature of the over- lying layers is increased. Thus helium ignites in a shell just outside the core, and hydrogen burns in a shell outside of that. The mass of the inert C-O core increases and it continues to contract. Correspondingly, nuclear burning in the shell continues to increase. The star's luminosity increases and it ascends the asymptotic giant branch. It is this shrinking core that causes the electrons to become degenerate. Figure 1.2, adapted from Shu (1982), p. 151, shows the structure of an asymptotic giant.

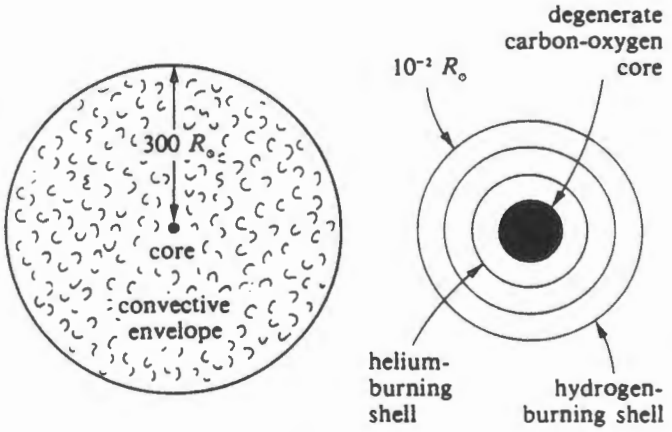

Figure 1.2: The structure of an asymptotic giant. The figure on the left shows the star from core to photosphere and the figure on the right shows an enlarged picture of the region near the core. (Reproduced from Shu, 1982.)

The mass of the C-O core on the AGB is larger than that of the He core during the giant-branch evolution, and the radius of the incipient C-O white dwarf is smaller. A smaller, more massive C-O degenerate core means the overlying shell will have higher pressure and temperature than the shell overlying the He core of the giant-branch stars, and thus AGB stars generate higher luminosities. The stars may reach $10^4 L_\odot$.

When the helium shell source becomes spatially thin, *thermal relaxation oscillations* occur. An overproduction of energy leads to a thermal runaway. The nuclear energy region is non degenerate, but it is a spatially thin shell. Thus, with the input of excess nuclear energy, the layer will expand. But the expansion of a thin shell does little to relieve the weight of the overlying material. As the weight hardly changes, the pressure that the thin shell

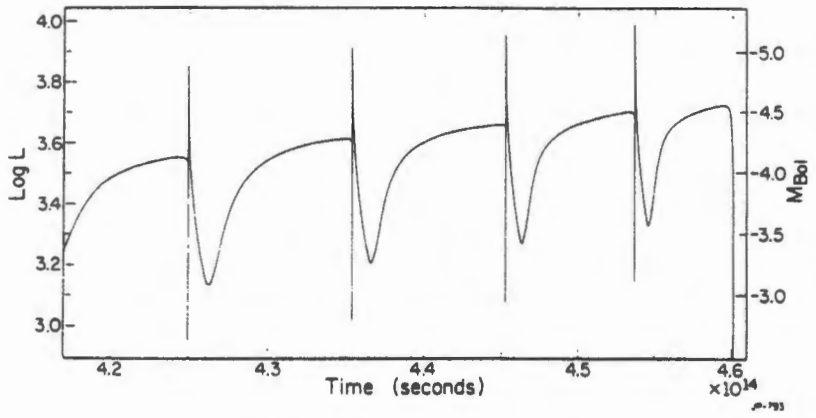

Figure 1.3: Surface luminosity (in solar units) as a function of time in a model star of mass $0.6M_{\odot}$, and initial composition (Y, Z)=(0.25,0.001) where Y and Z are, respectively, the abundances by mass of elements heavier than helium and of helium. Reproduced from Iben & Renzini (1983).

has to maintain to offset this weight also hardly changes. Meanwhile, the temperature has increased, and as the triple-alpha reaction is sensitive to temperature changes, the reaction increases further before the excess heat has a chance to diffuse away. Thus thermal runaway ensures. The runaway is checked only after considerable expansion and the appearance of the convective zone to carry away excess heat. But the basic problem remains. After the runaway is checked, and when the star tries to adopt the *natural* double shell burning of the AGB stage, it finds itself in the same difficulty. Thus the star undergoes a series of *thermal relaxation oscillations* which consists of one or more sharp pulses of extra energy generation followed by relatively long periods of quiet evolution. Each thermal runaway is followed by a development of a convection zone which extends from the helium-burning almost to the hydrogen-burning-shell. Figure 1.3, adapted from Iben & Ren-

zini (1983), p. 289, shows the luminosity variations associated with thermal pulsation. (The simplified model presented in the diagram does not include variations that are associated with dynamical pulsation, such as those active in Miras.)

In the event that the inner convective zone connects with the outer convective envelope through the hydrogen burning shell, products of helium burning, carbon and oxygen, as well as neutron-rich isotopes of the s-process, may be brought to the surface of the asymptotic red giant. The *dredge-up* of material that results from the development of a convective shell during the thermal pulses can change the surface carbon-to-oxygen abundance ratio (C/O) from a value around 0.5-0.6 to a value around 1.1-1.6 (Lambert 1990). According to Iben and Renzini 1983, the mass of the material dredged up during this thermal pulsation phase can be as high as $1M_{\odot}$ in the most massive intermediate-mass stars. **Thermal pulses** and the resulting **dredge-up** of material are indeed important features of the AGB.

1.2.2 Mass-Loss in Miras

Mira variables have stellar winds with velocities of $10 - 20kms^{-1}$, through which they are subject to great mass loss. The rate of mass loss varies between $10^{-8} - 10^{-4}M_{\odot}yr^{-1}$ (Whitelock et al 1991).

Mass loss creates an extended circumstellar shell of gas and dust around Miras, that is eventually ejected (violently or otherwise) into the Interstellar Medium (ISM). The dust grains, though they are a minute component of the circumstellar matter, absorb some visual light from the star and reradiate it

in the infrared. The effective temperatures of the star and the dust-shell are estimated at $2000 - 3000°K$ and $300 - 1000°K$ respectively. Therefore, in the blackbody approximation, the spectrum of the star and the shell consist of two separate but overlapping distributions (humps), the one for the shell being at the longer wavelengths. Dust shells of some stars have been resolved at 11.15 microns and inner radii of 2-7 stellar radii measured (Danchi et al 1994).

The cause of mass loss is believed to be linked to a two step process involving the pulsation of the star and the radiation pressure on the dust-grains. Pulsation, and the shock-waves that are dissipated as a result, acts to levitate stellar matter above the photosphere where the gas can be cooled and dust grains can form. Radiation pressure on the dust then drives the matter into the ISM (Morris 1987). However, recent hydrodynamical computations by Winters et al. (1995) show that there is a time-dependent dust structure across the circumstellar shell that may indicate that the relation between pulsation, dust formation, and radiation pressure is more complex than generally thought.

What is certain is that Miras lose mass at high rates, and that they have extended circumstellar shells. The mass loss must contribute to the evolution and fate of these stars. The resultant injection of material in the ISM contributes to the ISM's replenishment and evolution.

1.3 Summary of Thesis Goals

The main thesis goals were to study the properties of 101 galactic Mira candidates that were selected from the *IRAS* catalogue and to use the Miras as probes for low-mass populations. In particular, the goals were (1) to determine the periods and amplitudes of as many variables as possible, (2) to classify the variables into non-Miras and Miras, (3) to analyse the colours of all the variables, (4) to classify the Miras into oxygen-rich and carbon-rich stars, (5) to determine the bolometric magnitudes and distances of the Miras, (6) to determine galactic distributions of the O/C-rich Miras including their distances from the galactic plane (z); and wherever relevant (7) to answer statistical and astrophysical questions about the variables, (8) to examine different relevant reduction techniques, and (9) to compare the findings to those in astronomical literature. In addition to the above goals, a search for Miras in the Bulge of the Milky Way Galaxy was to be undertaken using APM-scanned I-plate data and computer reduction programs by Dr. Shaun Hughes (Royal Greenwich Observatory).

The study of the *IRAS* sources was done from the South African Astronomical Observatory in conjunction with the University of Cape Town, and the I-plate search was conducted during a two months studentship at the Royal Greenwich Observatory in Cambridge, England.

Chapter 2

Near- and Mid-Infrared Observations

One hundred and one *Infrared Astronomical Satellite* sources which lie in a region of low interstellar extinction close to the galactic plane: $-7.°3 < b < +1°$ and $282.°5 < l < 285.°5$ were observed (l and b are, respectively, galactic longitude and latitude). The sources were expected to be mass-losing Long Period Variables or Miras but they included some cool Semi-Regular Variables.

2.1 Source Selection

The region in which stars were chosen was one in which searches for long period variables were being made by Shaun Hughes (RGO) using I-plates taken with the Anglo-Australian Schmidt Telescope (Schmidt Field 127). *IRAS* point sources were selected to provide a diagonal strip across the

Schmidt Plate (Field 127) as follows:

(RA,Dec)	to	**(RA,Dec)**
9 47, –57 00	to	10 29 59, –58 59 59
9 46, –58 00	to	10 30 59, –59 59 59
9 45, –59 00	to	10 31 59, –60 59 59
9 44, –60 00	to	10 32 59, –61 59 59
9 43, –61 00	to	10 33 59, –62 59 59
9 42, –62 00	to	10 34 59, –63 59 59.

All stars with measured $12\mu m$ fluxes in the selected region were extracted. Out of these, those with visual counterparts too bright for the objects with the given *IRAS* fluxes to be Miras were rejected. Some more stars were rejected when the objects had $JHKL$ colours (eg. in comparison with Miras from Whitelock *et al.* (1991) which indicated that the stars were not Miras. This was done prior to the author's involvement in the project. During the course of the $JHKL$ observations, some objects had to be abandoned due to crowding which precluded accurate photometry. Specific reasons for program stars that were abandoned during the course of the observations will be outlined together with other discussions of results in chapter 3.

2.2 Near-Infrared Photometry

Near-infrared observations were obtained at the $JHKL$ (1.2, 1.65, 2.2, 3.45μm) bands using the Mk III photometer attached to the SAAO 1.9-m telescope.

2.2.1 The 1.9m Reflector

This telescope was built in 1938-48 for the Radcliffe Observatory in Pretoria. Its home is now at an elevation of 1767m in Sutherland, South Africa, together with other smaller national optical/infrared telescopes administered by SAAO. The 1.9m *Radcliffe* telescope was used at the $f/50$ Cassegrain focus, $\approx 2.2''mm^{-1}$. The optical diagram for the f/50 Cassegrain system (which is used with the infrared photometer) on the 1.9m reflector, reproduced from the SAAO facilities Manual, is presented in Figure 2.2.

Controls, Settings, Computer System, and selected Accessories

The motion of the telescope is done by two separate drives for quick and slow motion on each axis. The setting of positions for any desired equinox are derived and displayed by computerised encoders at an accuracy of 30 arcsecs over most of the sky. There are three separate computers installed for the following respective functions: (1) to derive the position of the telescope

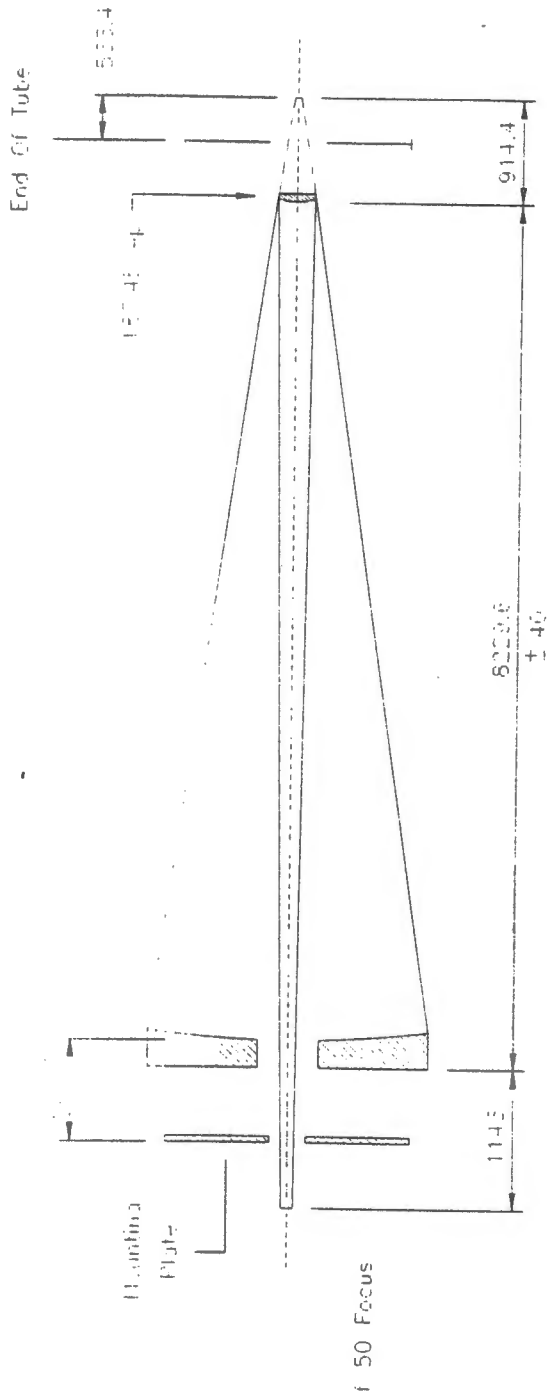

Figure 2.2: Optical diagram of the 1.9m reflector. All dimensions are in millimetres. (Reproduced from the SAAO Facilities Manual, 1994.)

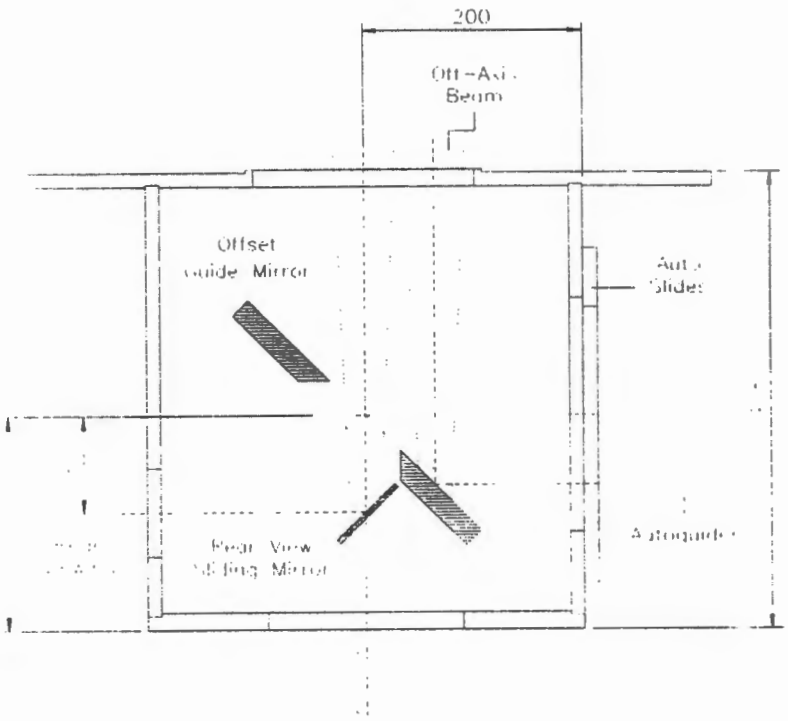

Figure 2.3: The 1.9m telescope acquisition box. All Sizes are in millimetres. (Reproduced from the SAAO Facilities Manual, 1994.)

and control the dome motion accordingly, (2) to run the software for the IR photometer, and (3) to control the CCD-based acquisition TV.

2.2.2 The Mk III Photometer

In the infrared, the sky is very bright and varies rapidly. To cancel for the sky background during an infrared measurement of a star, the detector is rapidly switched from a stellar observation (the star beam) to a nearby patch of the sky (the reference beam) by a chopping secondary, and the measurement from the star beam is appropriately corrected with that from

the reference beam.

The Mk III Infrared photometer is used with the f/50 chopping secondary on the 1.9-m telescope. The acquisition box for the IR photometer, which is presented in Figure 2.3, has two 45^0 mirrors for off-set guiding and rear-viewing. Light coming from the telescope first encounters a piece of glass at 45^0 to the beam with an aluminized spot (the rear-viewing mirror) in its centre. During an infrared measurement, the central part of the field is reflected by the spot into the InSb detector Dewar, but during acquisition the glass is moved sideways to the *view* position, allowing the whole field to reach the graticule in the focal plane and then the CCD detector of the TV acquisition system. Guiding is done with the same CCD that is used for acquisition. The InSb (JHKLM) Dewar is cooled by liquid nitrogen. The JHKLM filters have 0.5 inch diameters, and the apertures are $0'', 3'', 6'', 9'', 12''$ and $18''$. Manuals for the Mk III Photometer and the Infrared Data Acquisition Program, BRUCE, are available at the SAAO library and the telescope domes.

2.2.3 The Observations

The $JHKL$ data were obtained largely between 1992 and 1996, firstly by Dr. Whitelock, Prof. Feast, and Dr. Catchpole, and during 1995 also by the writer. The observations were made through a 12-arcsec aperture and with a 30-arcsec chop whenever possible. Under conditions of poor seeing, an 18-arcsec aperture was used while a few of the crowded sources were measured through a 9-arcsec aperture under good conditions. Chop amplitudes other

than 30 arcsec were used as necessitated by objects in the reference beam. In a few instances, J and H magnitudes could not be obtained because of interfering sources or because the programme star was too faint. The magnitudes are on the SAAO system as defined by Carter (1990) and are estimated to be accurate to about 0.03 mag in JHK and 0.05 mag in L.

Spectroscopic surveys of selected sources had been planned with collaborators in Chile, but bad weather managed to prevail over good observing conditions. With better luck, some spectroscopic data will be obtained in the future.

2.2.4 Correction for Extinction

Interstellar material absorbs and scatters light. Along the line of sight between the star and the observer interstellar dust attenuates starlight in a phenomenon known as Interstellar Extinction or Interstellar Reddening. The *reddening* refers to the fact that blue light is more heavily extinguished than red so that an apparent reddening of the starlight is observed. The general trend of increasing extinction at shorter wavelengths is, with some exceptions, known to be broadly true not only over visual wavelengths but also from infrared to ultraviolet (Williams 1992).

In the Galaxy, the extinction is severe in the plane, and confined to a relatively thin layer. The sample presently studied has on average $b = -3.^\circ3$ and $l = 283.^\circ4$; thus, it lies in a region of moderate interstellar extinction. Note that in general, interstellar material and thus also extinction have an

irregular spatial structure.

Differences in extinction at different wavelengths, λ and λ', lead to a colour access $E_{\lambda-\lambda'} = A_\lambda - A_{\lambda'}$, or $E_{B-V} = A_B - A_V$ for $\lambda = 0.54\mu m$ (V light) and $\lambda = 0.42\mu m$ (B light). From a comparison of reddened and unreddened stars, and since the extinction becomes very small at long wavelengths, it is possible to derive a ratio of blue and violet extinction R so that $A_V = \mathbf{R}E_{B-V}$. The visual extinction then simply becomes

$$A_V = 3.05E_{B-V}, \tag{2.1}$$

a formula that is very useful if E_{B-V} can be determined.

In the present paper, A_V is determined from a map of *The Spatial Distribution of the Interstellar Extinction* by Neckel and Klare (1980). The extinction at the observed near-infrared bands: J ($1.25\mu m$), H ($1.65\mu m$), K ($2.2\mu m$), and L ($3.5\mu m$), is then calculated from the following ratios

$$\begin{aligned} A_J &= 0.246A_V \\ A_H &= 0.141A_V \\ A_K &= 0.088A_V \\ A_L &= 0.046A_V, \end{aligned}$$

adopted from Feast et al. (1990).

The Neckel and Klare (1980) maps were designed for $|b| \leq 7.°6$; and the present sample being at $-7.°3 < b < +1°$ was within the covered galactic

belt. In the maps, A_V is dependent on galactic l and b, and the distance r to the observed source. Galactic regions that have a similar $A_V(r)$ relation are demarcated and designated by l,b where (l, b) are the coordinates for the regions' centres. For each region l,b, there is a $A_V(r)$ diagram where, if r is known, A_V can be determined.

On average the present sample is at galactic coordinates $l = 284.°3$ and $b = -3.°28$. The field thus corresponds to the region designated by l,b is **280,–5** in the Neckel and Klare (1980) maps, and consequently a $A_V(r)$ relation that has a constant $A_V = 0.7$ for $1kpc \leq r \leq 14kpc$. Now according to the Period-Luminosity (see section on distance determination) and using the uncorrected K magnitudes , an average distance for the present sample was determined to be 6kpc, with only one star under 1kpc and 6 over 14kpc. An average visual extinction $A_V = 0.7$, derived from the Neckel and Klare (1980) maps, is therefore adopted in the present paper and applied to the ratios listed above to derive near-infrared extinction at the J H K and L bands. The corrected J H K and L magnitudes are the uncorrected magnitudes minus their respective extinctions.

As a second check and for exercise, A_V was also determined by using the cosecant law

$$E_{B-V} = 0.032(\csc|b| - 1)[1 - \exp -10r\sin|b|], \qquad (2.2)$$

that was adopted from Feast et al. (1990). An average $b = -3.°28$ and $r = 6kpc$ were used. $E_{B-V} = 0.51$ corresponding to $A_V = 1.5$ was derived.

Although the difference in the A_V of the two methods is large ($\Delta A_V = 0.8$), the effect at K is small ($\Delta A_K = 0.088 * 0.8 = 0.07$). The effect in the $JHKL$ colours is also generally small ($\Delta A_{J-H} = 0.08, \Delta A_{H-K} = 0.04, \Delta A_{J-K} = 0.1, \Delta A_{K-L} = 0.03$).

2.3 Mid-Infrared Data

All but twelve sources have $IRAS$ fluxes at 12 and 25μm. The other twelve have 12μm fluxes but only upper limits on the 25μm fluxes. Since this paper uses two-colour diagrams that include the [12μm]-[25μm] colour for all the stars, estimates of the 25μm flux had to be made for the stars with only upper limits on the fluxes. The relation $\mathbf{(25\mu m)}$=0.334$\mathbf{(12\mu m)}$+0.004 was derived from a first order polynomial fit to the data with both 12 and 25μm points, and thus the missing 25μm fluxes were calculated. In all cases the derived 25μm fluxes were below the given $IRAS$ flux limits.

2.3.1 Colour Correction

Deriving true flux densities requires a knowledge of the intrinsic energy distribution of the stellar sources and the spectral response of the observing system. If the energy distribution is not constant for a flux measured in an observing band a 'colour correction' must be applied to the measured flux densities (*IRAS Point Source Catalogue - Explanatory Supplement* (PSC-ES) 1988).

The mid-infrared (IRAS) fluxes presented in this paper were colour cor-

rected using the flux correction formula

$$f_{v_0}[corrected] = f_{v_0}[uncorrected]/K, \tag{2.3}$$

adopted from the *IRAS* PSC-ES (1988). In the formula, v_0 is the effective frequency corresponding to the 12 or 25μm effective wavelength, and f_v is either the corrected or the uncorrected flux density of the source. K is the correction factor which is a function of the uncorrected 12/25μm fluxes as listed in table VI.C.6 of the *IRAS* PSC-ES (1988). In the present paper, ratios of the uncorrected fluxes at 12 and 25μm were calculated, the respective Ks obtained from the table and applied in the correction formula, and the respective corrected fluxes determined.

2.4 Period Determination

Periods were determined using a period fitting routine. A function is evaluated and attains an extremum at a trial frequency equal to the correct signal frequency. A plot of a period finding function with such an extremum is called a periodogram. In the present paper, periodograms were generated using a full least-squares fitting program from the STAR computer package written by Dr. L. Balona of the SAAO.

It was assumed that the data value, y_i, at time t_i is given by

$$y_i = A\cos(\omega t_i + \phi) + \varepsilon_i \tag{2.4}$$

where ω is the signal frequency and ε_i is an unknown error which can be written as

$$\varepsilon_i = y_i - a\cos\phi\cos\omega t_i + a\sin\phi\sin\omega t_i. \tag{2.5}$$

The sum of the squares, $\Sigma{\varepsilon_i}^2$, is minimised using standard multivariable least-squares procedures to produce equations of state from which the unknowns $a\cos\phi$ and $a\sin\phi$ as well as the rms of the fit, σ^2, may be determined. For convenience, the quantity

$$P = \frac{1}{s^2 - \sigma^2} \tag{2.6}$$

is used as a discriminant to search for the best value of the frequency ω. Here $s^2 = \Sigma{y_i}^2$ and $\sigma^2 = \Sigma{\varepsilon_i}^2$. A periodogram plot of P for trial values of ω is constructed and the best value of ω is the one which maximises P (ie. the highest peak in the periodogram). Thus a periodicity is revealed.

The calculation is computer intensive but suitable for Mira period analysis where typically not more than 20 data points will have been obtained. However the technique is intended for sinusoidal curves, which not all Miras have, and the obtained period may have to be improved by off-setting it slightly and analysing the phased light-curve. The improvement is done mindful of the fact that problems can occur in period calculation of Miras because of differences in the stars from one pulsation cycle to the next.

Period detection can be undermined by aliasing and noise. In determining periods from the observations discussed here, signal to noise was

very good, so aliasing was the only factor that needed serious consideration. Aliasing refers to a result where by a related *alias* frequency is detected instead of or together with a correct signal frequency. The *alias* frequency can be a harmonic of the true frequency or a frequency related to the spacing of the input data. When the input data are sampled at gaped or equally spaced time intervals, Δt, so that sinusoids of frequencies $v_0 \pm n(\Delta t)^{-1}$ can fit the data equally well (Fueller 1986), data sampling *alias* frequency will be detected.

Since the data discussed here were obtained in periodically gaped times, ie. during the season (about one half of a year) when the objects were available for observation, there was a risk that yearly aliasing sometimes impeded or precluded detection of objects' periods. Small deviations from equal sampling can make aliasing unimportant (Fueller 1986), so period detections in problematic (aliased) data sets were made possible by stretching the observations to the very beginning and end of the objects' season. For objects with periods of nearly a year, observations were practically impossible at certain phases, and nothing could be done to ensure that their full light curves were obtained.

Periodicity for a few objects, semi-regular variables and others, could not be determined even after many observations and repeated analysis. In the discussion of results (chapter 3) for the affected objects, the relevant reasons will be explained.

2.5 Classification of O-rich and C-rich Miras

Epchtein *et al.* (1987) showed that on the basis of near- and mid-infrared photometry, mass-losing long period variable stars (Miras) with oxygen-rich and carbon-rich shells can be discriminated in two-colour diagrams. The physical reason for this separation lies in the different ratios of near-infrared to mid-infrared opacities for the carbon-rich and oxygen-rich dusts (Le Berte *et al.* 1994). A $K-L$ (*i.e* [2.2μm]–[3.6μm]) or K–[12μm] versus [12μm]–[25μm] two-colour diagram can be designed to separate the oxygen-rich and carbon-rich mass-losing stars. The most useful two-colour diagram is $K-L$ versus [12μm]–[25μm], on which carbon-rich Miras are found in the lower right of the diagram (region *c* in the Epchtein nomenclature) and oxygen-rich Miras are found above this region (regions *o2* and *o3*, see Figure 3.6).

A few sources in the sample, for which there were spectral classifications, by the *IRAS* Low Resolution Spectra (LRS) and other methods (see Table 3.3), were plotted on the $K-L$ vs. [12μm]–[25μm] diagram and presented in Figure 3.7 (a). The regions of oxygen-rich and carbon-rich Miras were demarcated. Since the wavelength for the window L and criteria for the source selection used were different from those Epchtein *et al.* 1987 used, the regions shown in Figure 3.7 do not necessarily coincide with those of Epchtein (Figure 3.6).

Figure 3.7 (b) shows oxygen-rich and carbon-rich regions as marked out on the K–[12μm] versus [12μm]-[25μm] colour diagram. For the most part, O-rich and C-rich Miras fall in different regions on this diagram, but there is

a region of mixing. Therefore, the K-[12μm] versus [12μm]-[25μm] diagram cannot be used as the *overall* discriminating tool for O-rich and C-rich Miras, but it can be used to check the classifications that result from the $K - L$ versus [12μm]-[25μm] diagram.

2.5.1 Test for Two Independent Samples

When two samples are drawn, one from each of two possibly different populations, it is useful to apply a statistical test to determine if the two distribution functions associated with the two samples are identical. In this paper, the Kolmogorov-Smirnov two-sample test is applied on the period distributions of oxygen-rich and carbon-rich Mira variables. Since the oxygen-rich and carbon-rich Miras in the present paper had mean periods of 346 days and 402 days respectively, there was reason to believe that the samples came from significantly different populations.

One advantage of the Kolmogorov-Smirnov test is that it is sensitive not only to the difference in means or medians but also in variances; in fact, it is sensitive to all types of differences that may exist between two distribution functions (Conover 1971). Furthermore the test is non-parametric; that is, it does not require that the distribution functions be of any specified (Gaussian, exponential, etc.) form. The test assumes that the samples are random and independent. In this paper, the samples are random because they were selected purely on the basis that the members were observed Miras that could tentatively be classified, and are independent because the Miras were classified as either oxygen-rich or carbon-rich, with no star classified

as both.

The Kolmogorov-Smirnov two-sample test involves the integration of each histogram associated with the concerned samples to form two representative cumulative distribution functions. The test statistic, **T**, is then defined as the greatest vertical distance between the two cumulative distribution functions. From the Kolmogorov-Smirnov tables (such as Table 16 and 17 in Conover 1971) **T** is matched against significance level quantiles that indicate the probability that the distribution functions associated with the two samples are identical. This probability is then a quantitative measure of the sameness (or difference) between the two independent samples.

2.6 Bolometric Magnitude Determination

Bolometric Magnitude is a measure of the total energy radiated by a star. Usually the apparent bolometric magnitude (m_{bol}) is determined first, and then if the distance modulus for the star is known, the absolute bolometric magnitude (M_{bol})is calculated. In practice (m_{bol}) is determined by calculating the best approximate sum of the energies observed or available at each constituent wavelength of the star's spectrum. The calculation involves fitting a function to the energies, which are usually in terms of fluxes, and then integrating between appropriately selected endpoints below the function.

In this paper m_{bol} was determined by fitting a spline curve to $J\ H\ K\ L$ $12\mu m$ and $25\mu m$ fluxes. An additional rough m_{bol} determination was done by fitting a Planck function to $J\ H\ K$ and L fluxes. This second m_{bol} fitting

was done just as an exercise to check the values determined from the spline curve fit, and the Planck function was fitted just as an interpolation formula. The Planck function technique provides a good estimate of the bolometric flux when the effects of the dust shell are negligible.

2.6.1 Apparent bolometric magnitude from J H K L $12\mu m$ and $25\mu m$ fluxes.

The bolometric magnitudes of the Long Period Variables presented in Table 3.5 were calculated by integrating under a spline curve fitted to the mean J H K L $12\mu m$ and $25\mu m$ fluxes as a function of frequency (where the means used are an average of minimum and maximum fluxes, see Table 3.3). At the high frequency endpoint a line joining the K flux was extrapolated through a point that lies between the H and J fluxes; and at the other end point, an extrapolation was made by assuming zero flux and zero frequency. Note that this procedure is similar to that adopted by Whitelock *et al.* (1994).

The curve fitting was made on fluxes converted from dereddened set of mean J H K L magnitudes by using calibration constants from Wilson *et al.* (1972) that are listed below:

Flux Density Corresponding to a Zeroth-Magnitude Star	
λ_e	$F_v(\lambda_0)$
(μ)	$(10^{-23} W m^{-2} Hz^{-1})$
1.25	1.52
1.65	0.98
2.2	0.62
3.5	0.28

The table gives the wavelength dependence of the flux density of α Lyr which is taken as a zeroth-magnitude star at all wavelengths (Wilson *et al.* 1972). The extinction and colour correction for near- and mid-infrared data respectively are explained in previous sections.

2.6.2 Apparent bolometric magnitude from $J\ H\ K\ L$ fluxes.

As an exercise to check the m_{bol} values determined by fitting a spline curve, a second m_{bol} determination was made integrating under a blackbody fitting. The blackbody spectrum described by Planck's function:

$$I_v = \frac{2hv^3}{c^2} \frac{1}{e^{hv/kT} - 1}, \tag{2.7}$$

was used as an interpolation, extrapolation device. In the equation, I_v is the intensity per unit frequency v, h is Planck's constant, c is the velocity of light, and k is Boltzmann's constant. As in the above section, the magnitude to fluxes conversion was done by using constants from Wilson *et al.* (1972). Note that this m_{bol} from $JHKL$ fluxes determination procedure is similar

to the m_{bol} from JHK procedure used by Feast *et al.* (1989). Therefore the exercise of deriving m_{bol} by blackbody fitting here was important since the aim of finding luminosity (by spline) in this paper was so that they could be used with the Feast *et al.* (1989) period-luminosity relations that were derived from blackbody fits to near-infrared photometry.

Though there are various arguments about which fitting technique gives the best estimation for the luminosity, the spline curve seems suitable for the red sources such as thick-dust shelled Miras studied here, while the blackbody fitting procedure may be more appropriate for relatively bluer sources. Whitelock *et al.* (1989) discusses some systematic differences and presents brief arguments concerning the two techniques.

2.7 Distance Determination

Distances to Mira variables can be determined by applying various Mira Period-Luminosity relations that have been shown to exist for stars in the Large Magellanic Cloud (LMC). The evidence of this came from the work of Robertson & Feast (1981), Glass & Lloyd Evans (1981) and later Glass & Feast (1982) who demonstrated that a Mira Period-Luminosity ($P-L$) relation ($\sigma = 0.22$ mag) existed at JHK and M_{bol} by observing 11 Miras in the LMC. Feast (1984) found that oxygen-rich and carbon-rich Miras in the LMC followed the same $P-L$ relation at K, and Glass et al. (1987) obtained a $P-L$ relation with a scatter of $\sigma = 0.15$ mag.

In this paper the precise $P-L$ relations from Feast *et al.* (1989) with

$\sigma = 0.16$ for oxygen-rich Miras and $\sigma = 0.13$ for carbon-rich Miras were used to determine distances to the galactic Miras that were being studied. The equations, which are presented in Table 2.1, resulted from least-squares solutions of the form

$$m_0 = \rho \log P + \delta, \tag{2.8}$$

that were applied to observations of long period variables as explained by Feast *et al.* (1989). The equations were converted to relations in absolute magnitude by adopting a LMC modulus of 18.57 (Feast 1995), and applying

$$M = m_0 - Modulus. \tag{2.9}$$

Using the absolute magnitudes, distances were calculated from the distance relation,

$$M = m + 5 - 5 \log r. \tag{2.10}$$

The periods, magnitudes, and oxygen and carbon-rich classifications used in calculating distances were determined as explained in the above sections. Preliminary distances were calculated from relations at K and the final distances were calculated from relations in the m_{bol} that were determined from J H K and L magnitudes and 12 and 25μm fluxes as outlined in the sections above. It is understood that while the relation at K is the most practical (due to relative insensitivity of K to interstellar reddening and other reasons), the relation in m_{bol} is the most important for comparing observation with the theory of stellar evolution. Furthermore, while the

relation at K breaks down when applied to stars with thick shells, the relation in m_{bol} prevails even when used with these very red stars, since flux absorbed from the star by the shell is reradiated and emitted at the $IRAS$ fluxes. The drawback of the $P-L$ relation in m_{bol} is that, while it is established for periods less than 420 days, it is less understood for larger periods. As shown by Whitelock *et al.* (1994), extrapolating the relation for periods larger than 420 days may produce systematic errors.

Table 2.1 Period-luminosity relations. (Adapted from Feast *et al.* 1989.)

Group	Mag	$\rho \pm s.e.$	$\delta \pm s.e.$	σ	Solution
O-Miras	K_0	$-3.47 \pm .19$	$19.48 \pm .45$	0.13	(a)
C-Miras	K_0	$-3.30 \pm .40$	$18.98 \pm .98$	0.18	(b)
O-Miras	m_b	$-3.00 \pm .24$	$21.35 \pm .57$	0.16	(c)
C-Miras	m_b	$-1.86 \pm .30$	$18.73 \pm .74$	0.13	(d)

Chapter 3

Results

The present study contains observations of 101 *IRAS* Galactic Long Period Variables (LPVs), which include Miras and non-Miras as defined in relevant sections. The LPVs are listed in Table 3.1, together with their 12 and 25μm *IRAS* fluxes (not colour corrected) and their respective uncertainties (Unc). Also tabulated are the *IRAS* variability index (Var) and the LRS spectral type (LRS). A definition of these parameters as well as the procedure for making the colour corrections can be found in version 2 of the *IRAS Point Source Catalogue - Explanatory Supplement* (PSC-ES) (1988). As in associated studies by Whitelock *et al.* (1994), the common names of the *IRAS* stars previously identified are also listed, with preference given to a variable star designation (Kukarkin *et al.* 1982; GCVS) if available; alternatively the Stephenson **S** or Carbon Star numbers (Stephenson 1984, 1989) are quoted.

Table 3.1 *IRAS* Galactic Long Period Variables

Star	IRAS Name	12μm (Jy)	25μm	Unc	Var (0.1%)	LRS		Name
1	09421–6223	4.44	1.71	AA	5	-	-	NT Car
2	09433–6233	5.47	2.44	BB	8	-	-	-
3	09509–6013	0.86	0.34	BC	3	-	-	-
4	09510–6247	0.81	0.35	AC	8	-	-	KM Car
5	09519–6007	13.29	5.45	AB	4	14	-	V363 Car
6	09533–6021	30.39	18.97	CB	9	42	-	C2663
7	09568–6056	0.48	0.25L	B_	-	-	-	-
8	09570–6051	0.66	0.19	ED	1	-	-	-
9	09571–5930	1.31	0.75	BB	8	-	-	-
10	09579–6203	1.17	0.45	BB	3	-	-	-
11	09581–5936	0.47	0.25L	B_	-	-	-	-
12	09586–6150	6.26	3.87	DC	9	-	-	-
13	09595–6141	0.83	0.42	BC	0	-	-	-
14	09597–5927	0.66	0.40	DC	1	-	-	-
15	10001–5929	1.30	0.62	CB	6	-	-	-
16	10003–6207	0.35	0.25L	C_	-	-	-	-
17	10004–6235	5.11	1.74	BB	1	-	-	GY Car
18	10008–6115	0.41	0.16	BD	0	-	-	-
19	10010–6025	1.53	0.92	BB	3	-	-	-
20	10015–6212	0.84	0.25L	C_	-	-	-	-
21	10019–5946	0.33	0.25L	C_	-	-	-	-
22	10021–5903	2.08	0.69	BC	1	-	-	-
23	10023–5946	1.58	0.48	BC	5	-	-	C2692
24	10026–5849	5.61	1.91	BB	0	-	-	-
25	10029–5856	6.43	2.99	CC	9	-	-	-
26	10033–5950	27.54	20.99	BB	9	29	-	-
27	10034–6207	1.12	0.60	BE	2	-	-	-
28	10038–6055	0.99	0.37	BC	4	-	-	S657
29	10040–6020	6.33	3.43	BB	0	-	-	-
30	10044–5803	1.51	0.92	BD	4	-	-	-
31	10045–5955	2.81	1.16	AB	1	-	-	S661
32	10048–5820	0.98	0.43	BD	4	-	-	-
33	10050–6001	1.09	0.46	BC	2	-	-	-
34	10051–5817	2.48	0.97	BB	2	-	-	-
35	10052–5906	0.36	0.54L	C_	-	-	-	C2703
36	10053–6001	0.60	0.25L	C_	-	-	-	-
37	10053–5852	3.67	2.85	CC	9	-	-	-
38	10056–6223	0.73	0.33	EC	-	-	-	-
39	10057–6018	2.24	1.32	BB	4	-	-	-
40	10062–5824	2.54	1.65	BB	4	-	-	-

Table 3.1 *IRAS* Galactic Long Period Variables - *continued*

Star	IRAS Name	12μm (Jy)	25μm	Unc	Var (0.1%)	LRS		Name
41	10064–5757	3.20	1.42	BB	1	-	-	-
42	10071–5815	0.77	0.38	CD	2	-	-	-
43	10075–5747	0.61	1.46L	B_	-	-	-	-
44	10076–5944	1.52	0.75	BC	4	-	-	-
45	10078–5742	1.20	0.67	CC	6	-	-	-
46	10079–5914	0.52	0.41	CD	9	-	-	-
47	10080–5902	3.81	1.69	BB	1	-	-	-
48	10090–5744	1.00	0.88	BC	4	-	-	-
49	10098–5742	38.41	24.20	BB	9	42	-	-
50	10102–5841	0.51	0.22	CD	0	-	-	-
51	10104–5832	1.82	0.95	CC	6	-	-	-
52	10107–5814	1.24	0.63	BD	8	-	-	-
53	10109–5958	10.60	3.32	BB	0	-	-	C2720
54	10110–5734	1.55	4.11L	B_	-	-	-	-
55	10111–6102	0.59	0.30L	AB	-	-	-	-
56	10113–6142	0.30	0.25L	B_	-	-	-	-
57	10118–6038	50.66	30.91	CB	9	29	-	SU Car
58	10121–5836	16.14	6.84	BB	7	15	-	Z Car
59	10121–5846	16.54	6.83	AB	0	14	-	AF Car
60	10123–5753	1.87	1.03	CD	9	-	-	-
61	10136–5743	2.58	0.78	BE	0	-	-	C2729
62	10141–5837	4.07	1.74	BB	4	-	-	AN Car
63	10145–5714	1.25	1.96L	B_	-	-	-	-
64	10145–6046	5.59	2.09	AB	0	-	-	C1651
65	10146–5922	0.44	0.51L	B_	-	-	-	-
66	10148–6039	0.75	0.37	BC	0	-	-	-
67	10150–5703	1.06	4.03L	C_	-	-	-	-
68	10154–5828	0.52	0.18	CF	1	-	-	-
69	10157–5944	0.69	0.51	DF	-	-	-	-
70	10160–6041	1.18	0.39	BC	0	-	-	-
71	10161–5945	3.93	2.22	BB	2	-	-	-
72	10162–6010	1.56	0.50	BD	0	-	-	-
73	10163–6012	3.79	1.73	BC	8	-	-	-
74	10164–6005	0.48	0.60L	C_	-	-	-	-
75	10168–6013	2.03	0.70	BC	0	-	-	-
76	10173–5844	2.05	1.64	CC	9	-	-	-
77	10174–5704	41.80	60.39	BB	5	69	-	-
78	10175–5957	0.63	0.25L	C_	-	-	-	C1662
79	10176–5802	73.57	55.83	BB	5	28	-	-
80	10194–5816	3.76	2.94	CC	0	-	-	-

Table 3.1 *IRAS* Galactic Long Period Variables - *continued*

Star	IRAS Name	12μm (Jy)	25μm	Unc	Var (0.1%)	LRS		Name
81	10196–5718	2.82	1.69	BD	8	-	-	-
82	10198–5853	0.73	0.35	CE	3	-	-	-
83	10199–5801	28.31	16.51	CB	1	43	-	-
84	10207–5815	0.86	0.60	CD	7	-	-	-
85	10216–5813	0.63	1.68L	B_	-	-	-	-
86	10220–5858	3.17	0.90	DC	5	-	-	-
87	10222–5700	2.14	1.02	BB	2	-	-	-
88	10225–5925	0.79	0.41	CF	9	-	-	-
89	10229–5705	4.15	1.15	BC	9	-	-	-
90	10230–5744	1.05	0.95	CF	9	-	-	-
91	10231–5823	14.87	7.62	CB	9	43	-	-
92	10234–5820	0.76	1.65L	F_	-	-	-	-
93	10238–5852	1.07	0.65	BD	4	-	-	-
94	10246–5844	2.40	1.96	CB	3	-	-	-
95	10250–5904	1.29	0.50	BD	0	-	-	-
96	10256–5836	1.66	0.96	CC	9	-	-	-
97	10257–5854	0.90	1.28L	D_	-	-	-	-
98	10261–5717	4.60	3.43	BC	1	-	-	-
99	10262–5727	1.70	0.94L	B_	0	-	-	-
100	10277–5836	0.96	0.69	BC	0	-	-	-
101	10287–5733	84.77	69.80	BB	0	04	-	OH285.05+.07

The *near*-infrared data, totalling 1098 sets of observations at JHK and L, were made between JD 244 8314 and JD 245 0202. The complete data set is shown in Table 3.2. The times of the observations are given as Julian dates from which 244 0000 d has been subtracted. The errors of individual magnitude measurements are estimated to be about 0.03 mag in J H K and 0.05 mag in L. Photometry marked with a colon is uncertain and only accurate to ±0.1 mag. In the few instances (blanks in the mag columns in Table 3.2), J and H magnitudes could not be determined because the programme star was faint.

Table 3.2: Near-Infrared Observations

Date	J	H	K	L
1 IRAS 09421-6223				
8314.28	5.56	4.57	4.03	3.43
9006.56	5.42	4.45	3.99	3.44
8703.22	5.45	4.46	3.99	3.42
9143.22	4.95	3.96	3.56	3.17
9317.51	5.35	4.42	3.93	3.33
9356.44	5.18	4.22	3.78	3.24
9471.25	5.16	4.18	3.71	3.25
9518.21	5.53	4.54	4.00	3.53
9798.44	5.32	4.35	3.86	3.46
9904.20	5.54	4.59	4.07	3.49
2 IRAS 09433-6233				
8314.30	10.59	8.31	6.66	4.74
9020.49	11.84	9.43	7.66	5.61
9061.54	11.76	9.46	7.70	5.68
9112.25	11.77	9.43	7.67	5.68
8703.24	10.59	8.34	6.69	4.76
9147.22	11.58	9.28	7.56	5.60
9352.43	10.36	8.12	6.52	4.60
9434.47	10.79	8.44	6.78	4.80
9495.28	11.54	9.00	7.23	5.19
9791.46	11.70	9.11	7.22	5.07
9832.42	11.25	8.72	6.88	4.80
3 IRAS 09509-6013				
9056.32	13.36:	10.84	8.83	6.54
9112.26	13.44:	11.02	9.06	6.72
9147.24	13.48:	11.04	9.05	6.86
9172.30	13.65:	11.23	9.20	6.95
9352.45	13.82:	11.43	9.43	7.24
9376.40	13.47:	11.32	9.39	7.22
9471.24	12.97:	10.63	8.79	6.83
9518.25	12.62:	10.34	8.56	6.64
9791.47	13.14:	10.82	9.00	7.04
9879.20	12.99:	10.70	8.93	7.12
10122.52	11.61	9.48	8.01	6.20
10199.26	11.87	9.73	8.19	6.38
4 IRAS 09510-6247				
8314.34	7.00	6.05	5.64	5.12
9006.57	7.41	6.47	6.00	
9115.34	6.76	5.81	5.43	5.03
9152.18	6.98	6.10	5.67	5.25
9316.53	6.76	5.83	5.50	5.02
9355.43	6.65	5.72	5.35	4.89
9471.27	7.32	6.39	5.99	5.35
9496.31	7.28	6.32	5.86	5.26
9791.48	6.93	6.04	5.66	5.15
5 IRAS 09519-6007				
8315.32	5.06	3.84	3.19	2.64
8703.27	5.28	4.03	3.35	2.69
9061.55	5.39	4.07	3.38	2.80
9319.54	4.58	3.41	2.87	2.41
9356.45	4.97	3.76	3.14	2.63
9472.30	4.79	3.70	3.12	2.49
9519.20	4.84	3.76	3.17	2.54
9791.45	5.11	3.88	3.25	2.62
9832.43	4.88	3.74	3.12	2.54
10120.47	4.99	3.78	3.13	2.54
10199.27	4.62	3.57	3.00	2.34
6 IRAS 09533-6021				
8315.35	11.81	8.63	6.21	3.41
8703.28	13.35:	10.24	7.69	4.64
9056.35	11.65	8.55	6.17	3.31
9112.27	11.82	8.68	6.30	3.40
9147.25	11.82	8.64	6.24	3.42
9353.44	13.44:	10.25	7.66	4.46
9434.00	13.98:	10.59	7.99	4.82
9491.18	13.89:	10.52	7.90	4.73
9705.47	12.11:	8.91	6.43	3.49
9792.39	11.90	8.63	6.18	3.41
9879.21	12.28:	8.92	6.40	3.56
7 IRAS 09568-6056				
8315.38	10.03	8.38	7.22	6.09
8703.30	11.11	9.18	7.74	6.34
9056.36	10.73	8.88	7.55	6.30
9112.29	9.99	8.30	7.15	6.03
9147.27	9.80	8.12	7.00	5.89
9172.31	9.94	8.20	7.04	5.90
9355.44	10.48	8.70	7.46	6.22
9434.50	9.89	8.22	7.10	5.93
9495.28	10.28	8.53	7.33	6.15
9792.40	10.47	8.69	7.48	6.79
8 IRAS 09570-6051				
8317.31	7.66	6.55	6.03	5.61
9056.37	7.82	6.73	6.27	5.75
9115.35	7.73	6.58	6.14	5.70
9152.19	7.57	6.48	6.03	5.65
9172.32	7.66	6.50	6.05	5.68
9318.48	7.84	6.73	6.26	5.75
9355.44	7.83	6.74	6.28	5.77
9434.51	7.67	6.55	6.12	5.69
9495.29	7.77	6.61	6.14	5.75
9792.40	7.76	6.63	6.14	5.81
9 IRAS 09571-5930				
8315.40	9.12	7.56	6.68	5.93
8703.30	8.69	7.18	6.44	5.81
9056.38	7.96	6.61	5.96	5.24
9115.35	8.22	6.79	6.09	5.41
9152.21	8.35	6.96	6.23	5.56
9173.21	8.59	7.09	6.34	5.66
9355.45	8.89	7.46	6.63	5.74
9472.33	8.17	6.86	6.19	5.51
9519.21	8.08	6.72	6.06	5.41
9792.41	9.07	7.64	6.77	5.96
10 IRAS 09579-6203				
8317.32	7.59	6.53	5.95	5.40
8703.31	7.64	6.61	6.04	5.43
9061.55	7.52	6.49	5.93	5.36
9115.36	7.45	6.43	5.89	5.28
9152.21	7.42	6.48	5.95	5.30
9173.22	7.35	6.37	5.89	5.26
9355.46	7.33	6.25	5.73	5.20
9472.35	7.33	6.31	5.80	5.22
9519.22	7.36	6.35	5.86	5.24
9792.42	7.56	6.50	5.93	5.40
10122.53	7.54	6.50	5.93	5.38
10199.31	7.35	6.38	5.87	5.26
11 IRAS 09581-5936				
8317.33	9.24	7.77	6.91	5.93
8703.32	10.00	8.41	7.32	6.15
9056.40	9.95	8.42	7.40	6.31
9112.30	9.73	8.19	7.26	6.21
9147.27	9.86	8.27	7.28	6.18
9173.23	10.10	8.46	7.43	6.31
9355.46	10.48	8.85	7.66	6.47
9472.37	9.79	8.19	7.18	6.19
9519.23	9.77	8.13	7.12	6.11
9792.44	10.16	8.56	7.46	6.46
9880.27	9.47	7.96	7.01	6.00
10122.55	10.08	8.48	7.46	6.42
10199.33	9.88	8.35	7.40	6.32
12 IRAS 09586-6150				
8315.42	14.65:	11.17	8.35	
8703.33		11.63	8.88	5.62
9056.41		13.00:	10.06	6.56
9112.31		12.95:	10.06	6.62
9147.29		12.65:	9.73	6.37
9173.25	15.34:	12.18:	9.25	5.93
9355.47		11.30	8.52	5.33
9474.21		12.31:	9.49	6.15
9519.26		12.64:	9.85	6.47
9792.47	14.70:	11.17	8.38	5.27
9904.22		11.55	8.80	5.59

Table 3.2 Near-Infrared Observations *continued*

Date	J	H	K	L
13 IRAS 09595-6141				
8318.30	8.47	7.47	6.99	6.43
8703.34	8.21	7.25	6.85	6.38
9056.42	8.43	7.49	7.03	6.50
9112.32	8.11	7.14	6.76	6.30
9147.21	8.11	7.12	6.71	6.26
9173.27	8.19	7.19	6.75	6.30
9355.49	8.27	7.25	6.81	6.30
9474.23	8.02	7.06	6.68	6.20
9518.27	8.31	7.26	6.80	6.33
9792.48	8.13	7.18	6.76	6.32
14 IRAS 09597-5927				
8316.37	8.79	7.58	6.98	6.36
8703.35	8.54	7.32	6.80	6.21
9056.43	8.51	7.27	6.74	6.14
9112.32	8.83	7.59	7.03	6.40
9147.30	8.65	7.47	6.93	6.26
9173.28	8.45	7.29	6.78	6.26
9355.50	8.53	7.39	6.87	6.27
9474.26	8.66	7.45	6.89	6.32
9519.28	9.00	7.81	7.21	6.53
9792.49	8.33	7.18	6.70	6.19
15 IRAS 10001-5929				
8314.42	7.26	6.05	5.52	5.07
8703.35	7.41	6.28	5.72	5.16
9056.44	7.63	6.48	5.87	5.24
9115.36	8.32	7.13	6.41	5.72
9152.22	8.18	7.09	6.40	5.68
9173.29	8.13	7.03	6.34	5.64
9355.51	7.24	6.10	5.57	5.02
9474.26	8.23	7.04	6.28	5.57
9519.29	8.18	6.97	6.22	5.48
9791.51	7.72	6.51	5.91	5.34
9832.43	7.76	6.53	5.90	5.32
9879.24	7.70	6.55	5.92	5.36
10122.54	7.89	6.77	6.11	5.47
10199.35	7.99	6.85	6.18	5.49
16 IRAS 10003-6207				
8314.43	11.79	9.76	8.34	6.86
8703.36	11.47	9.59	8.22	6.73
9056.45	11.66	9.64	8.20	6.66
9112.34	11.93	9.91	8.43	6.95
9147.30	11.74	9.75	8.31	6.85
9173.31	11.64	9.71	8.29	6.88
9355.51	10.57	8.84	7.66	6.33
9434.51	10.99	9.22	7.96	6.58
9495.30	11.54	9.65	8.29	6.91
9791.52	10.81	9.06	7.84	6.53
9832.44	11.16	9.29	8.00	6.65
9904.23	11.52	9.69	8.34	7.01
17 IRAS 10004-6235				
8314.44	5.39	4.42	4.04	3.60
9006.58			3.47	
8704.22	4.97	3.97	3.58	3.22
9143.25	5.51	4.58	4.10	3.52
9317.52	4.87	3.91	3.54	3.12
9374.40	5.19	4.17	3.73	3.28
9474.27	5.33	4.39	3.95	3.42
9526.70	5.32	4.34	3.94	3.42
9791.52	5.36	4.40	3.96	3.37
9904.26	4.77	3.79	3.44	3.03
18 IRAS 10008-6115				
8316.38	7.86	6.82	6.34	5.73
8703.37	8.36	7.39	6.86	6.16
9056.46	8.40	7.34	6.78	6.08
9112.34	8.40	7.38	6.85	6.18
9147.33	8.15	7.18	6.66	5.99
9179.22	7.91	6.87	6.41	5.86
9355.52	8.45	7.26	6.67	6.12
9434.52	8.78	7.61	6.98	6.36
9495.30	8.37	7.35	6.81	6.16
9791.53	8.53	7.36	6.77	6.21
9832.46	8.68	7.48	6.86	6.30
9880.28	8.32	7.27	6.72	6.07
10122.58	7.94	6.79	6.26	5.75
10199.37	8.60	7.39	6.76	6.19
19 IRAS 10010-6025				
8316.40	8.01	6.67	5.95	5.26
8703.39	7.73	6.43	5.77	5.12
9056.47	7.47	6.22	5.59	4.87
9115.37	7.98	6.62	5.93	5.26
9152.23	8.32	6.99	6.22	5.49
9179.23	8.49	7.11	6.30	5.50
9355.53	7.38	6.26	5.68	4.89
9434.53	7.33	6.14	5.56	4.89
9495.32	7.72	6.45	5.82	5.19
9792.50	7.29	6.14	5.52	4.79
9832.49	7.38	6.14	5.51	4.74
9904.27	7.99	6.72	6.01	5.24
20 IRAS 10015-6212				
8703.40	11.49	9.51	8.00	6.45
9056.48	11.43	9.43	7.96	6.35
9112.35	11.11	9.16	7.75	6.29
9147.34	10.07	9.06	7.66	6.23
9179.24	10.87	9.02	7.69	6.25
9355.54	10.76	8.91	7.60	6.15
9474.28	11.03	9.17	7.82	6.41
9518.29	10.81	9.00	7.69	6.34
9792.50	10.96	9.06	7.70	6.31
9832.50	11.28	9.29	7.86	6.35
10122.57	10.33	8.51	7.26	5.99
10199.36	10.68	8.76	7.45	6.15
21 IRAS 10019-5946				
8404.20	7.95	6.81	6.32	5.78
8705.24	8.02	6.84	6.35	5.86
9056.49	8.04	6.88	6.42	5.88
9115.37	7.86	6.66	6.20	5.76
9153.29	7.80	6.61	6.15	5.74
9179.28	7.84	6.67	6.18	5.75
9355.55	8.05	6.88	6.43	5.94
9474.31	7.85	6.67	6.20	5.82
9526.18	8.11	6.94	6.41	5.98
9792.51	7.93	6.78	6.28	5.91
9880.29	7.98	6.88	6.40	5.88
22 IRAS 10021-5903				
8317.38	11.07	8.62	6.87	4.96
8703.41	10.98	8.70	7.06	5.34
9057.39	11.50	9.15	7.47	5.66
9112.36	11.09	8.81	7.21	5.58
9147.35	10.97	8.68	7.10	5.46
9179.27	10.82	8.60	7.09	5.46
9355.56	10.20	8.00	6.58	4.93
9474.32	11.21	8.76	7.19	5.56
9526.20	11.59	9.20	7.52	5.70
9792.52	10.27	8.08	6.56	4.96
9876.28	10.42	8.13	6.58	4.88
10122.60	11.80	9.25	7.47	5.60
10199.41	11.59	9.10	7.34	5.49
23 IRAS 10023-5946				
8318.31	7.05	5.62	4.94	4.22
9004.34	6.75	5.39	4.81	4.14
9061.56	6.84	5.46	4.84	4.17
9143.26	6.80	5.43	4.84	4.16
9317.52	7.16	5.72	5.02	4.30
9374.41	7.11	5.67	4.99	4.27
9440.25	6.93	5.53	4.90	4.22
9474.33	6.99	5.57	4.92	4.23
9496.29	7.01	5.59	4.94	4.25
9702.50	6.83	5.41	4.81	4.13
9791.60	6.87	5.47	4.87	4.16
24 IRAS 10026-5849				
8314.47	10.15	7.88	6.20	4.38
8704.25	11.02	8.38	6.53	4.57
9057.40	9.55	7.20	5.64	3.92
9147.36	9.85	7.42	5.78	4.09
9318.50	10.01	7.72	6.02	4.30
9355.57	9.85	7.60	5.95	4.29
9439.35	9.57	7.34	5.82	4.25
9491.20	9.48	7.29	5.80	4.18
9702.51	9.95	7.66	6.07	4.37
9792.52	10.07	7.83	6.20	4.59
10122.62	9.26	7.00	5.55	3.97
10199.43	9.52	7.20	5.66	4.07

Table 3.2 Near-Infrared Observations *continued*

Date	J	H	K	L
25 IRAS 10029-5856				
8314.48	6.03	4.93	4.36	3.67
8704.26	6.11	4.95	4.38	3.67
9057.41	6.20	5.11	4.53	3.76
9143.27	5.98	4.83	4.28	3.66
9317.58	6.89	5.71	4.99	4.22
9374.47	6.69	5.55	4.86	4.08
9440.25	6.17	5.03	4.44	3.71
9491.21	5.98	4.81	4.25	3.60
9702.51	6.82	5.62	4.95	4.27
9792.54	6.43	5.33	4.72	4.03
9876.29	5.98	4.80	4.27	3.66
26 IRAS 10033-5950				
8316.43	7.06	5.43	4.62	3.79
8704.27	7.07	5.43	4.64	3.86
9058.27	6.83	5.24	4.45	3.70
9143.29	7.08	5.47	4.68	3.83
9317.60	7.27	5.63	4.76	3.89
9374.39	6.86	5.22	4.45	3.57
9440.26	6.71	5.08	4.31	3.53
9491.21	7.27	5.67	4.80	4.01
9702.52	7.92	6.39	5.46	4.55
9792.54	7.48	5.93	5.05	4.06
9876.31	7.53	5.88	4.88	3.98
10122.63	7.72	5.95	4.92	3.97
10199.44	7.28	5.51	4.58	3.58
27 IRAS 10034-6207				
8316.44	7.53	6.38	5.80	5.28
8704.28	7.94	6.70	6.05	5.47
9058.28	7.81	6.65	5.99	5.33
9115.39	7.53	6.46	5.85	5.20
9153.31	7.49	6.45	5.86	5.19
9318.53	7.48	6.30	5.70	5.19
9356.36	7.74	6.50	5.85	5.29
9474.37	7.40	6.39	5.84	5.19
9526.21	7.13	6.10	5.58	5.01
9792.55	7.49	6.48	5.91	5.32
9876.32	7.12	6.08	5.58	5.03
28 IRAS 10038-6055				
8316.45	7.41	6.20	5.70	5.14
8704.28	7.21	6.08	5.62	5.10
9058.29	7.59	6.22	5.67	5.13
9116.24	7.26	6.12	5.68	5.07
9153.31	7.39	6.20	5.73	5.14
9318.51	6.92	5.59	5.05	4.52
9355.58	7.22	5.78	5.20	4.68
9474.39	7.45	6.21	5.71	5.19
9526.22	7.29	6.15	5.68	5.13
9792.55	7.57	6.11	5.49	5.00
9876.33	7.51	6.32	5.75	5.14
29 IRAS 10040-6020				
8314.51	13.96:	10.94	8.50	5.64
8704.29	12.37:	9.30	7.07	4.44
9058.30	12.96:	10.02	7.65	4.92
9112.40	12.57:	9.53	7.21	4.58
9147.37	12.44:	9.36	7.05	4.43
9352.50	13.23:	10.16	7.75	4.96
9438.56	14.06:	10.89	8.42	5.54
9491.23	14.19:	10.95	8.47	5.57
9703.46	12.55:	9.36	7.03	4.34
9792.56	12.46:	9.29	6.96	4.34
30 IRAS 10044-5803				
8315.47	9.39	7.59	6.56	5.58
8704.31	9.49	7.57	6.59	5.72
9058.31	9.32	7.48	6.51	5.68
9116.25	9.89	7.84	6.82	5.95
9153.33	9.78	7.84	6.79	5.90
9181.29	9.65	7.81	6.75	5.82
9352.47	8.62	6.81	6.01	5.23
9376.43	8.58	6.78	5.98	5.28
9474.41	9.25	7.33	6.38	5.61
9526.22	9.46	7.51	6.51	5.75
9792.57	8.53	6.72	5.87	5.13
9880.31	9.42	7.55	6.54	5.61
10122.64	9.38	7.65	6.64	5.45
10199.46	9.10	7.26	6.32	5.35
31 IRAS 10045-5955				
8314.53	6.79	5.71	5.25	4.61
8704.30	7.05	5.92	5.44	4.74
9061.56	7.14	6.01	5.48	4.89
9319.55	6.93	5.56	4.93	4.39
9356.46	7.29	5.82	5.20	4.72
9474.44	7.24	6.07	5.50	5.00
9526.23	6.83	5.78	5.28	4.74
9796.44	7.50	5.97	5.29	4.74
9880.32	6.82	5.68	5.15	4.44
9905.20	6.95	5.76	5.22	4.49
10122.64	6.82	5.38	4.76	4.09
10199.46	7.46	5.98	5.28	4.66
32 IRAS 10048-5820				
8316.47	10.10	7.99	6.83	5.73
8704.33	9.69	7.83	6.77	5.58
9058.32	10.58	8.66	7.45	6.31
9112.41	10.47	8.55	7.40	6.19
9148.20	10.31	8.44	7.31	6.03
9181.23	9.86	8.04	6.99	5.68
9352.48	10.00	7.90	6.78	5.52
9376.45	10.14	8.03	6.87	5.63
9475.20	10.78	8.63	7.31	6.23
9526.24	11.10	8.97	7.57	6.47
9796.45	9.88	7.95	6.82	5.59
33 IRAS 10050-6001				
8314.53	8.01	6.80	6.17	5.57
8704.34	8.05	6.84	6.23	5.60
9058.35	7.96	6.79	6.19	5.54
9116.26	8.38	7.11	6.50	5.83
9153.34	8.67	7.37	6.69	6.01
9353.44	7.70	6.60	6.10	5.42
9438.55	7.62	6.44	5.90	5.36
9491.23	7.95	6.77	6.18	5.59
9702.53	8.09	7.09	6.53	5.76
9796.47	7.47	6.34	5.84	5.26
34 IRAS 10051-5817				
8317.41	11.36	8.82	7.05	5.15
8704.34	10.82	8.26	6.58	4.82
9058.33	9.82	7.59	6.08	4.52
9112.42	10.14	7.73	6.19	4.68
9148.21	10.35	7.89	6.32	4.76
9181.22	10.61	8.15	6.54	4.96
9352.48	10.18	7.83	6.29	4.79
9475.22	9.45	7.23	5.85	4.47
9526.25	9.60	7.32	5.91	4.55
9796.48	9.84	7.56	6.10	4.77
10123.51	10.14	7.80	6.27	4.90
10199.47	9.77	7.56	6.10	4.81
35 IRAS 10052-5906				
8318.34	9.57	7.71	6.57	5.68
8704.35	9.42	7.60	6.53	5.65
9058.35	9.05	7.37	6.42	5.64
9116.27	9.36	7.54	6.51	5.69
9153.34	9.47	7.60	6.53	5.72
9353.45	9.15	7.43	6.51	5.71
9475.23	9.04	7.30	6.38	5.62
9496.30	9.13	7.35	6.41	5.63
9702.53	9.40	7.56	6.55	5.74
9796.49	9.08	7.36	6.44	5.68
9888.27	8.99	7.26	6.34	5.56
9905.28	9.02	7.28	6.35	5.63
36 IRAS 10053-6001				
8314.56	9.16	7.95	7.15	6.31
8704.36	9.25	7.96	7.20	6.46
9020.48	8.18	6.95	6.41	5.95
9062.44	8.56	7.27	6.66	6.16
9116.28	9.11	7.77	7.05	6.43
9168.26	8.74	7.55	6.89	6.22
9355.58	7.98	6.81	6.32	5.80
9475.25	8.51	7.22	6.59	6.06
9526.26	9.14	7.81	7.05	6.41
9796.50	8.17	7.02	6.51	5.96
9888.26	8.51	7.20	6.60	6.06
10123.53	8.80	7.63	6.99	6.24
10201.33	8.17	7.03	6.52	5.94

Table 3.2 Near-Infrared Observations *continued*

Date	J	H	K	L
37 IRAS 10053-5852				
8315.51	11.24	8.67	6.81	4.83
8704.38	9.90	7.57	5.98	4.18
9058.36	10.51	8.18	6.48	4.64
9112.43	10.74	8.23	6.52	4.70
9148.24	10.48	8.02	6.36	4.55
9181.20	10.02	7.66	6.05	4.23
9352.49	10.82	8.26	6.43	4.45
9475.26	11.44	8.98	7.06	5.04
9526.27	11.32	8.72	6.79	4.84
9798.46	10.35	7.82	6.07	4.20
38 IRAS 10056-6223				
8315.52	8.76	7.79	7.39	6.86
8704.39	8.58	7.61	7.25	6.76
9058.36	8.45	7.52	7.14	6.69
9116.28	8.42	7.44	7.05	6.52
9116.27	8.63	7.62	7.23	6.78
9353.46	8.55	7.53	7.15	6.66
9439.37	8.35	7.39	7.00	6.51
9491.37	8.44	7.42	7.03	6.56
9702.55	8.65	7.63	7.25	6.75
9798.49	8.56	7.61	7.25	6.78
10121.55	8.69	7.71	7.34	6.91
10201.34	8.46	7.45	7.12	6.68
39 IRAS 10057-6018				
8315.54	6.41	5.42	4.92	4.36
9003.44	6.38	5.47	4.99	4.35
8704.39	6.04	5.04	4.58	4.07
9062.45	6.09	5.12	4.68	4.18
9319.57	6.67	5.70	5.10	4.42
9371.51	6.22	5.29	4.80	4.15
9475.27	6.10	5.10	4.61	4.10
9526.27	6.48	5.43	4.89	4.40
9798.50	6.01	5.01	4.53	4.01
40 IRAS 10062-5824				
8315.56	7.97	6.54	5.64	4.82
9004.35	8.37	6.94	5.99	4.93
8704.40	7.58	6.25	5.45	4.64
9062.46	8.41	6.97	6.09	5.08
9319.59	7.69	6.30	5.51	4.76
9371.52	8.08	6.62	5.76	4.94
9475.28	8.06	6.61	5.70	4.80
9526.28	7.46	6.14	5.36	4.50
9798.51	8.41	6.98	5.95	4.88
10123.55	7.74	6.34	5.51	4.75
10201.35	8.08	6.60	5.68	4.76
41 IRAS 10064-5757				
8315.57	13.63:	10.96	8.75	6.06
8704.41	12.85:	9.95	7.80	5.40
9058.37	12.81:	10.08	8.04	5.82
9112.44	12.61:	9.77	7.76	5.62
9148.24	12.43:	9.65	7.72	5.55
9353.47	12.90:	10.31	8.26	5.91
9439.38	12.91:	10.41	8.40	6.18
9491.26	13.08:	10.40	8.29	6.07
9702.56	12.34:	9.53	7.58	5.49
9804.40	12.37:	9.73	7.79	5.59
9904.29	13.88:	10.76	8.52	6.15
10123.60	13.03:	10.54	8.41	6.04
10201.36	12.79:	10.02	7.87	5.52
42 IRAS 10071-5815				
8316.49	9.70	7.55	6.45	5.52
8704.42	9.45	7.38	6.34	5.39
9058.38	9.25	7.28	6.28	5.37
9116.29	9.21	7.16	6.23	5.36
9168.29	9.28	7.22	6.22	5.35
9353.48	9.14	7.09	6.14	5.24
9439.39	9.36	7.25	6.25	5.35
9491.28	9.44	7.30	6.27	5.35
9702.56	9.52	7.37	6.34	5.43
9804.41	9.13	7.09	6.18	5.28
43 IRAS 10075-5747				
8316.51	10.13	7.95	6.91	5.97
8704.43	10.23	8.09	7.05	6.09
9058.40	10.44	8.37	7.27	6.30
9112.46	10.27	8.10	7.06	6.17
9148.25	10.02	7.84	6.85	6.01
9353.49	10.73	8.47	7.31	6.28
9439.40	10.41	8.24	7.16	6.21
9491.29	10.38	8.18	7.11	6.14
9703.48	10.67	8.36	7.21	6.28
9804.42	10.56	8.36	7.25	
44 IRAS 10076-5944				
8320.28	7.80	6.55	5.86	5.18
9004.40	7.55	6.23	5.61	5.07
8704.45	8.07	6.82	6.07	5.33
9061.34	7.87	6.55	5.87	5.28
9116.29	8.00	6.65	5.95	5.32
9168.32	7.48	6.33	5.69	5.07
9355.59	7.02	5.79	5.22	4.69
9440.42	7.68	6.40	5.73	5.12
9475.30	8.06	6.73	5.99	5.33
9526.29	8.08	6.76	6.01	5.33
9804.45	7.42	6.17	5.57	5.02
45 IRAS 10078-5742				
8704.46	8.03	6.07	5.26	4.65
9058.41	8.07	6.17	5.34	4.79
9112.47	8.23	6.20	5.37	4.82
9148.26	8.24	6.23	5.40	4.86
9353.50	8.08	6.09	5.26	4.62
9440.27	8.18	6.17	5.36	4.77
9475.31	8.11	6.11	5.30	4.72
9496.31	8.08	6.07	5.28	4.71
9703.48	8.07	6.06	5.26	4.67
9829.22	8.11	6.12	5.30	4.70
9888.25	8.13	6.14	5.33	4.73
46 IRAS 10079-5914				
8320.31	9.57	8.18	7.58	6.77
8704.47	9.50	8.08	7.45	6.66
8815.24	9.35	7.95	7.38	6.59
9058.42	10.10	8.59	7.86	6.92
9113.22	10.61	8.98	8.18	7.14
9148.30	10.78	9.14	8.30	7.25
9353.51	9.46	8.06	7.43	6.60
9439.40	9.63	8.19	7.59	6.81
9491.30	9.61	8.17	7.53	6.74
9703.49	11.41	9.69	8.69	7.37
9829.23	10.14	8.54	7.77	6.80
47 IRAS 10080-5902				
8320.32	9.71	7.39	5.83	4.11
8704.48	10.29	7.96	6.34	4.62
9059.48	11.06	8.61	6.83	4.93
9113.23	11.22	8.70	6.91	5.05
9168.33	11.00	8.51	6.73	4.90
9353.52	9.94	7.51	5.87	4.08
9439.42	10.40	7.86	6.16	4.36
9492.19	10.97	8.32	6.59	4.72
9703.50	10.93	8.40	6.61	4.75
9829.25	9.86	7.46	5.87	4.13
48 IRAS 10090-5744				
8320.36	8.85	6.90	6.06	5.42
9004.38	9.15	7.07	6.21	5.49
8704.49	8.96	7.00	6.15	5.52
9061.35	8.87	6.90	6.06	5.43
9116.30	8.80	6.82	6.00	5.37
9148.32	8.82	6.84	6.01	5.38
9526.30	8.88	6.89	6.05	5.45
9355.59	8.75	6.80	5.97	5.37
9475.33	8.85	6.89	6.06	5.45
9791.55	8.88	6.93	6.09	5.44
9888.22	8.91	6.91	6.08	5.43

Table 3.2 Near-Infrared Observations *continued*

Date	J	H	K	L
49 IRAS 10098-5742				
8320.39	13.88:	10.46	7.43	3.88
8704.50	14.34:	11.30	8.38	4.77
8767.34		10.91	8.04	4.55
8813.24	13.66:	10.48	7.61	4.18
9059.49	13.51:	10.24	7.45	4.03
9113.24	13.95:	10.54	7.77	4.37
9148.33	14.16:	10.72	7.99	4.60
9355.60	13.71:	10.60	7.92	4.66
9434.54	13.14:	9.90	7.29	4.03
9495.32	12.80:	9.58	6.96	3.75
9791.57	13.72:	10.52	7.82	4.58
9832.47	13.90:	10.68	7.93	4.68
10126.49	12.49:	9.20	6.66	3.64
10201.37	12.65:	9.24	6.63	3.54
50 IRAS 10102-5841				
8320.42	9.24	7.38	6.46	5.66
8704.54	9.27	7.38	6.48	5.69
9059.51	9.53	7.54	6.55	5.73
9116.31	9.34	7.41	6.47	5.71
9148.34	9.30	7.37	6.44	5.70
9318.54	9.37	7.39	6.40	5.60
9354.60	9.38	7.40	6.40	5.63
9439.42	9.28	7.34	6.40	5.64
9475.34	9.28	7.34	6.40	5.65
9526.30	9.20	7.27	6.34	5.59
9791.58	9.38	7.41	6.46	5.65
51 IRAS 10104-5832				
8320.43	10.55	8.12	6.54	4.96
8704.54	10.44	8.09	6.48	4.93
9059.51	11.17	8.74	7.01	5.47
9113.26	10.61	8.27	6.66	5.19
9148.36	10.28	7.98	6.45	4.98
9318.60	10.46	8.12	6.57	5.06
9356.37	10.86	8.41	6.79	5.23
9440.43	11.31	8.80	7.11	5.55
9495.33	11.07	8.62	6.97	5.47
9804.46			6.85	
9829.21	10.82	8.39	6.82	5.26
9888.21	11.35	8.75	7.07	5.41
52 IRAS 10107-5814				
8320.46	8.53	6.77	5.89	5.14
9004.41	8.98	7.31	6.42	5.55
8705.25	8.43	6.63	5.76	4.99
9061.38	8.68	6.93	6.11	5.30
9116.32	8.72	6.87	6.03	5.31
9169.22	9.02	7.17	6.25	5.52
9356.38	9.32	6.61	6.61	5.69
9440.44	8.70	6.93	6.13	5.35
9495.35	8.53	6.74	5.90	5.20
9829.26	8.61	6.93	6.04	5.08
53 IRAS 10109-5958				
8398.29	7.03	5.37	4.19	3.22
9061.38	7.34	5.63	4.47	3.25
8705.26	7.21	5.45	4.25	3.20
9319.60	6.97	5.38	4.30	3.16
9371.53	6.77	5.15	4.10	2.93
9475.36	7.59	5.76	4.50	3.21
9526.31	8.02	6.08	4.73	3.38
9829.27	7.10	5.28	4.02	2.75
9887.25	7.71	5.79	4.44	3.01
10123.62	7.91	5.97	4.55	3.12
10201.38	7.22	5.39	4.11	2.73
54 IRAS 10110-5734				
8403.21	6.21	5.04	4.58	4.42
9005.35	6.30	5.14	4.62	4.05
8815.25	6.91	5.75	5.13	4.45
9061.39	6.82	5.67	5.08	4.49
9143.32	6.69	5.55	5.03	4.40
9319.60	6.68	5.50	4.94	4.42
9371.54	6.82	5.68	5.10	4.45
9475.36	6.39	5.22	4.78	4.27
9526.31	6.25	5.03	4.56	4.11
9829.28	6.28	5.11	4.62	4.18
55 IRAS 10111-6102				
8317.50	8.45	7.31	6.71	6.11
8705.26	8.24	7.07	6.49	5.97
8815.21	8.53	7.44	6.79	6.09
9059.52	7.93	6.83	6.29	5.80
9116.33	8.34	7.24	6.64	6.08
9169.23	8.72	7.56	6.89	6.25
9356.39	7.75	6.69	6.23	5.73
9440.44	7.91	6.80	6.28	5.79
9495.36	8.26	7.16	6.56	6.07
9829.29	7.92	6.80	6.26	5.72
56 IRAS 10113-6142				
8317.51	7.84	6.84	6.39	5.92
8705.27	8.35	7.31	6.80	6.24
9059.53	7.78	6.74	6.29	5.78
9116.37	7.93	6.86	6.38	5.94
9169.25	8.31	7.27	6.70	6.14
9353.53	7.86	6.82	6.34	5.89
9439.43	8.40	7.36	6.82	6.30
9490.42	8.24	7.24	6.74	6.16
9702.57	8.33	7.29	6.75	6.24
9829.30	7.85	6.80	6.37	5.87
57 IRAS 10118-6038				
8316.55	3.68	2.60	2.10	1.57
9062.47	5.20	3.95	3.12	2.21
9144.30	4.81	3.68	2.89	1.93
9316.54	3.70	2.75	2.21	1.46
9371.56	3.53	2.52	2.03	1.31
9475.39	3.79	2.71	2.18	1.59
9530.19	4.16	3.04	2.44	1.82
9829.31	3.73	2.86	2.30	1.51
58 IRAS 10121-5836				
8422.22	4.26	3.16	2.64	2.18
9062.48	3.83	2.86	2.43	1.93
9144.32	3.97	2.90	2.42	1.98
9317.55	4.50	3.47	2.91	2.26
9371.57	4.53	3.55	2.99	2.31
9475.42	3.79	2.81	2.39	1.90
9526.33	3.98	2.90	2.43	2.00
59 IRAS 10121-5846				
8422.21	3.75	2.77	2.38	1.90
9062.47	4.27	3.22	2.66	2.16
9144.31	3.94	2.99	2.53	2.00
9317.54	3.59	2.63	2.23	1.78
9371.57	3.60	2.60	2.17	1.74
9475.40	4.24	3.19	2.64	2.15
9526.33	4.08	3.08	2.54	2.05
9887.24	4.21	3.15	2.61	2.15
10121.64	4.20	3.22	2.77	2.28
10201.39	3.74	2.75	2.36	1.96

Table 3.2 Near-Infrared Observations *continued*

Date	J	H	K	L
60 IRAS 10123-5753				
8398.31	7.79	6.27	5.55	4.92
8705.29	8.02	6.51	5.75	4.99
9059.54	8.03	6.56	5.80	5.02
9116.37	7.87	6.28	5.53	4.89
9172.28	8.31	6.60	5.79	5.16
9352.52	8.51	6.95	6.11	5.30
9439.44	7.82	6.30	5.57	4.87
9490.42	7.85	6.25	5.49	4.87
9703.52	8.62	7.03	6.13	5.20
9829.32	7.99	6.39	5.62	4.94
9904.31	8.48	6.75	5.89	5.22
61 IRAS 10136-5743				
8422.24	7.87	6.05	4.98	3.86
8705.34	8.22	6.24	5.04	3.88
9061.40	7.64	5.80	4.75	3.64
9352.53	8.54	6.68	5.52	4.17
9374.51	8.60	6.72	5.53	4.16
9490.34	8.84	6.83	5.56	4.13
9703.52	9.28	7.14	5.74	4.17
9829.33	8.78	6.74	5.49	4.03
9887.24	8.60	6.60	5.39	2.98
9905.29	8.60	6.58	5.37	3.99
62 IRAS 10141-5837				
8422.24	6.04	4.94	4.38	3.72
8705.36	6.36	5.22	4.57	4.00
9062.48	6.05	4.90	4.32	3.80
9145.27	6.32	5.15	4.54	3.97
9316.56	5.61	4.51	4.08	3.54
9371.61	5.42	4.28	3.86	3.39
9490.34	6.32	5.19	4.54	3.96
9829.35	5.62	4.47	3.98	3.45
63 IRAS 10145-5714				
8705.38	14.35:	10.35	7.94	5.62
9059.56		10.37	7.92	5.56
9113.28	14.74:	10.26	7.86	5.55
9172.26	14.58:	10.21	7.81	5.50
9352.53		10.32	7.78	5.27
9490.35		10.54	7.95	5.57
9832.27	13.11:	9.32	7.08	5.04
10121.57	13.16:	9.40	7.14	5.09
10201.39	12.78:	9.11	6.95	4.94
64 IRAS 10145-6046				
8317.53	5.90	4.44	3.71	2.97
9005.42	5.94	4.47	3.76	3.01
9061.41	5.83	4.41	3.70	3.01
9145.26	5.86	4.40	3.68	3.01
9316.56	5.76	4.34	3.66	2.98
9371.58	5.65	4.24	3.59	2.91
9490.38	5.84	4.40	3.68	2.99
9703.53	5.68	4.28	3.61	2.91
9832.30	5.75	4.32	3.61	2.99
10142.52	5.67	4.30	3.61	2.97
10201.40	5.66	4.25	3.59	2.92
65 IRAS 10146-5922				
8422.25	8.68	7.10	6.47	5.91
8813.21	9.27	7.68	6.89	6.19
9059.57	8.86	7.27	6.53	5.91
9117.28	9.25	7.67	6.87	6.14
9169.28	8.98	7.43	6.71	5.98
9352.54	8.89	7.31	6.56	5.93
9439.44	9.09	7.52	6.81	6.12
9490.43	8.88	7.27	6.60	6.02
9703.54	9.01	7.45	6.71	5.89
9831.26	8.63	7.03	6.36	5.75
10142.53	8.82	7.23	6.52	5.94
10201.41	9.01	7.39	6.64	6.01
66 IRAS 10148-6039				
8316.59	7.72	6.45	5.86	5.35
9005.43	8.01	6.81	6.14	5.33
8815.26	8.28	6.87	6.12	5.46
9061.42	7.51	6.35	5.77	5.09
9117.29	7.40	6.19	5.61	5.00
9169.31	7.64	6.37	5.73	5.16
9352.55	8.11	6.93	6.27	5.57
9440.45	8.04	6.87	6.24	5.59
9495.36	7.58	6.38	5.82	5.35
9831.28	7.93	6.74	6.05	5.35
9905.20	7.40	6.20	5.63	5.03
10121.61	8.88	7.49	6.68	5.84
10199.49	8.62	7.39	6.60	5.74
67 IRAS 10150-5703				
8422.27	8.36	6.82	6.03	5.33
9005.46	8.09	6.58	5.87	5.20
8705.39	8.45	6.90	6.15	5.50
9061.43	8.39	6.83	6.05	5.38
9117.29	8.78	7.20	6.34	5.58
9117.35			6.34	
9169.32	8.57	7.00	6.18	5.39
9356.40	8.28	6.73	5.93	5.31
9434.55	8.98	7.45	6.51	5.63
9495.37	8.96	7.40	6.48	5.63
9831.29	8.66	7.14	6.33	5.53
9905.21	8.14	6.58	5.86	5.22
10121.60	8.86	7.37	6.54	5.66
10202.30	8.09	6.54	5.85	5.13
68 IRAS 10154-5828				
9495.40	8.32	6.84	6.24	5.75
9530.20	8.45	6.96	6.38	5.88
9703.55	8.17	6.70	6.14	5.59
9832.31	8.20	6.74	6.13	5.70
10126.61	8.04	6.61	6.06	5.61
10202.32	8.29	6.83	6.23	5.75
69 IRAS 10157-5944				
8403.28	9.66	8.19	7.36	6.44
8705.44	9.82	8.46	7.63	6.62
9060.41	10.78	9.19	8.12	7.04
9113.30	9.61	8.21	7.43	6.52
9169.32	9.52	8.04	7.24	6.36
9353.55	10.10	8.63	7.76	6.87
9439.45	10.88	9.29	8.24	7.18
9490.44	10.79	9.22	8.16	7.17
9703.55	9.32	7.86	7.18	6.27
9799.49	9.92	8.47	7.59	6.82
9832.52	10.17	8.64	7.71	6.91
10121.62	9.23	7.76	6.97	6.14
10202.33	9.68	8.25	7.41	6.54
70 IRAS 10160-6041				
8316.61	10.12	8.28	6.96	5.57
8705.46	10.35	8.58	7.17	5.78
9060.42	11.11	9.23	7.75	6.39
9113.34	10.57	8.79	7.39	6.08
9169.34	10.14	8.40	7.10	5.78
9353.56	10.65	8.75	7.41	6.00
9439.46	11.21	9.28	7.86	6.40
9492.20	11.20	9.19	7.86	6.30
9703.56	9.65	7.96	6.87	5.52
9799.54	10.23	8.40	7.21	5.90
71 IRAS 10161-5945				
8404.32	7.00	5.58	4.86	4.24
9061.44	7.74	6.40	5.56	4.63
9317.60	7.84	6.31	5.45	4.60
9375.43	9.00	7.26	6.15	5.09
9440.30	9.08	7.48	6.36	5.09
9492.34	8.66	7.16	6.10	4.91
9703.56	7.07	5.60	4.83	4.05
9831.31	8.41	6.65	5.53	4.55
9887.21	8.07	6.42	5.39	4.37
10126.56	6.88	5.41	4.64	3.85
10202.34	7.57	5.98	5.09	4.24

Table 3.2 Near-Infrared Observations *continued*

Date	J	H	K	L
72 IRAS 10162-6010				
8317.57	6.68	5.57	5.12	4.62
9004.43	6.76	5.66	5.18	4.60
9061.44	6.40	5.30	4.86	4.42
9145.30	6.78	5.58	5.07	4.63
9316.60	6.92	5.82	5.30	4.69
9375.44	6.67	5.57	5.11	4.58
9440.31	6.48	5.35	4.90	4.46
9492.35	6.65	5.48	4.96	4.54
9703.57	6.79	5.70	5.20	4.61
9831.31	6.50	5.34	4.84	4.43
9887.21	6.88	5.69	5.13	4.65
9905.30	7.01	5.81	5.21	4.73
73 IRAS 10163-6012				
8317.58	5.93	4.69	4.20	3.75
9061.45	5.90	4.76	4.30	3.80
9318.55	5.74	4.52	4.04	3.62
9375.48	5.89	4.68	4.19	3.74
9440.31	6.02	4.82	4.30	3.80
9492.36	5.91	4.74	4.24	3.74
9703.57	5.81	4.65	4.19	3.64
9831.32	5.76	4.53	4.08	3.66
9886.27	5.88	4.67	4.18	3.74
9905.31	5.98	4.75	4.23	3.77
74 IRAS 10164-6005				
8317.59	8.37	7.09	6.51	6.00
9060.43	8.38	7.09	6.51	6.07
9113.35	8.89	7.60	6.93	6.36
9170.21	8.93	7.67	7.01	6.36
9316.59	8.46	7.25	6.74	6.12
9354.61	8.30	7.06	6.53	6.03
9439.48	8.68	7.37	6.75	6.26
9492.37	9.16	7.83	7.11	6.49
9704.48	8.31	7.04	6.56	6.11
9798.53	8.36	7.11	6.52	5.99
9832.52	8.63	7.33	6.69	6.15
75 IRAS 10168-6013				
8317.62	10.63	8.55	6.95	5.20
8705.49	10.12	8.13	6.67	5.05
9060.44	10.68	8.47	6.88	5.19
9113.35	10.85	8.63	6.99	5.26
9170.22	10.86	8.66	7.02	5.24
9353.57	10.84	8.45	6.79	4.95
9439.49	11.20	8.84	7.14	5.30
9492.38	10.84	8.60	6.99	5.26
9704.48	9.52	7.59	6.35	4.99
9798.55	9.04	7.23	6.04	4.66
9832.32	9.23	7.35	6.08	4.71
10126.59	9.43	7.64	6.40	5.07
10202.35	9.51	7.73	6.47	5.12
76 IRAS 10173-5844				
8402.31	10.01	9.06	8.02	6.73
8705.52	10.16	9.27	8.51	6.80
9060.45	10.11	9.20	8.52	6.87
9113.38	10.15	9.20	8.55	7.00
9170.23	10.47	9.50	8.85	7.20
9353.58	10.26	9.30	8.72	7.22
9439.50	10.37	9.44	8.84	7.30
9492.39	10.07	9.12	8.40	6.75
9705.48	10.23	9.26	8.58	6.88
9798.56	10.37	9.48	8.74	7.01
10202.35	10.16	9.22	8.53	6.90
77 IRAS 10174-5704				
8374.42	5.39	4.23	3.69	3.01
8402.32	5.33	4.20	3.66	2.98
8767.36	5.22	4.10	3.61	3.05
9061.45	5.38	4.27	3.74	3.12
9316.61	5.34	4.24	3.71	2.97
9371.62	5.32	4.22	3.72	3.04
9490.38	5.23	4.07	3.53	2.84
9704.49	5.29	4.15	3.62	2.95
9798.60	5.22	4.08	3.55	2.88
9832.34	5.23	4.07	3.53	2.91
9886.24	5.27	4.11	3.59	2.91
9909.22	5.33	4.14	3.65	2.92
78 IRAS 10175-5957				
8402.33	8.43	6.75	5.75	4.98
9061.47	8.12	6.49	5.58	4.79
9318.58	8.26	6.57	5.63	4.82
9375.49	8.20	6.53	5.61	4.83
9440.32	8.20	6.52	5.60	4.82
9490.39	8.22	6.54	5.62	4.82
9704.50	8.50	6.78	5.78	4.93
9832.34	8.36	6.70	5.70	4.91
9886.24	8.29	6.64	5.68	4.88
9905.22	8.32	6.67	5.70	4.91
79 IRAS 10176-5802				
8404.34	4.82	3.36	2.71	2.05
9004.46	4.63	3.20	2.59	1.93
9061.47	4.73	3.29	2.66	2.00
9143.34	4.85	3.41	2.77	2.10
9318.59	4.67	3.26	2.69	2.03
9375.50	4.66	3.26	2.69	2.05
9440.32	4.64	3.22	2.65	2.01
9492.41	4.60	3.17	2.58	1.94
9704.52	4.66	3.20	2.59	1.93
9832.35	4.89	3.42	2.77	2.11
9886.23	4.87	3.43	2.80	2.10
80 IRAS 10194-5816				
9004.47	7.58	5.70	4.91	4.20
8440.30	7.29	5.44	4.68	4.00
8817.20	7.44	5.53	4.79	4.07
9061.48	7.47	5.61	4.85	4.18
9145.32	7.31	5.45	4.71	4.09
9352.56	7.40	5.56	4.79	4.13
9375.50	7.36	5.51	4.77	4.10
9490.40	7.31	5.44	4.67	4.01
9704.52	7.40	5.54	4.81	4.13
9832.36	7.34	5.45	4.69	4.03
9905.32	7.47	5.57	4.78	4.12
81 IRAS 10196-5718				
8440.32	14.39:	10.75	8.30	5.88
8702.36	14.02:	10.38	8.04	
9060.46	13.39:	9.71	7.48	5.28
9113.39	13.25:	9.76	7.53	5.32
9170.25	13.57:	10.05	7.77	5.50
9352.57	14.07:	10.57	8.19	5.81
9439.51	13.60:	10.08	7.86	5.65
9492.42	12.86:	9.55	7.43	5.31
9704.53	13.86:	10.28	8.01	5.66
9831.46	14.23:	10.85	8.50	6.02
82 IRAS 10198-5853				
8700.25	10.02	8.27	7.33	6.52
8767.37	9.72	8.10	7.21	6.35
9060.48	9.82	8.15	7.26	6.49
9113.39	10.25	8.51	7.52	6.65
9170.27	10.04	8.43	7.45	6.53
9356.43	9.23	7.67	6.88	6.03
9439.53	9.42	7.84	7.02	6.29
9831.33	9.09	7.51	6.72	
9832.41	9.09	7.49	6.68	5.93
9909.30	9.48	7.92	7.08	6.28
83 IRAS 10199-5801				
8700.26	10.46	7.39	5.32	2.84
8767.38	11.09	7.85	5.71	3.20
9060.49	12.59:	8.94	6.53	3.75
9112.47	12.40:	8.94	6.52	3.73
9148.28	12.92:	9.11	6.66	3.87
9353.30	10.89	7.66	5.46	2.86
9439.52	11.30	7.97	5.74	3.18
9493.35	11.92	8.47	6.17	3.53
9493.37	11.56	8.43	6.16	3.50
9530.21	11.92	8.79	6.48	3.79
9704.54	11.96	9.00	6.63	3.85
9832.37	11.99	9.03	6.64	3.89

Table 3.2 Near-Infrared Observations *continued*

Date	J	H	K	L
84 IRAS 10207-5815				
8700.30	8.86	7.02	6.11	5.32
8817.23	9.70	7.71	6.64	5.76
9060.50	8.63	6.81	5.95	5.20
9117.37	8.94	7.08	6.16	5.45
9170.28	9.48	7.61	6.60	5.79
9354.42	9.35	7.61	6.63	5.66
9434.58	8.73	6.92	6.06	5.30
9493.39	8.99	7.10	6.17	5.44
9704.55	9.39	7.52	6.48	5.50
9831.47	8.65	6.81	5.93	5.10
9886.22	8.70	6.84	5.95	5.16
85 IRAS 10216-5813				
8700.39	9.85	8.01	6.99	6.09
8768.19	9.66	7.89	6.95	5.99
9060.51	9.75	7.91	6.93	6.06
9115.24	9.88	8.01	7.01	6.10
9170.30	9.66	7.93	6.96	6.01
9354.44	9.01	7.22	6.38	5.66
9434.58	9.47	7.61	6.66	5.90
9493.20	10.17	8.22	7.14	6.24
9704.56	9.35	7.62	6.76	5.85
9831.48	9.26	7.40	6.50	5.76
86 IRAS 10220-5858				
8700.43	8.11	6.30	5.21	4.13
9060.51	8.57	6.66	5.42	4.30
9147.38	8.45	6.61	5.40	4.28
9316.57	8.20	6.35	5.20	4.04
9355.61	8.37	6.48	5.27	4.08
9434.59	8.73	6.75	5.45	4.17
9493.21	8.98	6.94	5.59	4.32
9704.57	8.49	6.61	5.44	4.20
9831.49	8.05	6.25	5.13	4.00
9903.27	8.30	6.43	5.23	4.05
9905.23	8.33	6.41	5.20	3.99
87 IRAS 10222-5700				
8398.35	14.01:	10.13	7.72	5.40
8705.54		11.40	8.75	6.15
9060.52		10.98	8.37	5.80
9115.25		11.36	8.70	6.09
9147.39		11.51	8.83	6.17
9354.60		10.48	8.01	5.52
9434.60		10.17	7.71	5.33
9493.22		10.23	7.82	5.40
9704.58		11.20	8.65	6.03
9831.50		10.68	8.16	5.65
88 IRAS 10225-5925				
8398.37	8.88	7.55	6.78	5.95
8817.25	8.08	6.70	6.07	5.45
9060.53	8.06	6.66	6.08	5.45
9117.38	8.12	6.72	6.11	5.54
9170.31	8.52	7.17	6.47	5.88
9354.46	7.96	6.58	5.98	5.39
9439.54	8.57	7.28	6.56	5.89
9493.23	8.81	7.45	6.69	5.99
9705.49	8.62	7.28	6.55	5.83
9831.52	8.44	7.14	6.45	5.64
89 IRAS 10229-5705				
8403.36	10.40	7.64	6.00	4.30
8705.55	11.15	8.23	6.32	4.58
9060.53	10.69	7.84	6.11	4.45
9115.26	11.10	8.21	6.35	4.66
9148.37	11.16	8.25	6.38	4.70
9354.47	10.45	7.71	6.01	4.41
9439.55	10.20	7.47	5.83	4.29
9493.26	10.28	7.54	5.87	4.33
9705.50	10.41	7.68	6.03	4.48
9831.52	10.05	7.45	5.95	4.47
90 IRAS 10230-5744				
9005.55	8.02	6.67	6.18	
8700.50	7.51	6.22	5.72	5.20
9061.50	7.63	6.38	5.79	5.25
9117.39	7.98	6.72	6.05	5.38
9170.33	7.89	6.63	6.02	5.34
9354.47	7.81	6.54	5.92	5.32
9439.56	7.79	6.53	5.97	5.34
9494.27	7.58	6.26	5.76	5.22
9705.51	7.89	6.66	6.09	5.45
9831.53	7.41	6.14	5.59	5.12
9886.20	7.90	6.64	6.03	5.50
10142.53	7.69	6.43	5.84	5.32
10199.50	7.81	6.56	5.94	5.34
91 IRAS 10231-5823				
8700.47	12.65:	9.75	7.51	4.93
8768.21	12.99:	10.03	7.76	5.10
9060.55	11.54	8.63	6.47	3.95
9115.27	11.73	8.83	6.64	4.11
9170.34	12.14:	9.20	6.97	4.36
9354.49	13.24:	10.15	7.80	5.07
9439.57	12.60:	9.66	7.38	4.73
9494.28	12.04:	9.16	6.94	4.40
9705.51	11.78	8.86	6.68	4.14
9832.21	13.43:	10.30	7.90	5.16
92 IRAS 10234-5820				
8700.48	9.27	7.07	5.99	5.11
8768.22	9.09	6.94	5.92	5.03
9060.56	9.23	7.08	6.03	5.12
9117.40	9.41	7.20	6.07	5.17
9171.21	9.26	7.09	5.99	5.09
9354.49	9.65	7.41	6.25	5.26
9440.33	9.36	7.16	6.10	5.20
9490.41	9.30	7.10	6.04	5.16
9705.53	9.24	7.04	5.97	5.03
9832.38	9.45	7.22	6.07	5.13
93 IRAS 10238-5852				
8701.28	8.64	7.20	6.39	5.54
9061.51	9.25	7.75	6.85	5.96
9117.41	8.89	7.51	6.71	5.87
9171.22	8.32	7.01	6.30	5.53
9005.57	9.34	7.82	6.91	
8817.26	8.10	6.74	6.01	5.26
9355.61	9.52	7.82	6.85	6.05
9440.45	9.42	7.75	6.78	5.89
9495.40	8.96	7.48	6.58	5.69
9791.62	9.52	7.87	6.88	5.97
9832.48	9.25	7.65	6.73	5.87
9909.30	8.48	7.16	6.45	5.57
10142.55	9.41	7.77	6.84	6.05
10202.38	9.29	7.70	6.78	5.92
94 IRAS 10246-5844				
8701.31	10.53	8.55	7.19	5.69
8768.24	11.20	9.14	7.71	6.20
9060.57	9.96	8.04	6.75	5.36
9115.28	10.08	8.08	6.80	5.50
9148.38	10.26	8.22	6.94	5.66
9354.50	10.70	8.54	7.24	5.80
9440.34	9.87	7.94	6.73	5.38
9494.29	9.63	7.67	6.46	5.15
9705.54	10.88	8.59	7.17	5.91
9832.22	11.40	8.90	7.32	5.80
95 IRAS 10250-5904				
8400.37	11.05	8.84	7.25	5.66
8705.56	11.66	9.24	7.55	5.76
9061.24	10.77	8.47	6.93	5.22
9115.30	11.30	8.91	7.28	5.51
9171.25	11.79	9.36	7.66	5.82
9354.52	11.74	9.34	7.60	5.73
9440.37	10.97	8.66	7.06	5.32
9490.45	10.91	8.56	6.96	5.27
9705.54	11.82	9.41	7.67	5.87
9832.24	11.35	9.00	7.36	5.72

Table 3.2 Near-Infrared Observations *continued*

Date	J	H	K	L
96 **IRAS 10256-5836**				
8701.37	7.77	6.48	5.79	5.10
9061.52	8.54	7.18	6.32	5.47
9117.42	8.65	7.26	6.38	5.46
9171.28	8.39	7.09	6.28	5.29
9354.53	7.70	6.38	5.72	5.02
9440.38	8.19	6.78	6.03	5.34
9494.31	8.08	6.68	5.93	5.21
9705.56	7.30	5.96	5.32	4.63
9832.25	8.44	7.08	6.20	5.40
9886.19	8.59	7.22	6.37	5.47
10126.62	7.45	6.14	5.53	4.89
10202.39	7.94	6.62	5.91	5.26
97 **IRAS 10257-5854**				
8701.38	11.34	8.93	7.29	5.51
8768.27	11.64	9.13	7.41	5.54
9061.27	12.33:	9.68	7.80	5.80
9112.49	12.06:	9.49	7.65	5.70
9148.29	11.75	9.24	7.48	5.59
9354.54	12.90:	10.21	8.24	6.07
9440.39	12.73:	10.02	8.12	6.12
9494.32	12.77:	9.91	8.04	6.08
9705.56	12.39:	9.72	7.91	5.91
9832.26	13.30:	10.44	8.45	6.36
98 **IRAS 10261-5717**				
8702.25	11.06	8.81	7.68	6.72
8768.29	11.18	8.87	7.74	6.77
9115.31	10.97	8.76	7.67	6.79
9171.27	10.79	8.62	7.61	6.79
9354.55	10.80	8.62	7.57	6.65
9061.28	11.10	8.82	7.69	6.74
9440.40	10.82	8.61	7.56	6.68
9494.33	10.92	8.69	7.61	6.70
9832.39	11.02	8.76	7.70	6.83
10142.56	10.72	8.54	7.51	6.70
10202.40	10.78	8.61	7.57	6.67
10202.41	7.06	5.41	4.76	4.17
99 **IRAS 10262-5727**				
8702.26	9.13	7.05	6.05	5.18
8768.30	9.44	7.34	6.28	5.42
9061.29	9.17	7.12	6.10	5.11
9117.43	9.11	7.02	5.99	5.08
9171.29	9.24	7.12	6.08	5.13
9354.56	9.77	7.75	6.62	5.59
9440.41	9.68	7.67	6.60	5.55
9492.42	9.92	8.25	7.34	6.53
9832.29	9.80	7.72	6.57	5.59
100 **IRAS 10277-5836**				
8702.36	8.39	6.81	6.14	5.54
9061.32	8.58	6.94	6.25	5.68
9117.44	8.62	6.96	6.27	5.72
9171.34	8.62	6.95	6.26	5.70
9354.58	8.37	6.74	6.07	5.51
9440.42	8.37	6.75	6.09	5.53
9494.34	8.38	6.76	6.10	5.56
9832.40	8.56	6.89	6.16	5.61
101 **IRAS 10287-5733**				
8702.31	10.29	7.32	5.34	3.04
8768.25	9.78	6.95	5.10	2.88
9061.33	9.40	6.54	4.81	2.61
9115.33	9.45	6.57	4.83	2.65
9172.22	9.53	6.64	4.91	2.74
9354.59	9.89	7.00	5.25	3.06
9439.58	6.21	7.28	5.48	3.28
9492.44	10.41	7.41	5.60	3.39
9705.58	11.31	8.11	6.11	3.81
9831.54	11.77	8.41	6.32	3.93
10126.64	12.08:	8.58	6.30	3.74
10202.42	11.25	8.05	5.89	3.38

Only one observation is listed for IRAS10261-5717 because the correct star was only observed during the last run.

The *near*-infrared data are summarised in Table 3.3. The values shown are the averages of maximum and minimum magnitudes for each filter. It was found (see Appendix A) that this gives a result similar to the intensity means derived from Fourier fitting. Also tabulated are Spectral Classifications of the stars with the references of available published information

and the indicators '(O)' or '(C)' of classifications tentatively determined, respectively, for oxygen-rich or carbon-rich Miras (see Sections 2.5 & 3.3). (Where the Spectral Classifications are left blank, the stars are non-Miras and tentative classifications could not be made using techniques employed in the present study.)

Table 3.3 Mean J H K & L Magnitudes and Spectral Classes

Star	IRAS Name	G. Coord. $l, b(°)$	J	H	K	L	Spectral Class	Ref.
				(mag)				
1	09421–6223	283.1,–7.2	5.26	4.28	3.81	3.35	Me	1
2	09433–6233	283.1,–7.3	11.10	8.79	7.11	5.14	C	2
3	09509–6013	282.5,–4.9	12.71	10.46	8.72	6.72		-
4	09510–6247	284.2,–6.9	7.03	6.09	5.68	5.12	(O)	-
5	09519–6007	282.6,–4.7	4.99	3.74	3.13	2.61	M5e	3
6	09533–6021	282.9,–4.8	12.81	9.57	7.08	4.06	C	6
7	09568–6056	283.6,–5.0	10.46	8.65	7.37	6.34	(C)	-
8	09570–6051	283.5,–4.9	7.70	6.61	6.16	5.71	(O)	-
9	09571–5930	282.7,–3.8	8.54	7.13	6.37	5.60	(O)	-
10	09579–6203	284.4,–5.8	7.48	6.43	5.88	5.31		-
11	09581–5936	282.9,–3.8	9.86	8.31	7.28	6.20	(C)	-
12	09586–6150	284.3,–5.6	14.99	12.08	9.21	5.94	(C)	-
13	09595–6141	284.3,–5.4	8.25	7.27	6.86	6.35	(O)	-
14	09597–5927	282.9,–3.6	8.67	7.50	6.95	6.33	(O)	-
15	10001–5929	283.0,–3.6	7.78	6.59	5.97	5.37	(O)	-
16	10003–6207	284.6,–5.7	11.25	9.37	8.04	6.67	(C)	-
17	10004–6235	284.9,–6.1	5.14	4.19	3.77	3.32	Me	1
18	10008–6115	284.1,–5.0	8.32	7.30	6.62	6.04		-
19	10010–6025	283.7,–4.3	7.89	6.63	5.91	5.12	(O)	-
20	10015–6212	284.8,–5.7	10.75	9.17	7.78	6.28	(C)	-
21	10019–5946	283.4,–3.7	7.96	6.78	6.29	5.86	(O)	-
22	10021–5903	283.0,–3.1	11.11	8.63	7.04	5.29	(C)	-
23	10023–5946	283.4,–3.7	6.95	5.55	4.92	4.21	C	6
24	10026–5849	282.9,–2.9	10.25	7.79	6.09	4.26	(C)	-
25	10029–5856	283.0,–2.9	6.43	5.26	4.62	3.93	(O)	-
26	10033–5950	283.6,–3.6	7.31	5.74	4.89	4.04	M	3
27	10034–6207	284.9,–5.5	7.53	6.39	5.81	5.24	(O)	-
28	10038–6055	284.2,–4.5	7.25	5.95	5.40	4.86	Se	7
29	10040–6020	283.9,–4.0	13.28	10.12	7.73	4.98	(C)	-
30	10044–5803	282.6,–2.1	9.21	7.28	6.35	5.54		-
31	10045–5955	283.7,–3.6	7.15	5.72	5.13	4.55	Se	7
32	10048–5820	282.8,–2.3	10.39	8.40	7.17	6.00	(C)	-
33	10050–6001	283.8,–3.7	8.07	6.85	6.27	5.64	(O)	-
34	10051–5817	282.8,–2.2	10.41	8.03	6.45	4.81	(C)	-
35	10052–5906	283.3,–2.9	9.28	7.48	6.46	5.65	C	4
36	10053–6001	283.9,–3.6	8.61	7.39	6.76	6.13	(O)	-
37	10053–5852	283.2,–2.7	10.67	8.28	6.52	4.61	(O)	-
38	10056–6223	285.3,–5.5	8.56	7.59	7.20	6.69	(O)	-
39	10057–6018	284.1,–3.8	6.34	5.36	4.82	4.21	(O)	-
40	10062–5824	283.0,–2.3	7.94	6.56	5.72	4.79	(O)	-

Table 3.3 Mean *J H K & L* Mags. and Spec. Classes – *continued*

Star	IRAS Name	G. Coord. $l, b(°)$	J	H	K	L	Spectral Class	Ref.
				(mag)				
41	10064–5757	282.8,–1.9	13.11	10.25	8.16	5.79	(C)/G2	8
42	10071–5815	283.0,–2.1	9.41	7.32	6.30	5.38	(O)	-
43	10075–5747	282.8,–1.7	10.38	8.15	7.08	6.14	(C)	-
44	10076–5944	283.9,–3.2	7.55	6.31	5.65	5.01	(O)	-
45	10078–5742	282.8,–1.6	8.14	6.14	5.33	4.74	C	-
46	10079–5914	283.7,–2.8	10.38	8.82	8.04	6.98	(O)	-
47	10080–5902	283.6,–2.6	10.46	8.05	6.37	4.56	(C)	-
48	10090–5744	282.9,–1.5	8.95	6.93	6.09	5.44	(O)	-
49	10098–5742	283.0,–1.4	13.57	10.44	7.67	4.26	C	3
50	10102–5841	283.6,–2.2	9.37	7.41	6.44	5.66		-
51	10104–5832	283.5,–2.0	10.82	8.39	6.78	5.24	(C)	-
52	10107–5814	283.4,–1.8	8.87	6.96	6.19	5.34	(O)	-
53	10109–5958	284.4,–3.9	7.34	5.56	4.28	2.99	Ce	2
54	10110–5734	283.1,–1.2	6.56	5.39	4.84	4.27	(O)	-
55	10111–6102	285.0,–4.1	8.24	7.12	6.56	5.98	(O)	-
56	10113–6142	285.4,–4.1	8.09	7.05	6.56	6.04	(O)	-
57	10118–6038	284.9,–3.7	4.36	3.24	2.58	1.76	M5-8e	3
58	10121–5836	283.8,–2.0	4.16	3.18	2.69	2.11	M6e	3
59	10121–5846	283.9,–2.1	3.93	2.91	2.47	2.01	M8	3
60	10123–5753	283.4,–1.4	8.20	6.64	5.81	5.09	(O)	-
61	10136–5743	283.4,–1.1	8.46	6.47	5.25	3.58	C	4
62	10141–5837	284.0,–1.9	5.89	4.75	4.21	3.70	(O)	-
63	10145–5714	283.3,–0.7	13.92	9.82	7.45	5.28	(C)	-
64	10145–6046	285.2,–3.6	5.80	4.36	3.68	2.96	C	4
65	10146–5922	284.5,–2.5	8.97	7.39	6.68	6.04		-
66	10148–6039	285.2,–3.5	8.14	6.84	6.15	5.42	(O)	-
67	10150–5703	283.2,–0.5	8.53	6.99	6.20	5.39	(C)	-
68	10154–5828	284.1,–1.6	8.25	6.79	6.22	5.74	(O)	-
69	10157–5944	284.8,–2.7	10.10	8.57	7.71	6.73	(O)	-
70	10160–6041	285.3,–3.4	10.43	8.62	7.37	5.96	(C)	-
71	10161–5945	284.8,–2.7	7.98	6.44	5.50	4.47	(O)	-
72	10162–6010	285.1,–3.0	6.70	5.56	5.07	4.57	(O)	-
73	10163–6012	285.1,–3.0	5.88	4.67	4.17	3.71	(O)	-
74	10164–6005	285.0,–2.9	8.73	7.43	6.81	6.24	(O)	-
75	10168–6013	285.2,–3.0	10.12	8.03	6.59	4.98		-
76	10173–5844	284.4,–1.7	10.24	9.28	8.43	7.02		-
77	10174–5704	283.5,–0.3	5.30	4.17	3.64	2.98	M	3
78	10175–5957	285.1,–2.7	8.31	6.64	5.68	4.88	C	4
79	10176–5802	284.1,–1.1	4.74	3.30	2.69	2.02	M	3
80	10194–5816	284.4,–1.2	7.44	5.57	4.79	4.10		-

Table 3.3 Mean *J H K* & *L* Mags. and Spec. Classes – *continued*

Star	IRAS Name	G. Coord. $l, b(°)$	J	H	K	L	Spectral Class	Ref.
				(mag)				
81	10196–5718	283.9,–0.3	13.63	10.20	7.70	5.65	(C)	-
82	10198–5853	284.8,–1.7	9.67	8.00	7.10	6.29	(O)	-
83	10199–5801	284.3,–0.9	11.69	8.25	5.99	3.37	C	3
84	10207–5815	284.5,–1.1	9.17	7.26	6.29	5.45	(O)	-
85	10216–5813	284.6,–1.0	9.59	7.72	6.76	5.95	(C)	-
86	10220–5858	285.0,–1.5	8.51	6.59	5.36	4.16	(C)	-
87	10222–5700	284.0,+1.0	-	10.82	8.27	5.75		-
88	10225–5925	285.3,–1.9	8.42	7.07	6.38	5.70	(O)	-
89	10229–5705	284.1,+0.1	10.60	7.85	6.11	4.49	(C)	-
90	10230–5744	284.5,–0.5	7.72	6.43	5.89	5.31	B7	8
91	10231–5823	284.9,–1.0	12.49	9.47	7.18	4.56	C	3
92	10234–5820	284.9,–1.0	9.37	7.18	6.08	5.15	(C)	-
93	10238–5852	285.2,–1.4	8.81	7.31	6.46	5.66	(O)	-
94	10246–5844	285.2,–1.2	10.51	8.40	7.08	5.67	(O)	-
95	10250–5904	285.4,–1.5	11.30	8.94	7.30	5.55	(C)	-
96	10256–5836	285.2,–1.0	7.98	6.61	5.85	5.05	(O)	-
97	10257–5854	285.4,–1.3	12.32	9.69	7.87	5.94	(C)	-
98	10261–5717	284.6,+0.1	9.12	7.14	6.25	5.50		-
99	10262–5727	284.7,–0.0	9.46	7.38	6.31	5.33	(C)	-
100	10277–5836	285.5,–0.9	8.49	6.85	6.17	5.62		-
101	10287–5733	285.1,+0.1	9.14	7.56	5.57	3.27	M	5

1. Bidelman and MacConnel (1982)

2. Guglielmo *et al.* (1993)

3. Olnon *et al.* (1986)

4. Stephenson (1973)

5. te Lintel Hekkert *et al.* (1991)

6. Stephenson (1989)

7. Stephenson (1984)

8. *IRAS* Science Team (1988)

3.1 Pulsation

Periods (P) were determined from periodograms generated using a Multi-variable Least-squares Analysis program (see Section 2.4) on the K light curves with at least 8 observations. The results including half peak-to-peak amplitudes (ΔJ, ΔK) of the best-fitting sine curve to the J & K data are given in Table 3.4. It should be noted that unlike in the general astronomical literature, the values of amplitudes listed and plotted in this chapter of 'results' are all **halves** of the **peak-to-peak** amplitudes. Periods (P_1) from the GCVS and other sources are also listed where available. In addition, preliminary periods (P_2) from an on-going I-plate study by Dr. S. Hughes (RGO) are listed. The differences between P and P_1 are below 3 percent, and may be due to limited data in the respective studies, or unrepeatability of particular light curves' cycles. Thirteen or just less than 14% of the stars presented in this paper had previously published periods in the GCVS or other literature, and the P_2 are presented to provide independently determined periods for comparison with the P. The P and P_2 periods vary by as much as 10% and in some cases integer and half-integer multiples of P, indicating different period determination due to aliasing in I-plate work and other reasons that will be explained in reports of on-going collaborative studies of Mira light curves that have been obtained from I-plate Mira searches by Dr. S. Hughes (RGO) and the near-infrared observations of the same stars that are being obtained by Dr. P. Whitelock and collaborators at the SAAO. The light-curve shapes marked with an asterisk in Table 3.4

indicate phased curves with very low amplitudes. In the same table, those periods and amplitudes marked with a colon can be regarded as uncertain. Where the amplitudes are not well determined, the relevant turning points and thus the mean magnitudes and colours are also determined with limited certainty.

Table 3.4 Periods, Half-amplitudes and **K** Light Curve Classification

Star	IRAS Name	Period (days)			Amplitude		**K** Light Curves	
		P	P_1	P_2	$\Delta J/2$	$\Delta K/2$	Quality	Shape
1	09421-6223	303	313		0.37	0.30	good	symm.
2	09433-6233	567		533	0.69	0.61	good	asymm.
3	09509-6013	614:					poor	irreg.
4	09510-6247	246	244	245	0.34	0.27	good	symm.
5	09519-6007	174		72	0.20	0.14	good	asymm.
6	09533-6021	716			1.01	0.86	good	symm.
7	09568-6056	288		280	0.64	0.37	good	symm.
8	09570-6051	284		294	0.11:	0.12:	fair	irreg.*
9	09571-5930	497		443	0.54	0.36	good	symm.
10	09579-6203	464:		528:			poor	irreg.
11	09581-5936	390		630:	0.56:	0.35:	fair	irreg.
12	09586-6150	510			0.93	0.87	good	symm.
13	09595-6141	177		176	0.18	0.14	good	asymm.
14	09597-5927	194			0.27	0.21	good	asymm.
15	10001-5929	349		170:	0.49:	0.39:	fair	irreg.
16	10003-6207	399		788:	0.59:	0.35:	fair	irreg.
17	10004-6235	294	305	303	0.26	0.27	fair	symm.
18	10008-6115	420:		423:	0.23:	0.37:	poor	irreg.
19	10010-6025	398		405	0.62:	0.45:	fair	asymm.
20	10015-6212	193		1540:	0.29	0.15	good	asymm.
21	10019-5946	278		299	0.17	0.16	fair	asymm.
22	10021-5903	536			0.53:	0.42:	fair	irreg.
23	10023-5946	581			0.16:	0.09:	fair	asymm.*
24	10026-5849	519			0.47:	0.29:	fair	irreg.
25	10029-5856	383		383	0.45:	0.36:	fair	asymm.
26	10033-5950			202:			poor	
27	10034-6207	340		313	0.37:	0.26:	fair	symm.
28	10038-6055	379		391		0.33:	fair	asymm.
29	10040-6020	565			0.91	0.82	good	symm.
30	10044-5803	402:		423:	0.58:	0.39:	poor	irreg.
31	10045-5955	394		405	0.57:	0.38:	fair	asymm.
32	10048-5820	532		539	0.60	0.43	good	asymm.
33	10050-6001	391		407	0.66	0.54	good	symm.
34	10051-5817	450		1492:	0.84:	0.51:	fair	asymm.
35	10052-5906	445			0.30:	0.11:	fair	asymm.*
36	10053-6001	434	427		0.56:	0.38:	fair	irreg.
37	10053-5852	552		1556:	0.65	0.44	good	symm.
38	10056-6223	468			0.16	0.14	fair	asymm.
39	10057-6018	347		175:	0.45:	0.36:	good	symm.
40	10062-5824	199:		383	0.41:	.23:	fair	asymm.

Table 3.4 Periods, Half-amplitudes and **K** Light ... – *continued*

Star	IRAS	Period (days)			Amplitude		Light Curves	
	Name	P	P_1	P_2	$\Delta J/2$	$\Delta K/2$	Quality	Shape
41	10064-5757	566			0.48:	0.43:	fair	irreg.
42	10071-5815	195:				0.1:	poor	irreg.
43	10075-5747	394			0.30:	0.22:	fair	asymm.
44	10076-5944	408		409	0.67	0.47	good	asymm.
45	10078-5742	128					poor	irreg.
46	10079-5914	589		554	0.71	0.45	good	asymm.
47	10080-5902	516		501	0.74	0.55	good	symm.
48	10090-5744	288	288	808:	0.12:	0.08:	fair	asymm.*
49	10098-5742	533			0.65	0.54	good	symm.
50	10102-5841						poor	
51	10104-5832	468		459	0.52:	0.34:	fair	asymm.
52	10107-5814	388		398	0.58:	0.49:	fair	asymm.
53	10109-5958	210			0.47	0.29	good	asymm.
54	10110-5734	281			0.33	0.29	good	asymm.
55	10111-6102	399		387	0.46	0.35	good	asymm.
56	10113-6142	244		257	0.30	0.26	good	asymm.
57	10118-6038	566	575.6		0.80	0.52	good	symm.
58	10121-5836	397	384	407	0.33	0.31	good	asymm.
59	10121-5846	444:	453		0.29	0.18	fair	irreg.
60	10123-5753	350:		173			fair	
61	10136-5743	173			0.23	0.11	fair	asymm.
62	10141-5837	408	407.6	403	0.48	0.36	good	asymm.
63	10145-5714	441				0.42	fair	irreg.
64	10145-6046						poor	
65	10146-5922	158:	-	274:			poor	irreg.
66	10148-6039	414		417	0.60	0.44	good	
67	10150-5703	296			0.36:	0.23:	fair	irreg.
68	10154-5828	360					fair	
69	10157-5944	453		467	0.79	0.52	good	asymm.
70	10160-6041	468		444	0.67	0.48	good	symm.
71	10161-5945	447		445			fair	
72	10162-6010	353			0.35:	0.27:	fair	irreg.
73	10163-6012	528	550	537	0.12:	0.09:	fair	asymm.*
74	10164-6005	367			0.43:	0.35:	fair	asymm.
75	10168-6013			1478:			poor	
76	10173-5844						poor	
77	10174-5704	322			0.07:	0.09:	fair	symm*
78	10175-5957	100			0.14:	0.08:	fair	symm*
79	10176-5802	234:		117			good	asymm
80	10194-5816	116:			0.18:	0.17:	poor	irreg

Table 3.4 Periods, Half-amplitudes and **K** Light ... – *continued*

Star	IRAS Name	Period (days) P	P_1	P_2	Amplitude $\Delta J/2$	$\Delta K/2$	Light Curves Quality	Shape
81	10196-5718	481			0.60:	0.51:	fair	asymm.
82	10198-5853	464		425	0.50	0.34	good	asymm.
83	10199-5801	668					fair	asymm.
84	10207-5815	393		401	0.54:	0.39:	fair	irreg.
85	10216-5813	445		385	0.38:	0.28:	fair	irreg.
86	10220-5858	610			0.45	0.23	good	asymm.
87	10222-5700	513			0.65	0.54	good	symm.
88	10225-5925	271		269	0.42	0.37	good	symm.
89	10229-5705	459			0.49	0.23	fair	asymm.
90	10230-5744	269:		265:			poor	irreg.
91	10231-5823	548			0.88	0.55	good	symm.
92	10234-5820	102	103		0.16	0.11	good	asymm.
93	10238-5852	396			0.65:	0.37:	fair	asymm.
94	10246-5844	500			0.77	0.47	good	asymm.
95	10250-5904	495			0.54	0.40	good	asymm.
96	10256-5836	379		397	0.41:	0.27:	fair	irreg.
97	10257-5854	438			0.77	0.48	good	symm.
98	10261-5717						poor	
99	10262-5727	448	430		0.46	0.37	good	asymm.
100	10277-5836	581:		349:			poor	
101	10287-5733	1760	1584		1.45	0.78	good	

Figure 3.1 shows K light curves as a function of phase, illustrating, among other things, that the accuracies in period, and thus also amplitude, vary from star to star depending on the number of observations, the repeatability of the cycles, and the shape of the light curves. (The periodograms used in the period detection were generated assuming a sinusoidal light curve, and the periods thus derived were then corrected for possible off-set deviations – a method with a small, though undeniable error margin. [In doing the correction, phased light curves were plotted at periods slightly different from the one detected and the period that produced the best phased light curve was selected.])

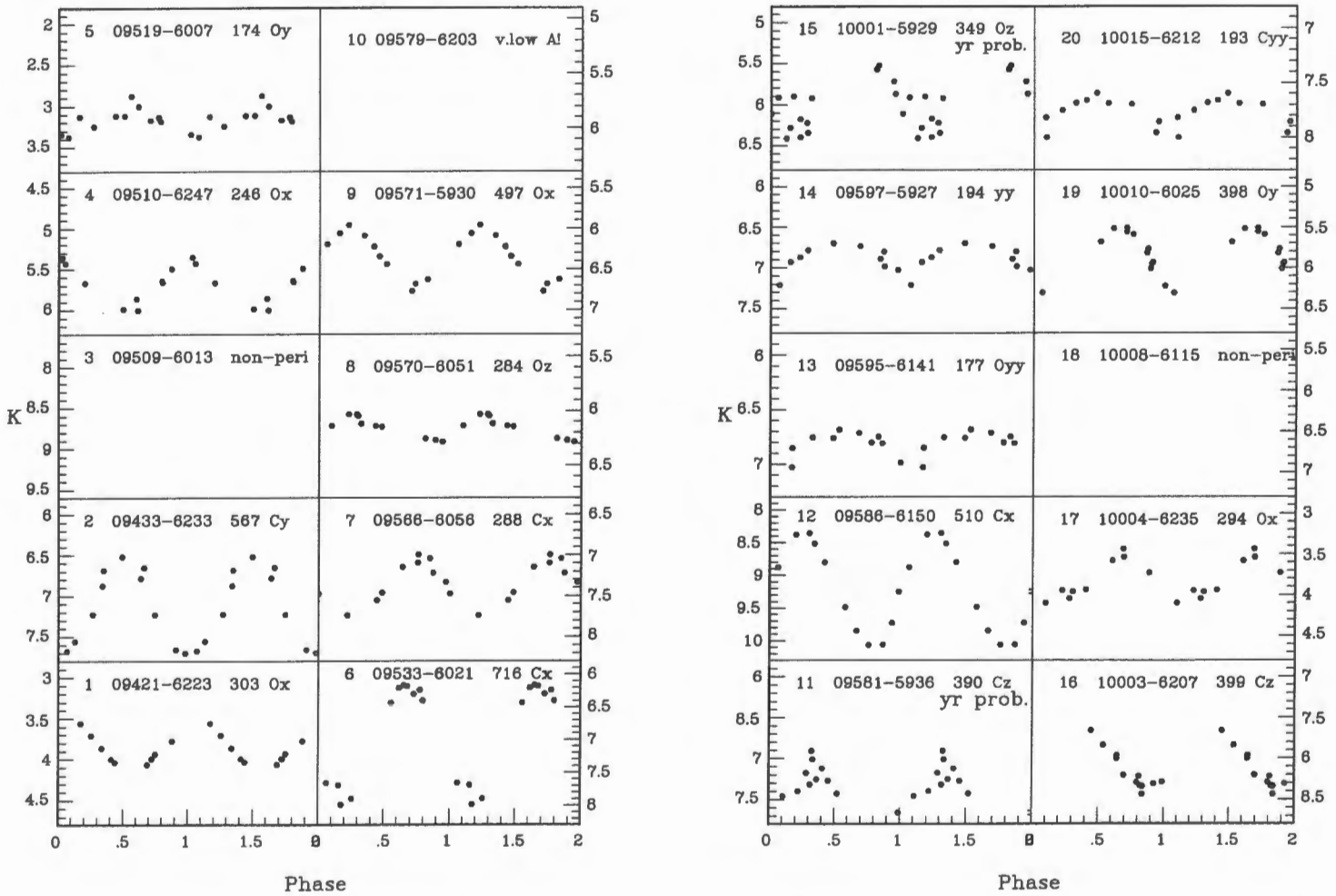

Figure 3.1: K light curves for the LPVs. Note that each point is plotted twice and the choice of zero phase is arbitrary. The *IRAS* name, period (P) and classifications by O/C richness and light curve shape are given for each object. The colon, asterisk, and double -asterisk indicate uncertain K-curve P, P from the literature, and P from the I-plate study.

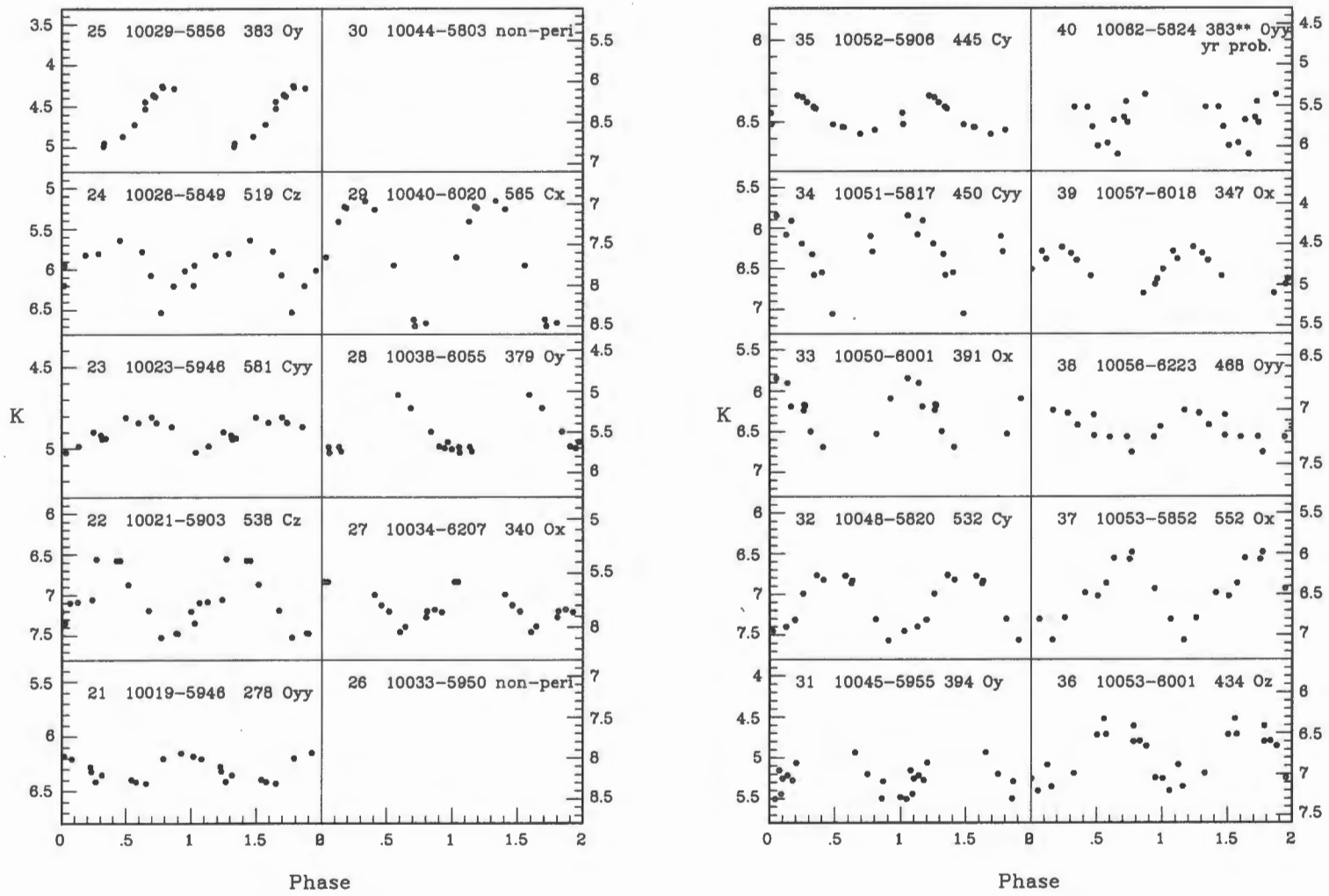

Figure 3.1 *K* Light Curves ... – *continued*

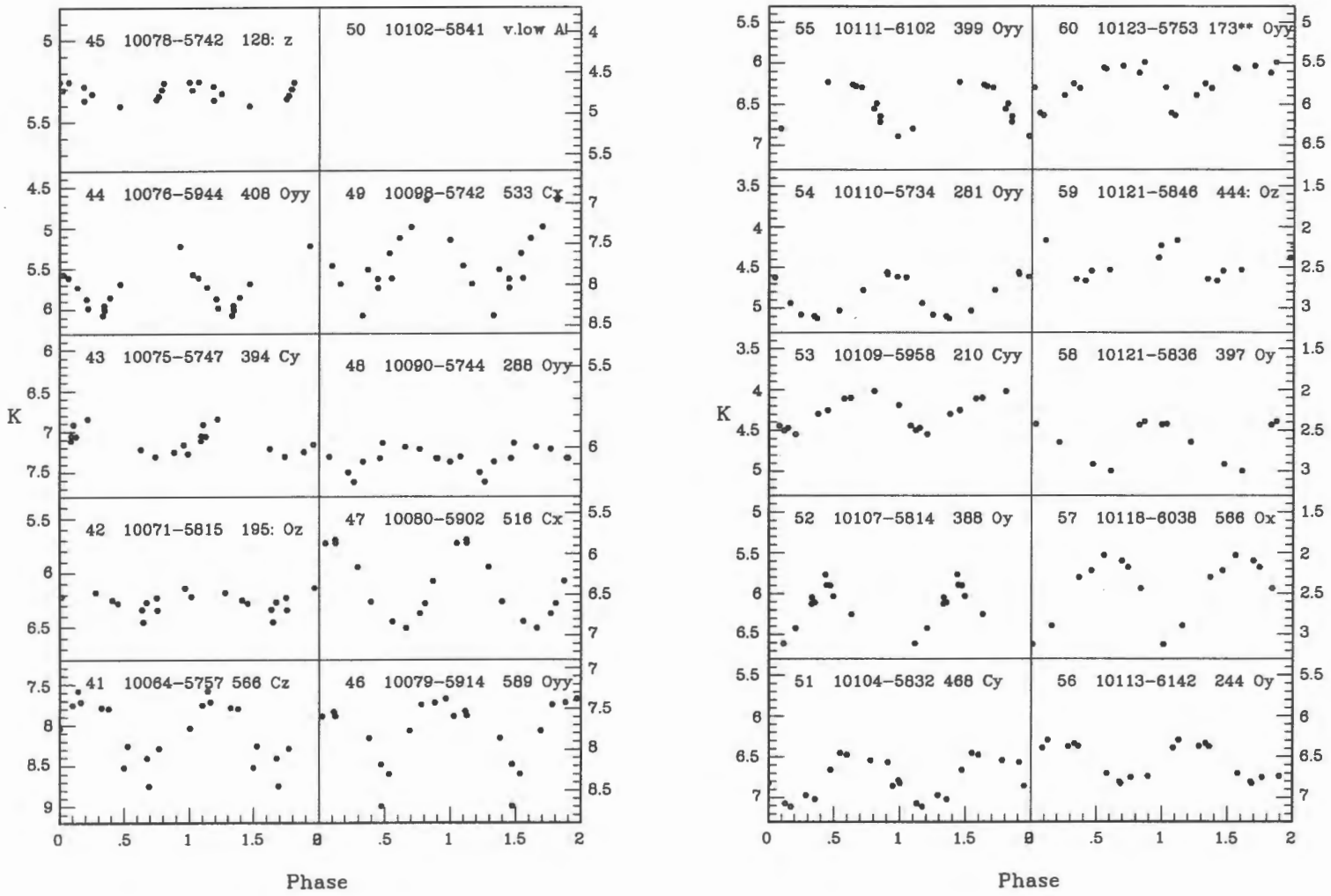

Figure 3.1 *K* Light Curves ... – *continued*

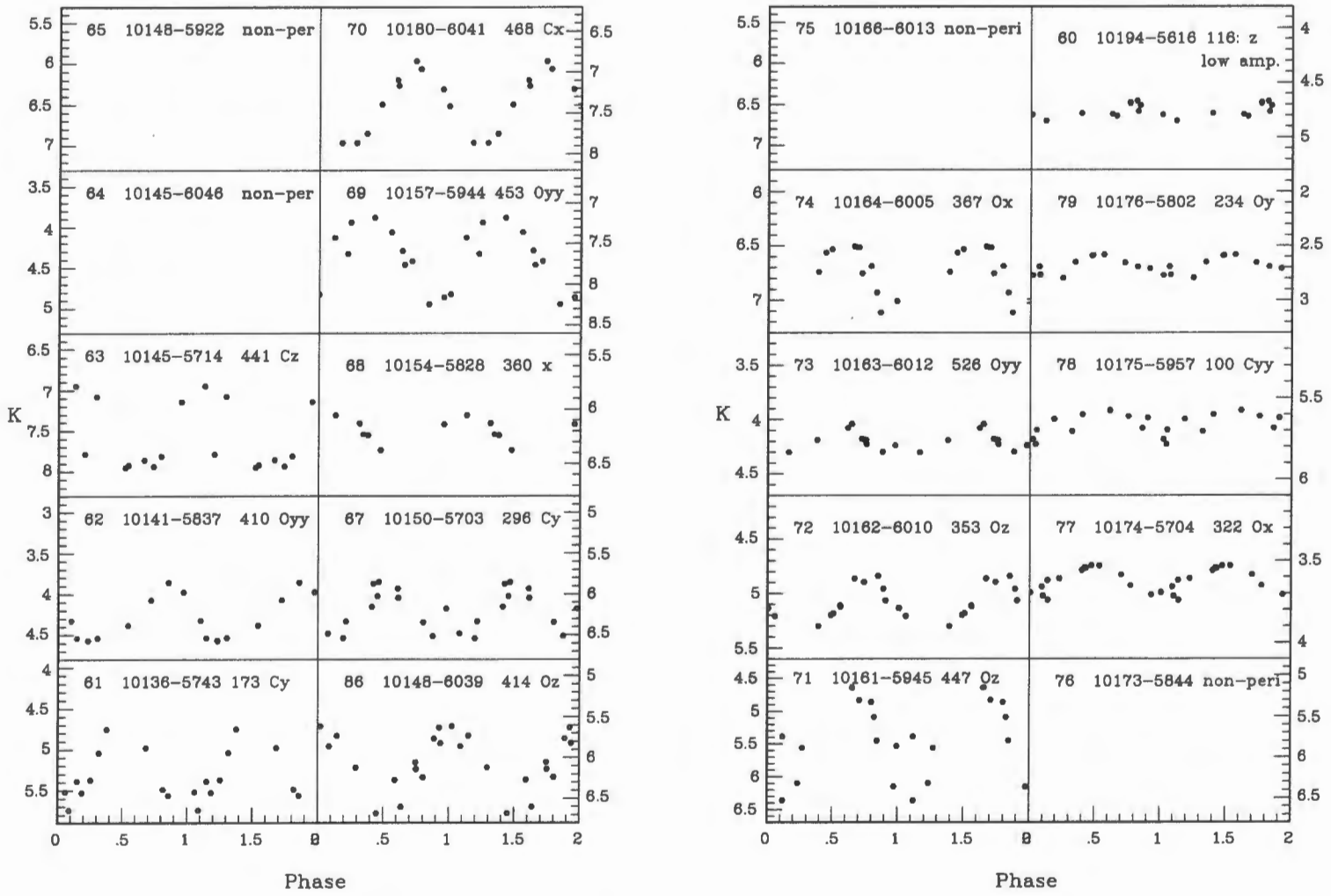

Figure 3.1 *K* Light Curves . . . – *continued*

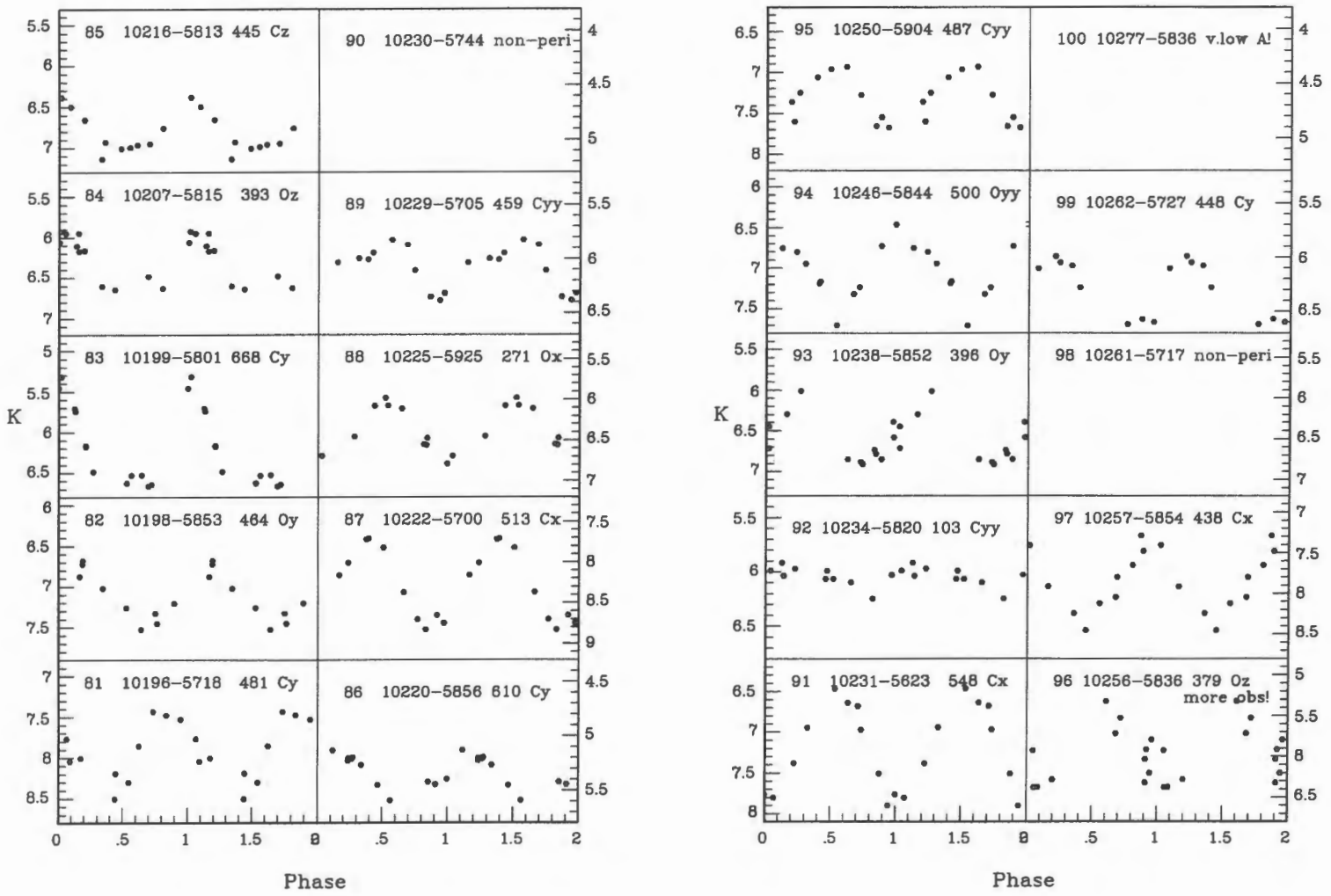

Figure 3.1 *K* Light Curves . . . – *continued*

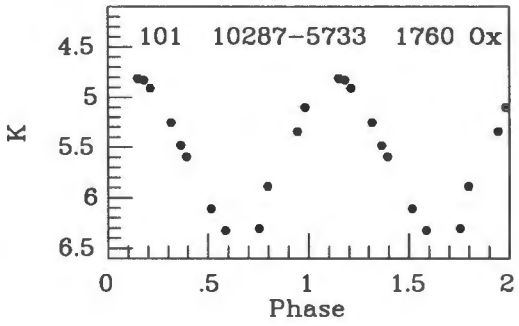

Figure 3.1 K Light Curves ... – *continued*

Each phased light curve was classified for **quality** and **shape** as listed in Table 3.4. The categories for **quality** were *good, fair* and *poor* and were derived subjectively according to phase coverage and scatter. In general the phased light curves classified *good* had well determined periods and amplitudes, the *fair* had well determined periods but not necessarily amplitudes, and the *poor* had neither well determined periods nor amplitudes. The curves in the *poor* category were of objects that were either non-periodic or else periodic, but for which no good data were obtained. The categories for **shape** were *symmetric* (symm. in Table 3.4 and **x** in Fig 3.1), *asymmetric* (asymm. and **y**) and *irregular* (irreg. and **z**) and were determined, also subjectively, according to the symmetry of the curve about its rise and fall. The *asymmetric* category was further divided into **y** and **yy** for curves were the rise was steeper than the fall and for the curves were the fall was steeper than the rise, respectively, as indicated in Figure 3.1.

New periods were determined for 82 stars of the 101 whose K light curves were obtained and analysed. This includes 13 stars which already had

published periods. For the two objects IRAS10062–5824 and IRAS10123–5753, periods (P_2) from the I-plate study were adopted as they produced very good K phased light curves. There is therefore a total of 84 (82 + 2) new periods available from this study. Of the 84, 42 have K phased light curves that are regarded as *good* and 42 as *fair* . No clear periodicity could be determined for 17 objects and their phased light curves were given the quality-class *poor* .

The new periods (P) are accurate to ±15 days for periods less than 550 days and to ±25 days for longer periods or those given in brackets. Periods around 365 days present a particular problem; although the periods are accurate to ±15 days, their amplitudes are not well determined.

3.1.1 Amplitude Variability

Figure 3.2 (a) shows the half peak-to-peak K amplitude (as listed in Table 3.4) versus period of the Mira variables. Amplitudes of Miras in the solar neighbourhood are known to increase with period, and this is clearly shown in the figure. An estimated fit marking the proportional increase is drawn for the Miras with well determined amplitudes (solid circles). About half of the Miras with amplitudes thought to be uncertain (open circles) are grouped around ($\Delta K/2$,Per) = (0.35 mag,400d) and fall on the fit in Figure 3.2 (a). These stars have periods close to a year and the fact that their periods and amplitudes have been classified as uncertain is caused by incomplete phase coverage due to the spacing of the observations. Most of the other stars with uncertain amplitudes and that do not lie on the fit, have

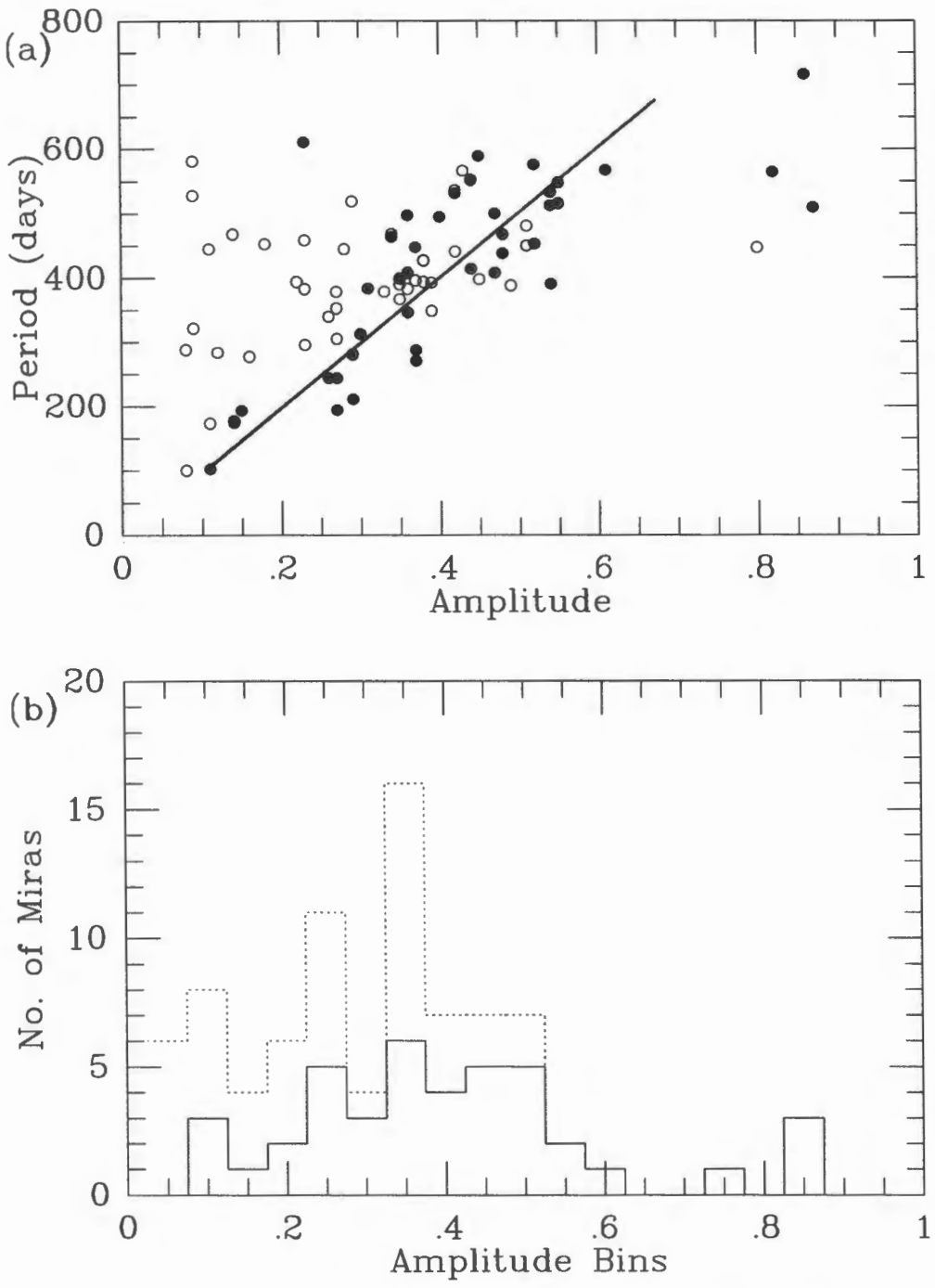

Figure 3.2: The plot of the half peak-to-peak K amplitude versus period and histograms of the half-amplitude distributions. In (a) the solid and open circles, respectively, represent variable stars with light curves of *good* (well determined amplitudes) and *fair* (uncertain amplitudes) qualities. In (b) the solid and dotted lines, respectively, represent stars with the *good* and *fair* light curves.

K half-amplitudes less than 0.3. It is interesting that they are not on the fit since other workers in this field would not classify variable stars with K half-amplitudes less than 0.3 as Miras; but, before drawing conclusion about their position in this diagram, it must be noted that their amplitudes have been determined with limited certainty. All said, it must be pointed out that the increase of amplitude with period is clearly exhibited (the marked sequence in Figure 3.2 (a)) for Miras with well determined periods and amplitudes in the presently studied sample.

The distribution of the half-amplitudes at K in 0.05 mag intervals is shown in Figure 3.2 (b). Miras with well determined amplitudes (solid-line histogram) have a mean half-amplitude of 0.4 mag and their largest half-amplitude is 0.85 mag. The stars with uncertain half-amplitudes peak at 0.35 mag (for reasons explained in the above paragraph). The half-amplitude distributions of oxygen-rich and carbon-rich Miras are plotted in subsequent sections and provide interesting comparisons.

3.1.2 *IRAS* Variability Index

The 'variability index' (Var, listed in Table 3.1) is an estimate of the percentage probability that an *IRAS* source is a variable. Weinberg *et al.* (1992) assumed that sources with $Var = 90$ were Miras and thus used the 'variability index' for selecting Miras from the *IRAS* catalogue. Whitelock *et al.* (1994 & 1995) showed that selecting *IRAS* sources with Var=90 was an effective way of selecting Mira variables. In the present paper there are 15 sources with $Var = 90$, and 12 of them are Miras. There were also 6 sources

with $Var = 80$ and 2 with $Var = 70$ which were all found to be Miras. The three sources classified as non-Mira here with $Var = 90$ are IRAS10033–5950 (#26), IRAS10173–5844 (#76), and IRAS10230–5744 (#90). Object # 26 is a M giant with an oxygen-rich envelope (Olnon *et al.* 1986) and may need further near-infrared observation. Object # 90 was identified as a Mira in the on-going I-plate searches of Mira variables by Shaun Hughes (RGO) and also needs further near-infrared observations. Object # 76 is a $IRAS$ point source that has been eliminated from the discussion with other Mira variables because its near-infrared data was confused by its bright companion.

Consistent with the findings of Whitelock *et al.* (1994 & 1995) and others, it is clear that $Var = 90$ is a clear way of selecting Miras from $IRAS$ sources. Though there is not enough evidence, there are indications in the present paper that $Var = 80$ and even 70 may also be an efficient way of selecting Miras. The reverse is not true; for instance, 45 of the Miras in this paper had Var between 0 and 70, and another 20 had no Var values listed. As Whitelock *et al.* (1994) noted, there is no characteristic difference between Miras of $Var = 90$ and the others, indicating that the difference is most probably a feature of the distribution of the $IRAS$ observations in time.

3.2 Infrared Colours

Figure 3.3 shows the near-infrared colours derived from the mean magni-

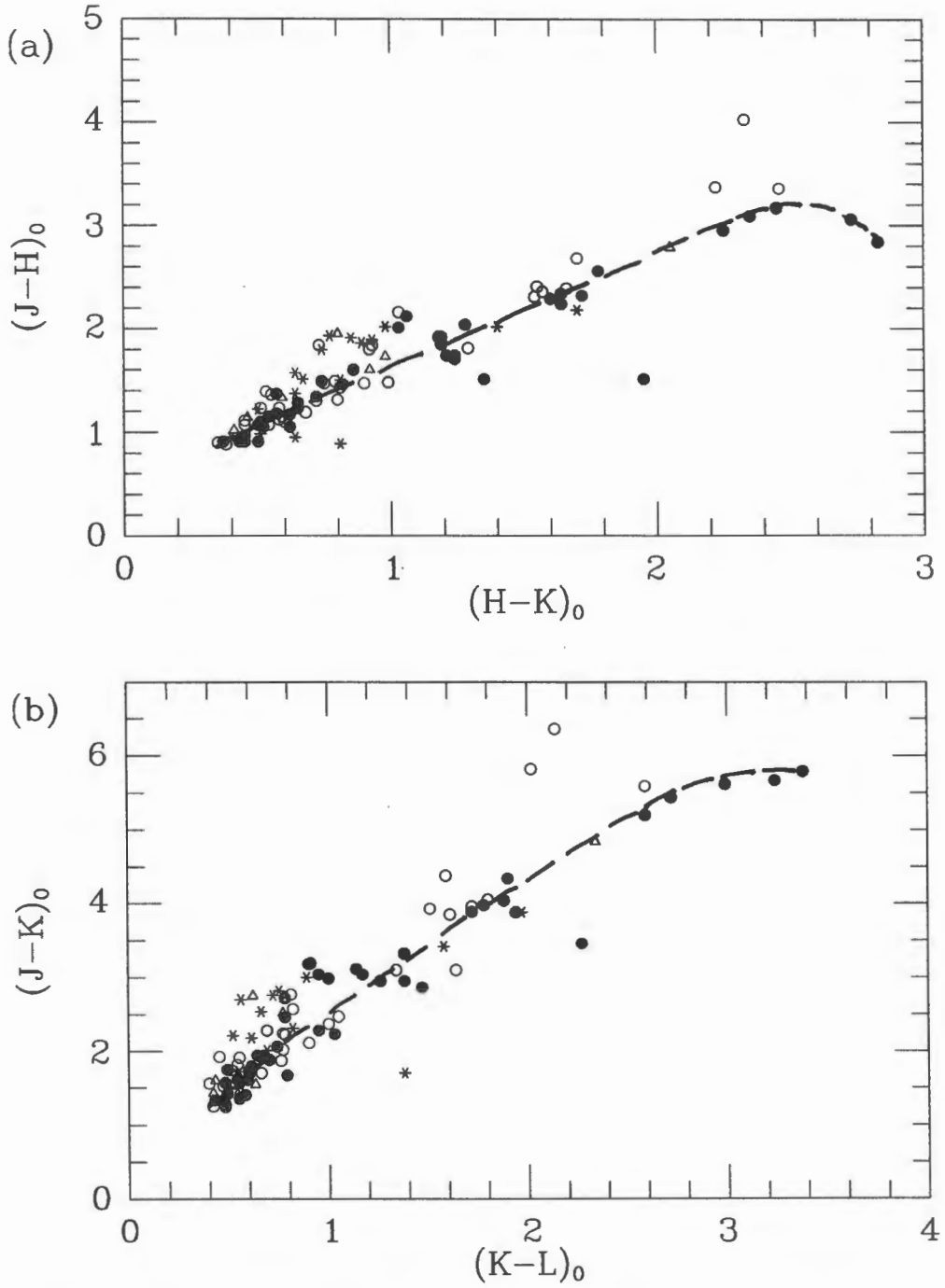

Figure 3.3: Reddening corrected near-infrared two-colour diagrams. The symbols signify the quality of K light curves that were derived for each star presented: solid circles are for *good* , open circles for *fair* , open triangles for *fair* with low amplitudes, and asterisks for *poor* curves.

tudes in Table 3.3. A well defined sequence is seen for the objects with *good* light curves (solid circles) and the dashed line is a mean fit by eye, with a mean scatter of 0.008 mag as measured perpendicular to the fit. The scatter is an indicator of the range of abundances for the very blue objects (Bessel *et al.* 1989). In Figure 3.3 (a), the $J - H$ and $H - K$ colour diagram, the sequence bends for the cool stars at the top. The *bending* is noted mindful of the fact that it is only defined by two stars in Figure 3.3, but that it is also manifested in similar diagrams of Carbon Miras by Whitelock (1996b). A group of stars with light curves other than *good* are bunched in a small area to the upper left of the sequence. The separation between this group and the sequence is not as clear as in the separation of Miras and non-Miras plotted in similar diagrams by Menzies and Whitelock (1985) or Whitelock *et al.* (1994, 1995). Preliminary assumptions in the present paper are that light curves classified as *good* and with half peak-to-peak K amplitudes over 0.2 mag (or >0.14 mag for stars with periods between 100 and 200 days) are Miras, those classified as *fair* are strong Mira candidates, and those with half-amplitudes under 0.14 mag or classified as *poor* are Semi-Regular long period variables.

Individual Stars Conspicuously off the Sequence: The object marked with a solid circle to the right of the sequence in Figure 3.3 (b) at $(J-K, K-L) = (3.46, 2.27)$ is the OH/IR Mira IRAS10287–5733 (# 101), with a period of 1584 days (Le Berte 1993). The colour of this object relative those of the other stars is peculiar because though it has a thick shell, its $J - K$

colour is bluer than those of other stars with the same $K - L$. The object marked with an asterisk to the right of the lower sequence at $(J-K, K-L)$ = (1.70, 1.38) is IRAS10173–5844 (# 76), an *IRAS* point source that has been eliminated from the discussion with other Mira variables because its near-infrared data was confused by its bright companion. The two objects marked with open circles in Figure 3.3 (a) are IRAS10145–6046 (# 63) at $(J-K, K-L)$ = (6.36,2.14) and IRAS10199–5801 (# 83) at $(J-K, K-L)$ = (5.59,2.59). The objects have periods of 441 and 668 days respectively. Their deviation from the sequence is not understood.

3.2.1 Fluxes from the Star and the Shell

Figure 3.4 is a two-colour plot showing $K - [12\mu m]$ against $[12\mu m] - [25\mu m]$. The *IRAS* magnitudes, $[12\mu m]$ and $[25\mu m]$ are calculated as described in Chapter 2 of the present paper and in the *IRAS Point Source Catalogue - Explanatory Supplement* (1988) after colour correcting the data. The K and $[12\mu m]$ fluxes originate, respectively, from the star and the shell, so $K - [12\mu m]$ provides a measure of the thickness of the shell and thus also the mass-loss rate. The larger is $K - [12\mu m]$, the thicker is the shell (Whitelock *et al.* 1994). The $[12\mu m]$–$[25\mu m]$ colour provides a measure of the temperature of the shell.

Figure 3.4 (a) presents the stars according to their classification by the quality of their K light curves, while Figure 3.4 (b) presents the stars according to their classifications as Mira or non-Mira. The two presentations are complementary and necessary in the following discussions. The positions

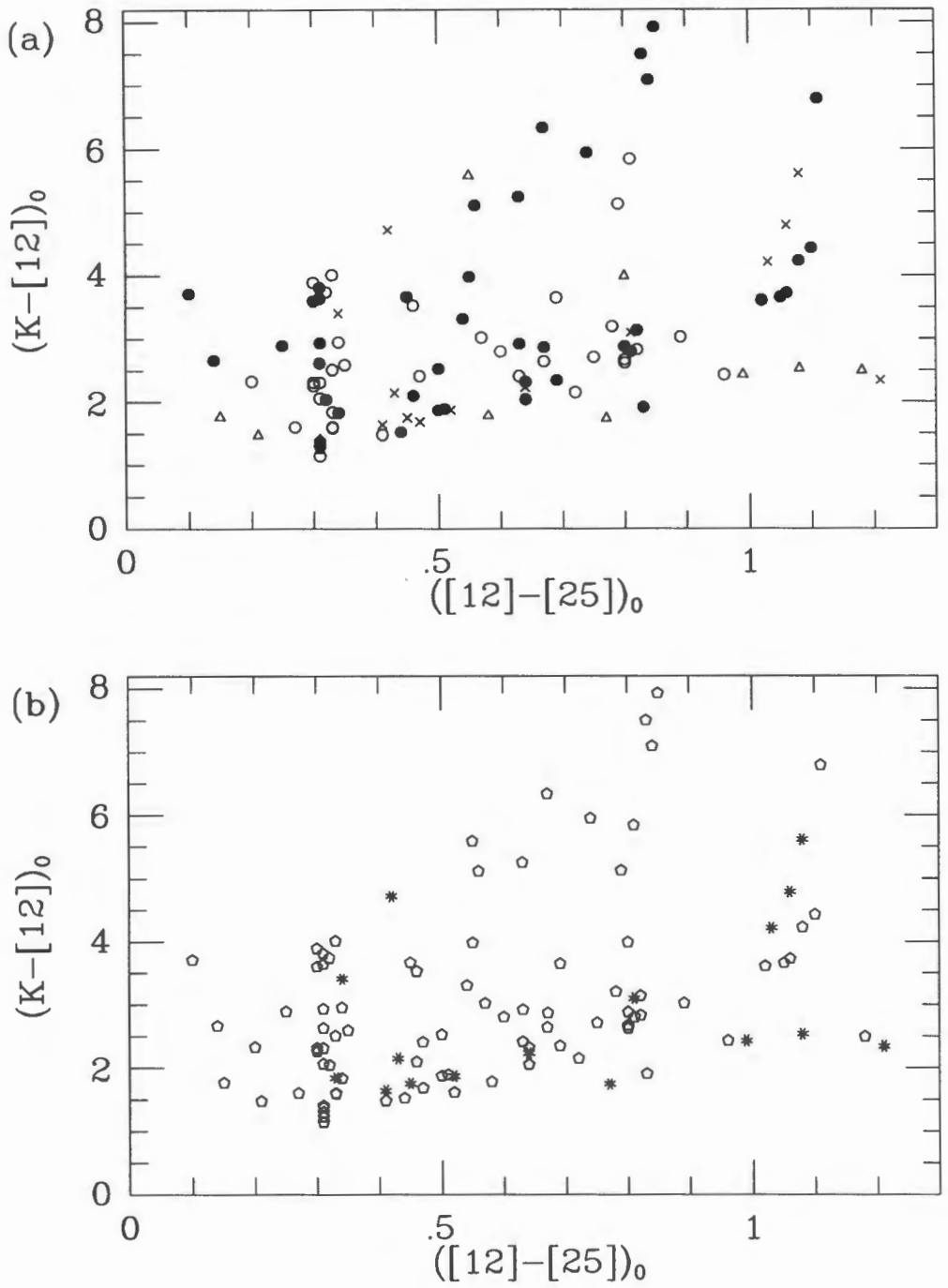

Figure 3.4: Reddening corrected $K - [12\mu m]$ vs. $[12\mu m] - [25\mu m]$ diagram. The symbols in (a) are the same as in Figure 3.2. In (b) the open pentagons and the asterisks, respectively, signify Miras and non-Miras as determined from the stars' K light curve quality and pulsation half-amplitudes as described in previous subsections.

of Miras and non-Miras in Figure 3.4 are not clearly split, but as apparent in a close look at Figure 3.4 (b), they are different. Most of the non-Miras have K–[12μm]< 2.5, indicating that they have moderate to thin shells. The stars with shells of moderate thickness are positioned in the region between $K - [12\mu m] = 2$ and 3.2. As shown in Figure 3.4 (a) this region contains most of the stars whose light curves were classified as *fair* (or strong Mira candidates). The location of these stars here may explain why the stars' Mira characteristics – the large amplitudes and so forth, were not as easily discernible as those of the stars in the region K–[12μm]> 3.2. The region K–[12μm]>3.2 is the region of stars with thick shells, and in Figure 3.4 (b) and (a), it is respectively, noticeably populated by Miras and by stars whose light curves were classified as of *good* quality.

The stars clustered at $[12\mu m] - [25\mu m] \simeq 0.3$ in Figures 3.4 (a) & (b) are those stars for which 25μm fluxes were estimated (see Section 2.3) since only upper limits on their 25μm fluxes were available. The estimation was made from a relation of the 25μm flux as a function of the 12μm flux and thus the systematic clustering on the $[12\mu m] - [25\mu m]$ axis.

Miras with Thin Shells

'Thin shelled' here is used for stars with K–[12μm] < 1.7. The objects discussed below all had light curves classified as *good* , so (unless their [12μm] fluxes were uncertain) the $K - [12\mu m]$ calculated for them must be a good approximation of the thickness of their shells. They are IRAS09421–6223

(# 1) at $(K - [12\mu m], [12\mu m] - [25\mu m]) = (1.52, 0.44)$, IRAS10110–5734 (# 54) at (1.37,0.31), and IRAS10113–6142 (# 56) at (1.30,0.31) in Figure 3.4. The determined periods are 313, 281, and 214 days for # 1, 54, and 56, respectively. Stars of these shorter periods frequently do not have thick shells.

Non-Miras with Thick Shells

The non-Miras with thick shells, *ie.* those with K–$[12\mu m]$>3.2, are probably interesting. They are IRAS09509–6013 (# 3) at $(K - [12\mu m], [12\mu m] - [25\mu m]) = (4.72, 0.42)$, IRAS10033–5950 (# 26) at (4.79,1.06), IRAS10168-6013 (# 75) at (3.41,0.34), IRAS10173-5844 (# 76) at (5.61,1.08), and IRAS10261-5717 (# 98) at (4.21,1.03) in Figure 3.4. Objects # 75 and #98 have uncertain mean magnitudes because of observing confusing caused by nearby stars; in fact, only one observation of the correct star was obtained for object #98. Objects # 3, # 26, #75 and #98 were classified as non-Miras because their periods couldn't be determined and not because they had low amplitudes; they probably need further investigation. It has all ready been noted that objects # 26 and # 76 have *IRAS* Variability index $Var > 90$ and would therefore be expected to be Mira variables (see Section 3.1.2). Furthermore it was noted that according to Low Resolution Spectra analysis by Olnon *et al.* (1986) # 26 is a M giant star with an oxygen-rich envelope.

3.2.2 Carrying the Colour Discussion Further

Comparing Figure 3.4 and 3.5 with similar diagrams from Epchtein *et al.*

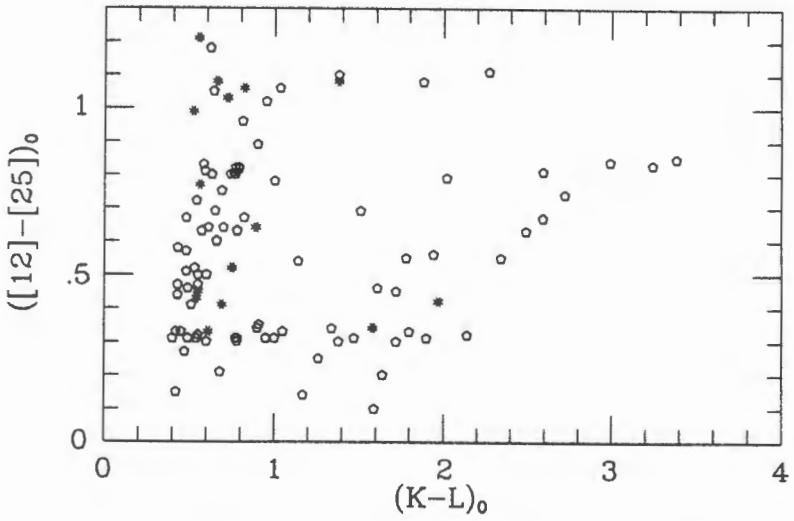

Figure 3.5: Reddening corrected near-and-mid-infrared two-colour diagram. The Open pentagons and the asterisks, respectively, signify Miras and non-Miras as determined from the stars' K light curve quality and the $J-H$ versus $H-K$ diagrams in previous subsections.

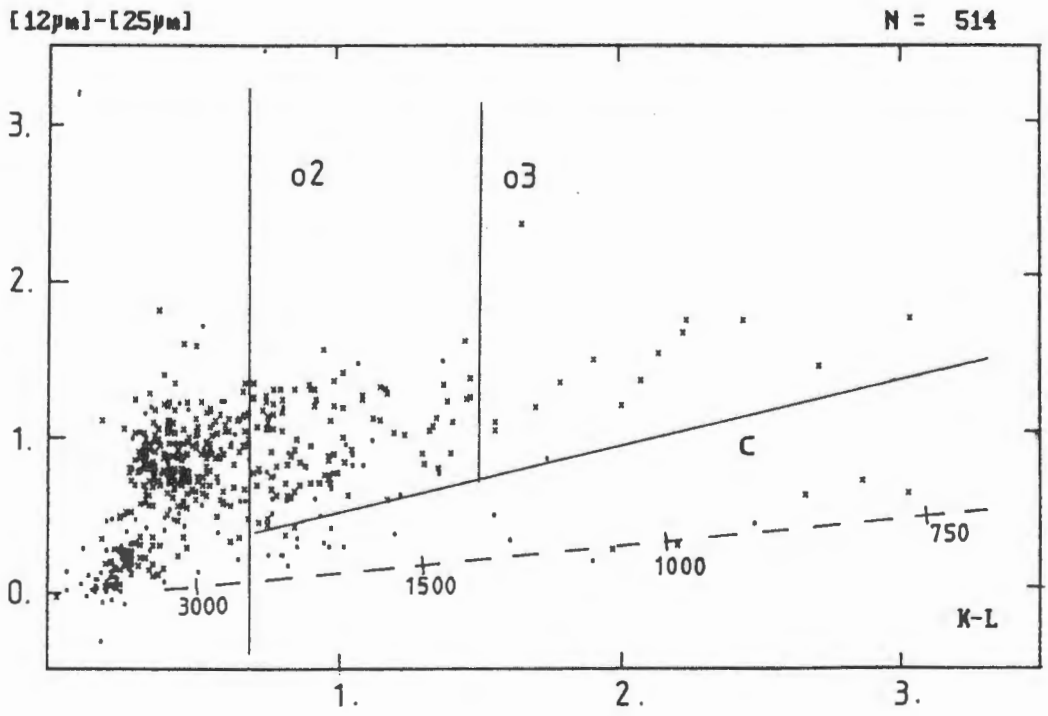

Figure 3.6: A reproduction of the Epchtein *et al.* (1987) oxygen-rich (o1,o2,o3) and carbon-rich (c) star regions in the K-L versus [12μm]-[25μm] two-colour diagram.

(1987) (one of which is reproduced in Figure 3.6, it is clear that the Miras observed in the present paper have both oxygen-rich and carbon-rich shells. In two-colour diagrams, particularly the $K - L$ versus $[12\mu m] - [25\mu m]$, designed to exhibit the different infrared excess of oxygen-rich and carbon-rich mass-losing long period variables (Le Berte *et al.* 1994), Carbon Miras will be found in the lower right of the diagram and the Oxygen Miras above this region. Stars with published spectra and observed in the present study were used to design such two-colour diagrams and the Miras with unknown spectra were classified as carbon-rich or oxygen-rich. (See Section 2.5.2 in the present paper.) The rest of the discussion focusses only on stars assumed to be Miras as indicated in Table 3.4, and the Carbon and Oxygen stars are differentiated.

3.3 Oxygen and Carbon Miras

Figure 3.7 (a) shows the oxygen-rich and carbon-rich regions in a $K - L$ versus $[12\mu m]$–$[25\mu m]$ diagram. The stars plotted (11 O-rich and 10 C-rich) had spectral classifications in literature (see Table 3.3) and were used to determine the demarcation of the regions. The demarcations are based on those from similar diagrams by Epchtein *et al.* (1987) (one of which is reproduced in Figure 3.6), but since the wavelength for the window L and criteria for source selections that they use are different from those used here, the regions shown in Figure 3.7 (a) do not coincide with those of

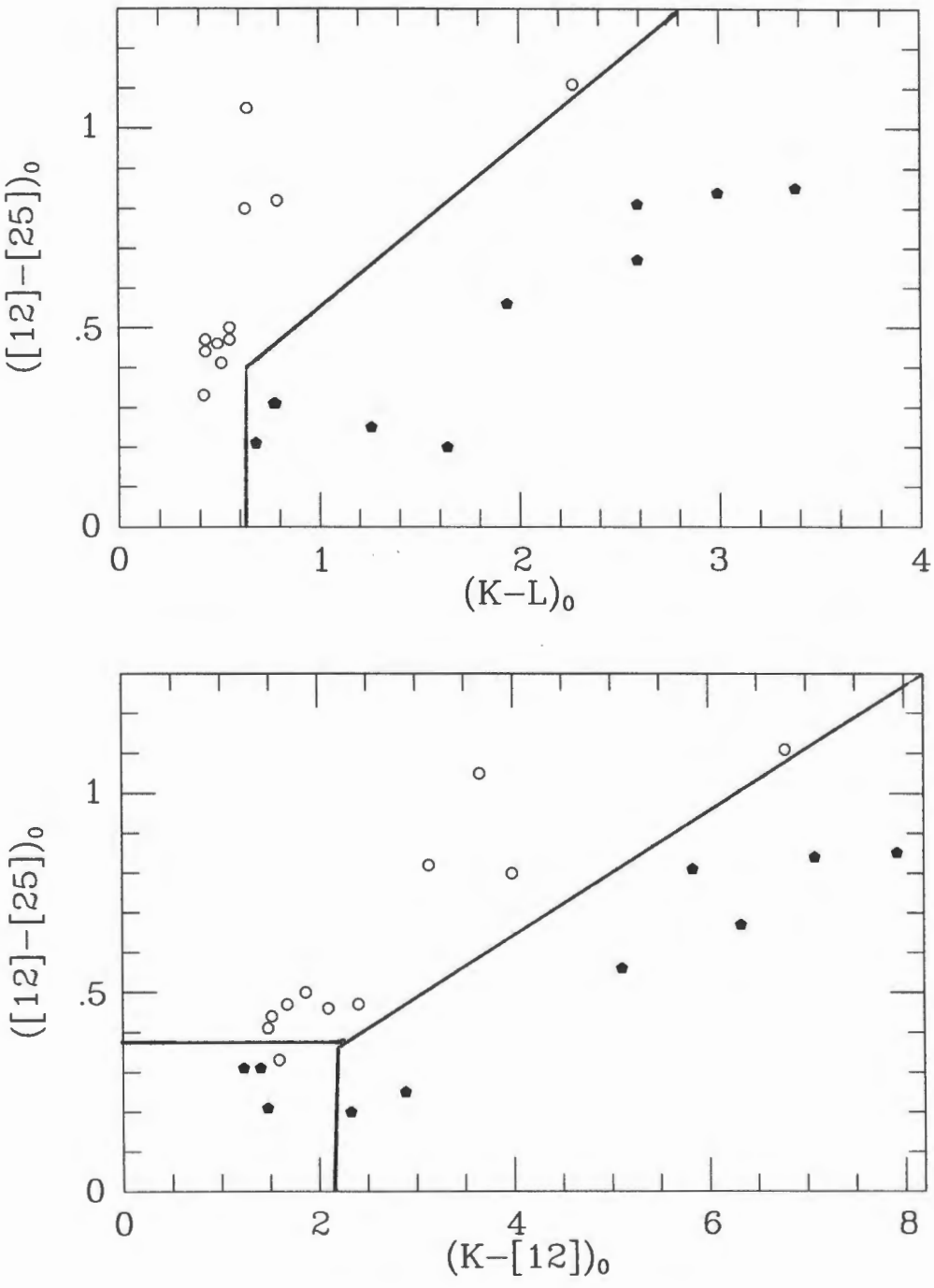

Figure 3.7: Oxygen-rich and carbon-rich Mira regions in infrared two-colour diagrams. Open circles and solid pentagons, respectively, signify Oxygen and Carbon Miras in the present sample and for which there were published spectral classifications.

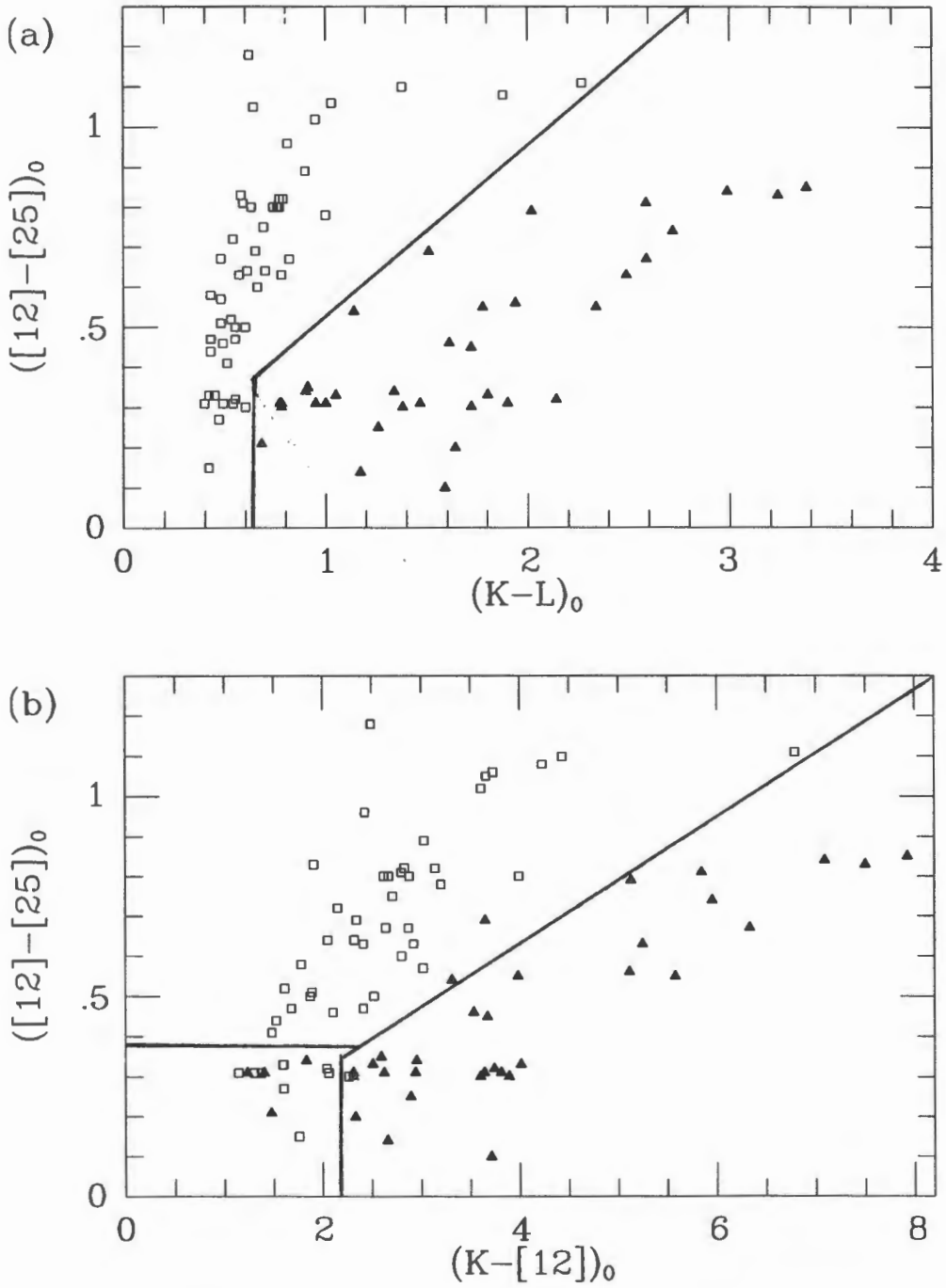

Figure 3.8: Two-colour diagrams with the oxygen-rich (open squares) and carbon-rich (solid triangles) Miras that were tentatively classified using the $K - L$ versus [12μm]–[25μm] diagram and those for which there were published spectral classifications. In (a) notice the clear separation of the O-rich and C-rich Mira locations and in (b) the small mixing region at ($K - [12\mu m] < 2.2$, $[12\mu m] - [25\mu m] < 0.38$).

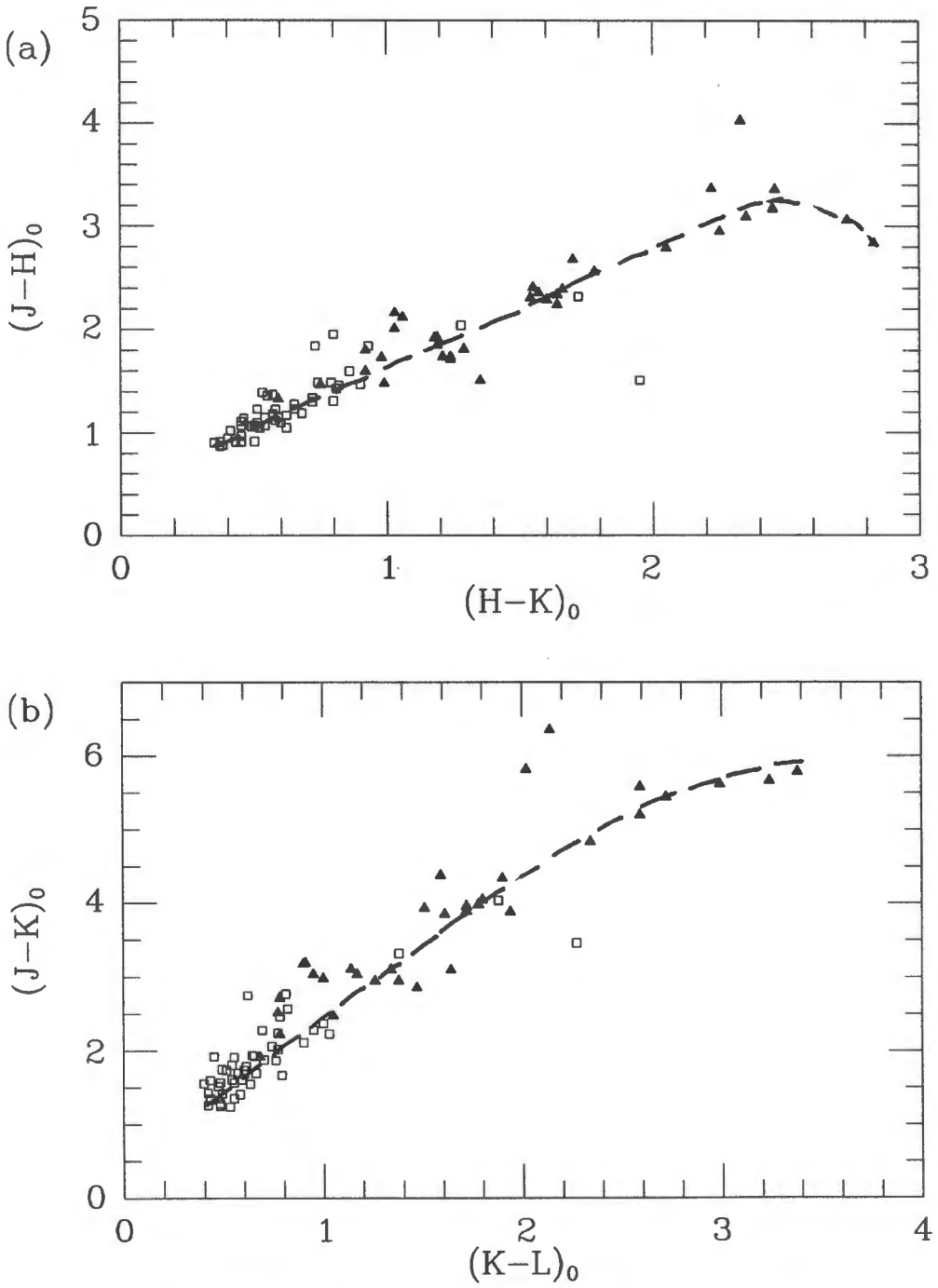

Figure 3.9: Near-infrared two-colour diagrams to exhibit the redder C-rich Miras (solid triangles) to the top right and the bluer O-rich Miras (open squares) to the bottom left. Notice the difference in the scatters of the O-rich and C-rich Miras about the estimated sequences that are marked in the diagrams.

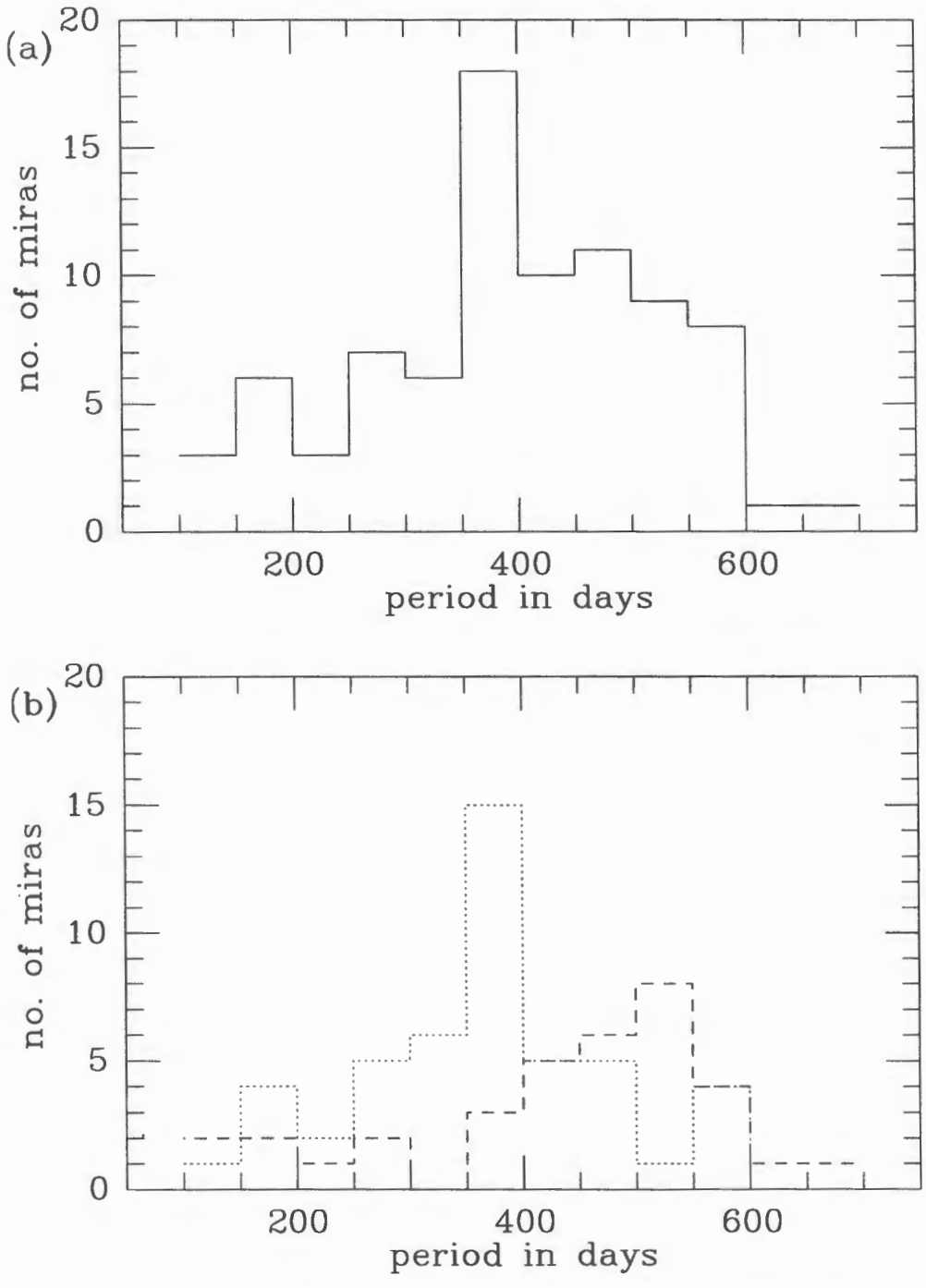

Figure 3.10: The solid-line histogram in (a) is for all Miras presented in the current paper, except for one object (# 101) with P=1584 which is off the diagram. In (b) the dotted-line histogram is for O-rich Miras and the dashed-line histogram is for C-rich Miras.

Figure 3.6. The carbon-rich region in Figure 3.7 is to the bottom right of the diagram and starts at $K - L = 0.65$; the oxygen-rich region is to the top left. In Figure 3.7 (b) the regions for the two groups are marked out as described above but there is a small region of mixing centred at $K - [12\mu m] = 1.7$ and $[12\mu m] - [25\mu m] = 0.25$. Therefore the $K - [12\mu m]$ versus $[12\mu m] - [25\mu m]$ diagram is not used as the *overall* discriminating tool for oxygen-rich and carbon-rich Miras but rather to check the classifications that result from the $K - L$ versus $[12\mu m] - [25\mu m]$ diagram. Since the $IRAS$ fluxes are averages of only a small number of observations by the $IRAS$ satellite, a scatter is expected in the designated oxygen-rich and carbon-rich locations on these discriminating two-colour diagrams. The tentative classifications are presented in Figure 3.8. Inclusive of the Miras which had spectral classifications, the resultant tallies of carbon-rich and oxygen-rich in the present sample are 36 and 49, respectively.

Figure 3.9 is presented to exhibit the positions of O-rich and C-rich Miras in near-infrared two-colour diagrams. These diagrams cannot be used to discriminate oxygen-rich and carbon-rich Miras in contrast to diagrams of Figure 3.7, but they do tell us the general colours of the stars in the two groups. In Figure 3.9 (a) the Carbon Miras are all above $H - K = 0.9$, but for stars # 23 at $(J - H, H - K) = (1.3, 0.6)$ and # 67 at $(J - H, H - K) = (1.50, 0.75)$. The star # 23 has P=552 days and an exceptionally low K amplitude; it was noted as possibly interesting in the section on light curve analysis. The star #67 has P=296 days and has not shown any peculiarities besides its currently discussed enigmatic position, given its

carbon-rich classification, in this diagram. In Figure 3.9 (b) the Oxygen Miras are all below $J-K=2.9$, but for stars # 37 at $(J-K, K-L)=(4.05, 1.9)$, # 94 at $(J-K, K-L)=(3.3, 1.4)$ and #101 $(J-K, K-L)=(3.45, 2.3)$, with the respective long periods 552, 500, and 1584 days, the longest of the periods in the group. Therefore in general, the Oxygen Miras in the $J-H$ versus $H-K$ plot are in a tight group at the bottom left (bluer) as in similar diagrams of Whitelock *et al.* (1994, 1995), while the Carbon Miras are in a less tight group to the top right (redder) of the diagram.

The Miras in the near-infrared two-colour diagrams of Figure 3.3 form sequences that are marked with dashed-lines on those diagrams. In Figure 3.9 the scatter of the C-rich Mira colours about the sequence is larger than that of the O-rich Mira colours. Whitelock (1996b) noted that O-rich Miras exhibited a tighter trend than C-rich Miras in such $J-H$ versus $H-K$ two-colour diagrams.

Figure 3.10 shows histograms of the numbers of Miras versus period in 50-day intervals. The top histogram (Figure 3.10 a) is for both the O-rich and the C-rich Miras. The periods extend from P=100 days to P=716 days and are concentrated between 350 days and 600 days, with most stars (18) in the 350-to-400-day interval. The actual average period is P=401 days, which does not include the one Mira (# 101) of P=1584 days which is off the diagram. The bottom histogram (Figure 3.10 b) compares the distribution of the O-rich (dotted-line) and the C-rich (dashed-line) Miras. The O-rich Miras peak at 375 days (15 stars), have a maximum of P=600 days, and and average of P=386 days. Again this analysis does not include (# 101). The

C-rich Miras peak at 525 days (9 stars), have a maximum of P=716 days, and an average of P=444 days. The minimum period for the two types is about the same just over 100 days. That C-rich Miras have an average period larger than that of O-rich Miras is interesting and consistent with studies of Miras in the Large Magellanic Clouds (Feast *et al.* 1989). Although it should be noted that the present sample is *IRAS* selected whereas the LMC sample of Feast *et al.* (1989) was taken mainly from *I*-plate surveys.

3.3.1 Amplitudes For O/C-rich Miras

Figure 3.11 shows the pulsation half-amplitude at K as a function of $K-L$, $K-[12\mu m]$ (shell thickness) and $[12\mu m]-[25\mu m]$ (shell temperature). For oxygen-rich Miras with thin shells, $K-L$ is a function of stellar temperature. However for stars with thick dust shells, $K-L$ is strongly influenced by the reddening of the shell (Whitelock *et al.* 1991). Moreover the oxygen-rich and carbon-rich shells absorb stellar radiation and influence $K-L$ differently. Separate oxygen-rich and carbon-rich correlations of $K-L$ with amplitude are shown in Figure 3.11 (a), indicating that the two group of stars have different $K-L$ colours at any given amplitude, in particular that the carbon-rich stars are redder at any given amplitude. The correlation for the oxygen-rich stars has a notably smaller scatter. The meaning of the separation of oxygen-rich and carbon-rich in (Figure 3.11 (a)) is not clear; however it seems the division is primarily because of the $K-L$ colour difference of the two groups of stars (as shown in near-infrared two-colour diagrams, Figure 3.9) and not so much because of the difference in the

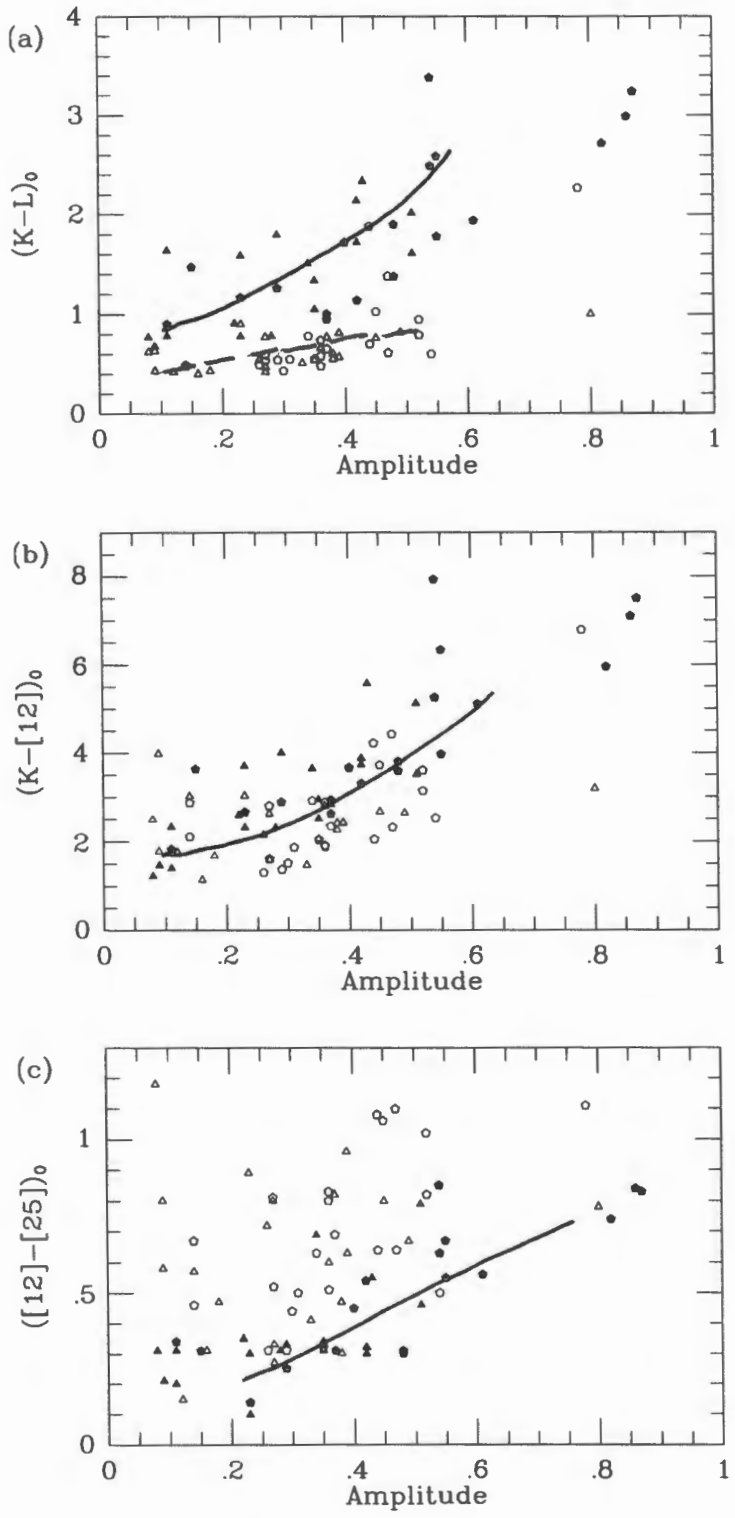

Figure 3.11: The half peak-to-peak K amplitude as a function of various colours. The symbols are as follows: solid pentagons and triangles, respectively, are for C-rich Miras with well determined and uncertain amplitudes; open pentagons and triangles, respectively, are for O-rich Miras with well determined and uncertain amplitudes.

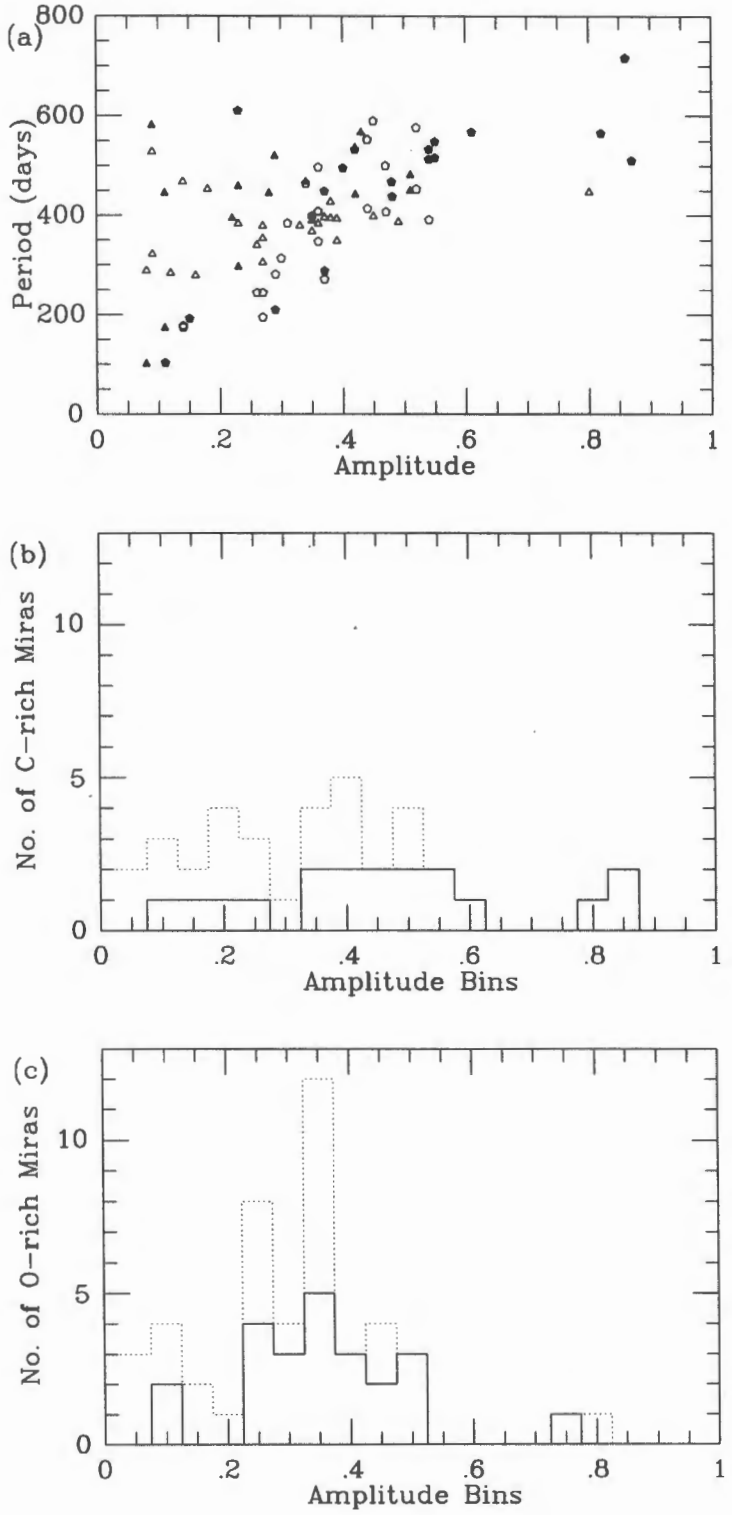

Figure 3.12: The half peak-to-peak K amplitude versus period (a); and the half-amplitude distributions of C-rich (b) and O-rich (c) Miras. Symbols in (a) are as in Figure 3.10. In (b) and (c) the solid-line and dotted-line histograms, respectively, are for Miras with well determined and uncertain amplitudes.

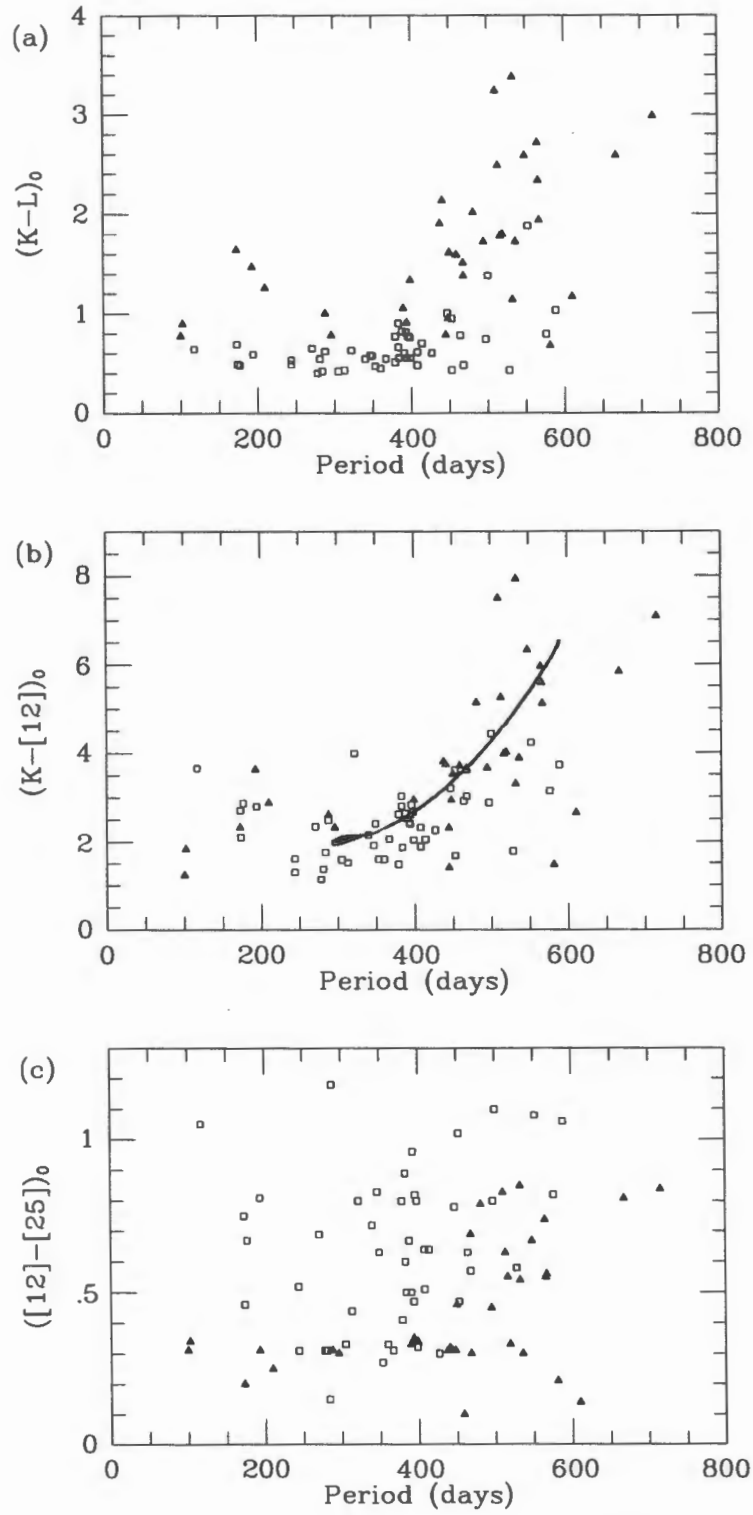

Figure 3.13: The period as a function of various colours. The symbols are as follows: solid triangles for C-rich Miras and open squares for O-rich Miras.

amplitudes of oxygen- and carbon stars.

In Figure 3.11 (b) the correlation of $K-[12\mu m]$ with pulsation-amplitude is shown. The $K-[12\mu m]$ correlation has a large scatter probably because the $[12\mu m]$ is not an average over the full light curve but only over the part sampled by *IRAS*. In Figure 3.11 (c), the carbon-rich stars show a correlation of $[12\mu m]-[25\mu m]$ with amplitude while the oxygen-rich stars do not. There is a considerable scatter here again probably because of the few *IRAS* observations.

The discussions of amplitude versus period and amplitude distributions that began in Section 3.1.1 and were based on Figure 3.2 are continued with special emphases on the difference between oxygen-rich and carbon-rich Miras. The increase of period with amplitude has already been discussed. One of the points to note in Figure 3.12 (a) is the large number of carbon-rich stars with half-amplitudes larger than 0.53 mag, which are all well determined. The histograms in (b) and (c), respectively, show that the carbon-rich stars are bunched up between pulsation half-amplitudes of 0.35 and 0.55 mag while the oxygen-rich stars are concentrated between 0.25 and 0.45 mag. In particular, the average half-amplitudes for the carbon-rich stars is 0.46 mag and that of the oxygen-rich stars is 0.36 mag.

Figure 3.13 shows the period as a function of $K-L, K-[12\mu m]$ and $[12\mu m]-[25\mu m]$ colours. These diagrams provide interesting comparisons with Figure 3.11, the diagrams of pulsation-amplitude as a function of the same colours. The correlations in Figure 3.13 and Figure 3.11 have different scatters but in general they behave alike, which is expected since ampli-

tude has been shown to be correlated with period for both oxygen-rich and carbon-rich Miras for which these quantities are well determined.

3.3.2 Statistical Test For The O/C-rich Groups

To check and quantify the significance in the difference between the oxygen-rich and carbon-rich Miras, the Kolmogorov-Smirnov statistical test, described in section 2.8, was performed on the period distribution of the two groups. The results of the test affirms the apparent difference between the two groups.

The maximum vertical distance between the cumulative distribution functions based on the oxygen-rich and carbon-rich Mira samples was **T** = 0.4648, corresponding to a significance level, **P** = 5.5x10^{-4}. In other words, according to the Kolmogorov-Smirnov two-sample test, there was only a probability of 0.00055 that the period distribution functions of the oxygen-rich and carbon-rich Miras classified in this paper came from the same populations.

3.4 Bolometric Magnitudes and Distances

The apparent bolometric magnitudes (m_{bol}), which are listed in Table 3.5, were calculated by integrating under the spline curve fit to the $JHKL, 12, 25_{\mu m}$ fluxes as a function of frequency (see section 2.6.1). An additional rough m_{bol} was calculated for the comparisons illustrated in Figure 3.14. This second m_{bol} was determined by fitting a Planck function, as an interpolation

formula, to the $JHKL$ fluxes (see section 2.6.2).

Due to incomplete light-curve coverage, there is an estimated rms uncertainty of about 0.2 mag in the bolometric magnitudes derived in this paper. The rms for the redder stars in the sample is probably as high as 0.3 mag (Whitelock *et al.* 1994). One source of the uncertainty is the $IRAS$ means, which are averages of only a few observations taken over a short time-interval. The problem is not too severe because the $IRAS$ amplitudes are thought to be relatively small and in most cases the fluxes contribute only a small amount to the derived m_{bol}. The mean $JHKL$ observations are good approximations to the mean fluxes of ordinary Miras (Appendix A, Menzies & Whitelock 1985, and Glass *et al.* (1995), and do not contribute significantly to this rms.

Table 3.5 Derived Data: Periods, m_{bol}, Distances ...

Star	IRAS Name	Period (days)	$\Delta K/2$	m_{bol}	J-K (mag)	K-[12μm]	Distance (kpc)	z
1	09421–6223	313*	0.30	6.96	1.34	1.52	2.15	–0.27
2	09433–6233	567	0.61	9.57	3.88	5.11	8.06	–1.02
3	09509–6013	-	-	11.35	3.88	4.72	-	-
4	09510–6247	244*	0.27	8.69	1.24	1.60	4.12	–0.49
5	09519–6007	174	0.14	6.53	1.75	2.10	1.24	–0.10
6	09533–6021	716	0.86	8.07	5.62	7.09	4.41	–0.37
7	09568–6056	288	0.37	10.87	2.98	2.63	11.40	–0.99
8	09570–6051	284	0.12:	9.40	1.43	1.76	6.25	–0.53
9	09571–5930	497	0.36	9.74	2.06	2.88	10.23	–0.69
10	09579–6203	-	-	9.12	1.49	2.15	-	-
11	09581–5936	390	0.35	10.70	2.47	2.51	11.80	–0.79
12	09586–6150	510	0.87	9.77	5.67	7.50	8.50	–0.83
13	09595–6141	177	0.14	9.86	1.28	2.87	5.82	–0.55
14	09597–5927	194	0.27	10.19	1.61	2.79	7.16	–0.45
15	10001–5929	349	0.39	9.31	1.70	2.41	6.79	–0.43
16	10003–6207	399	0.35:	11.36	3.10	2.97	16.13	–1.60
17	10004–6235	305*	0.27	6.82	1.26	1.59	1.99	–0.21
18	10008–6115	-	-	9.95	1.59	1.76	-	-
19	10010–6025	398	0.45:	9.25	1.87	2.67	7.14	–0.53
20	10015–6212	193	0.15	10.92	2.86	3.64	10.05	–0.99
21	10019–5946	278	0.16	9.65	1.56	1.14	6.93	–0.45
22	10021–5903	536	0.42:	10.04	3.96	3.89	9.80	–0.53
23	10023–5946	581	0.09:	8.37	1.92	1.46	4.68	–0.30
24	10026–5849	519	0.29:	9.03	4.05	4.01	6.08	–0.30
25	10029–5856	383	0.36:	7.90	1.70	2.80	3.75	–0.19
26	10033–5950	-	-	7.73	2.31	4.79	-	-
27	10034–6207	340	0.26:	9.13	1.61	2.15	6.15	–0.59
28	10038–6055	379	0.33:	8.82	1.74	1.48	5.69	–0.44
29	10040–6020	565	0.82	9.48	5.44	5.95	7.72	–0.54
30	10044–5803	-	-	9.78	2.75	3.10	-	-
31	10045–5955	394	0.38:	8.54	1.91	2.41	5.12	–0.32
32	10048–5820	532	0.42	10.50	3.11	3.30	12.08	–0.48
33	10050–6001	391	0.54	9.58	1.69	2.52	8.23	–0.53
34	10051–5817	450	0.51:	9.58	3.85	3.53	7.43	–0.29
35	10052–5906	445	0.11:	10.08	2.71	1.39	9.32	–0.47
36	10053–6001	427*	0.38:	10.12	1.74	2.25	11.12	–0.71
37	10053–5852	552	0.44	9.34	4.04	4.23	9.06	–0.43
38	10056–6223	468	0.14	10.15	1.25	3.01	11.92	–1.15
39	10057–6018	347	0.36:	7.99	1.41	1.92	3.68	–0.25
40	10062–5824	383**	0.23:	9.04	2.11	3.03	6.34	–0.25

Table 3.5 Derived Data: - *continued*

Star	IRAS Name	Period (days)	$\Delta K/2$	m_{bol}	J-K (mag)	K-[12μm]	Distance (kpc)	z
41	10064–5757	566	0.43:	10.25	4.84	5.58	11.02	–0.36
42	10071–5815	-	-	9.84	3.00	2.24	-	-
43	10075–5747	394	0.22:	10.59	3.19	2.59	11.26	–0.32
44	10076–5944	408	0.47	9.03	1.79	2.32	6.55	–0.37
45	10078–5742	-	-	8.95	2.70	1.74	-	-
46	10079–5914	589	0.45	11.17	2.23	3.74	21.88	–1.07
47	10080–5902	516	0.55	9.32	3.98	3.98	6.94	–0.32
48	10090–5744	288	0.08:	9.63	2.75	2.49	7.01	–0.18
49	10098–5742	533	0.54	7.91	5.79	7.93	3.67	–0.09
50	10102–5841	-	-	10.04	2.82	1.86	-	-
51	10104–5832	468	0.34:	9.94	3.93	3.65	8.90	–0.32
52	10107–5814	388	0.49:	9.63	2.57	2.64	8.38	–0.26
53	10109–5958	210	0.29	7.64	2.95	2.89	2.29	–0.16
54	10110–5734	281	0.29	8.19	1.61	1.37	3.56	–0.08
55	10111–6102	399	0.35	9.86	1.57	2.03	9.48	–0.67
56	10113–6142	244	0.26	9.79	1.42	1.32	6.83	–0.48
57	10118–6038	576*	0.52	5.78	1.67	3.14	1.80	–0.12
58	10121–5836	384*	0.31	5.82	1.36	1.87	1.44	–0.05
59	10121–5846	453*	0.18	5.63	1.35	1.67	1.46	–0.05
60	10123–5753	173**	-	9.26	2.28	2.71	4.35	–0.10
61	10136–5743	173	0.11	8.47	3.10	2.33	3.12	–0.06
62	10141–5837	408	0.36	7.53	1.57	1.89	3.28	–0.11
63	10145–5714	441	0.42	10.30	6.36	3.74	10.27	–0.12
64	10145–6046	-	-	7.15	2.01	1.64	-	-
65	10146–5922	-	-	10.20	2.18	1.85	-	-
66	10148–6039	414	0.44	9.56	1.88	2.06	8.44	–0.51
67	10150–5703	296	0.23:	9.66	2.22	2.31	6.60	–0.06
68	10154–5828	360	-	9.71	1.92	1.61	8.31	–0.24
69	10157–5944	453	0.52	10.92	2.28	3.60	16.66	–0.77
70	10160–6041	468	0.48	10.54	2.95	3.60	11.73	–0.70
71	10161–5945	447	0.80:	8.81	2.37	3.20	6.25	–0.29
72	10162–6010	353	0.27:	8.37	1.52	1.61	4.43	–0.23
73	10163–6012	528	0.09:	7.52	1.60	1.78	3.82	–0.20
74	10164–6005	367	0.35	10.23	1.81	2.07	10.69	–0.54
75	10168–6013	-	-	9.74	3.42	3.41	-	-
76	10173–5844	-	-	10.60	1.70	5.61	-	-
77	10174–5704	322	0.09:	6.65	1.55	3.99	1.90	–0.01
78	10175–5957	100	0.08:	9.28	2.52	1.24	3.70	–0.18
79	10176–5802	234	-	5.91	1.94	3.66	0.74	–0.01
80	10194–5816	116	0.17:	8.29	2.54	2.53	2.19	–0.04

Table 3.5 Derived Data: - *continued*

Star	IRAS Name	Period (days)	$\Delta K/2$	m_{bol}	J-K (mag)	K-[12μm]	Distance (kpc)	z
81	10196–5718	481	0.51:	10.15	5.82	5.12	9.90	–0.06
82	10198–5853	464	0.34	10.53	2.46	2.91	14.12	–0.41
83	10199–5801	668	-	7.89	5.59	5.84	3.95	–0.06
84	10207–5815	393	0.39:	9.81	2.77	2.42	9.18	–0.17
85	10216–5813	445	0.28:	10.30	2.72	2.32	10.31	–0.18
86	10220–5858	610	0.23	8.78	3.04	2.67	5.76	–0.15
87	10222–5700	513	0.54	10.46	5.89	5.25	11.70	0.20
88	10225–5925	271	0.37	9.79	1.93	2.33	7.27	–0.25
89	10229–5705	459	0.23	9.24	4.38	3.71	6.40	0.01
90	10230–5744	-	-	9.23	1.72	2.34	-	-
91	10231–5823	548	0.55	8.75	5.20	6.33	5.46	–0.10
92	10234–5820	102	0.11	9.67	3.18	1.84	4.46	–0.07
93	10238–5852	396	0.37:	9.87	2.24	2.83	9.48	–0.23
94	10246–5844	500	0.47	9.99	3.32	4.43	11.52	–0.24
95	10250–5904	495	0.40	10.35	3.89	3.67	10.97	–0.28
96	10256–5836	379	0.27:	9.23	2.02	2.62	6.87	–0.12
97	10257–5854	438	0.48	10.82	4.34	3.81	13.02	–0.29
98	10261–5717	-	-	9.36	2.76	4.21	-	-
99	10262–5727	448	0.37	9.76	3.04	2.94	8.06	0.00
100	10277–5836	-	-	9.66	2.21	2.42	-	-
101	10287–5733	1584*	0.78	6.95	3.46	6.79	5.67	0.01

Distances to the objects were calculated by applying $P - L$ relations in m_{bol} for oxygen-rich and carbon-rich Miras (see section 2.7). The distance, z, of the objects above the galactic plane were subsequently calculated by multiplying the radial distance with the sine of galactic latitude (*ie.* $z = dsin(b)$). In addition to m_{bol}s and distances, Table 3.5 lists all the derived periods, half peak-to-peak K amplitudes and $J-K$ and $K-[12\mu m]$ colours. Periods listed in Table 3.5 are the periods used in deriving all the listed relevant quantities. The asterisks and double-asterisks, respectively, indicate the periods which were adopted from literature and the I plate study as described in previous sections. The presentation and derivations

of amplitudes and colours are also as described in previous sections; *eg.* colons signify uncertain amplitudes. The negative values of z indicate distances below the galactic plane. The objects for which periods, amplitudes, and distances are not listed were classified as non-Miras.

Figure 3.14 (a), (b) and (c) illustrate correlations in the colours of the Miras and the difference between the luminosity or m_{bol} determined by the spline curve technique and that by the Planck function. The correlation of the fitting techniques with, or at least their dependence on, colour is expected since the fittings are to frequency dependent fluxes. The correlation with the least scatter in these diagrams is of the oxygen-rich stars in Figure 3.14 (c), *ie.* the plot with the K-[12μm] colour. It has already been pointed out that K-[12μm] is a measure of the shell thickness, and its correlation to the difference in Planck and Spline m_{bol}s is not surprising; however the correlation's small scatter for the oxygen-rich stars is interesting, especially in view of the carbon-rich stars correlation which has a larger scatter. The difference in the two m_{bol}s for carbon-rich (or cooler) stars is on average larger than it is for the oxygen-rich (or hotter) stars. In other words, the redder are the stars, the larger are the differences in the luminosities calculated by the two techniques. Furthermore, and particularly for the carbon-rich stars, the thicker are the shells, the bigger are the differences in the luminosities calculated from the two fitting techniques. This difference in the luminosities is less than 0.1 mag for almost all stars with 2<K-[12μm]<4 and 2<J-K<3.2, and less than 0.2 mag for almost all stars with K-[12μm]<4.2 and J-K<3.2, while it is greater than 0.2 mag for about

10 red, thick shelled, long period Miras in the sample. It is clear that for the very red Miras with thick shells and long periods, the two fitting techniques produce very different m_{bol}s, and that the Spline curve makes the better estimates of the stars' total luminosities because it includes the *IRAS* data which makes a significant contribution for the stars with thick shells.

Preliminary distances were calculated using the $P-L$ relation at K. In Figure 3.15 the derived distances are compared with those calculated from the $P-L$ relation in m_{bol}. Though the $P-L$ at K relation is the most practical (due to the relative insensitivity of K fluxes to interstellar reddening and other reasons), the relation breaks down when applied to stars with thick shells. Figure 3.15 (g) shows the increase of $(K-M_K)_0-(m_{bol}-M_{bol})_0$ with increasing $(K-[12\mu m])_o$ or the thickness of shells. In Figure 3.15 (e) a similar though less correlated increase of $(K-M_K)_0-(m_{bol}-M_{bol})_0$ with $(J-K)_0$ or the stars colour is illustrated. In all the diagrams of Figure 3.15, the $(K-M_K)_0-(m_{bol}-M_{bol})_0$ for the oxygen-rich stars (except for a few stars with large periods) are less than and close to zero. This may indicate that for the oxygen-rich stars, distances derived from the $P-L$ relation at K are as good as those derived from the relation in m_{bol}. The $P-L$ relation at K for carbon-rich stars has a bigger scatter ($\sigma=0.18$) than the one ($\sigma=0.13$ (Feast *et al.* 1989)) for the oxygen-rich stars. Figure 3.15 (h) illustrates that the distances derived from the $P-L$ relations at K and in m_{bol} are similar for stars with shorter periods, but cover a broad range of differences for stars with longer periods. The stars with longer periods have thicker shells, so it is not surprising to see them exhibiting this broad range

of $(K - M_K)_0 - (m_{bol} - M_{bol})_0$. Furthermore, the $P - L$ relation in m_{bol} breaks down for stars with periods greater than 420 days (Feast *et al* 1989).

Figure 3.16 shows the final derived distances plotted against colours and periods. Carbon-rich *IRAS* stars, being mostly red, can be seen to much farther distances than the oxygen-rich *IRAS* stars. At the shorter distances in Figure 3.16 there are mainly oxygen-rich stars. For any given distance the carbon-rich stars have redder colours than those of the oxygen-rich stars. The few oxygen-rich stars with long periods are again an exception in this. There is no obvious correlation of distance with period. However z, the distance above the galactic plane, provides more information of galactic distributions and this is discussed in subsequent sections.

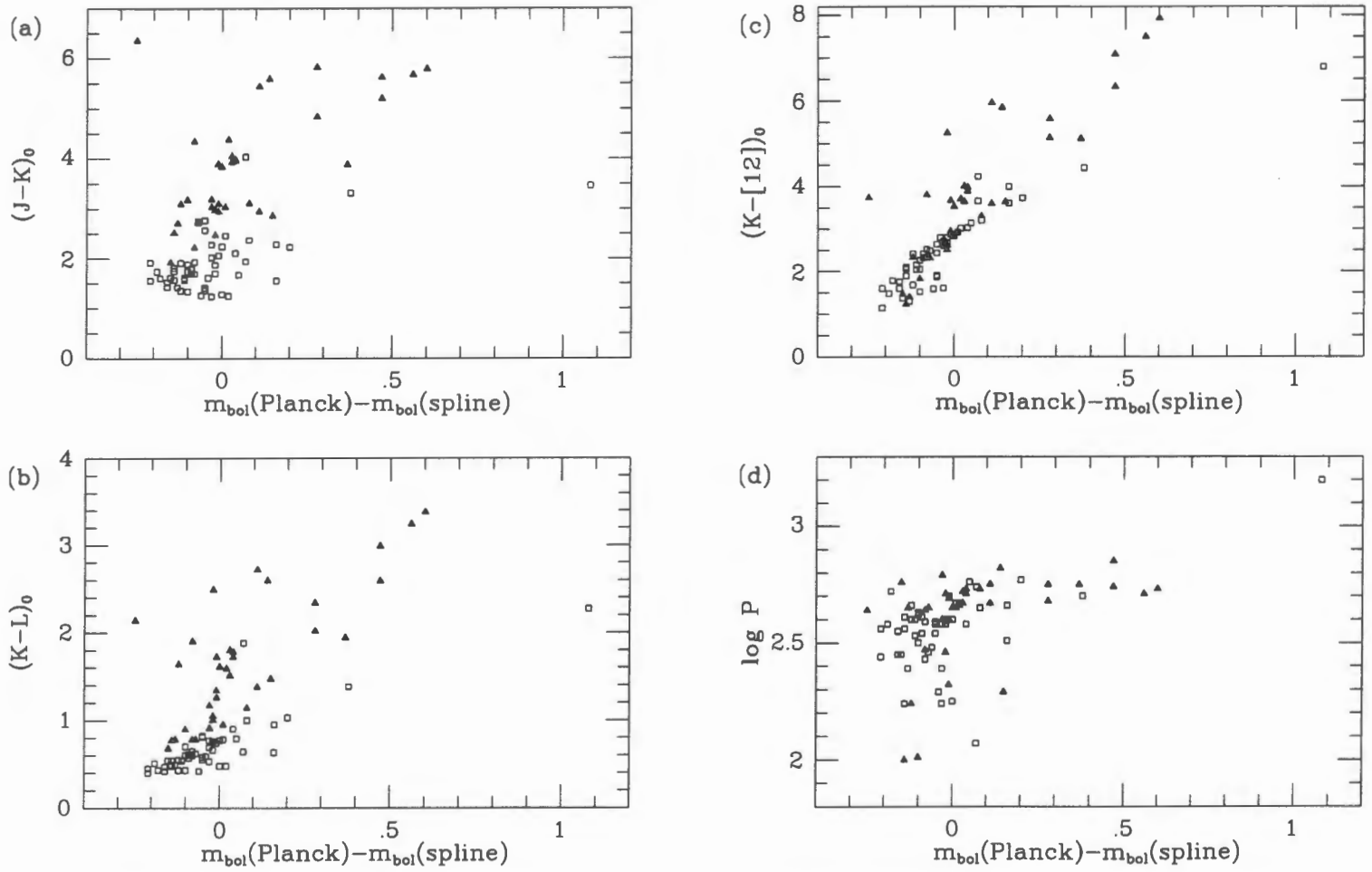

Figure 3.14: The colours and periods exhibited against the difference in the m_{bol}s determined by the blackbody and spline curve fitting techniques. Open squares and solid triangles are for oxygen-rich and carbon-rich Miras, respectively.

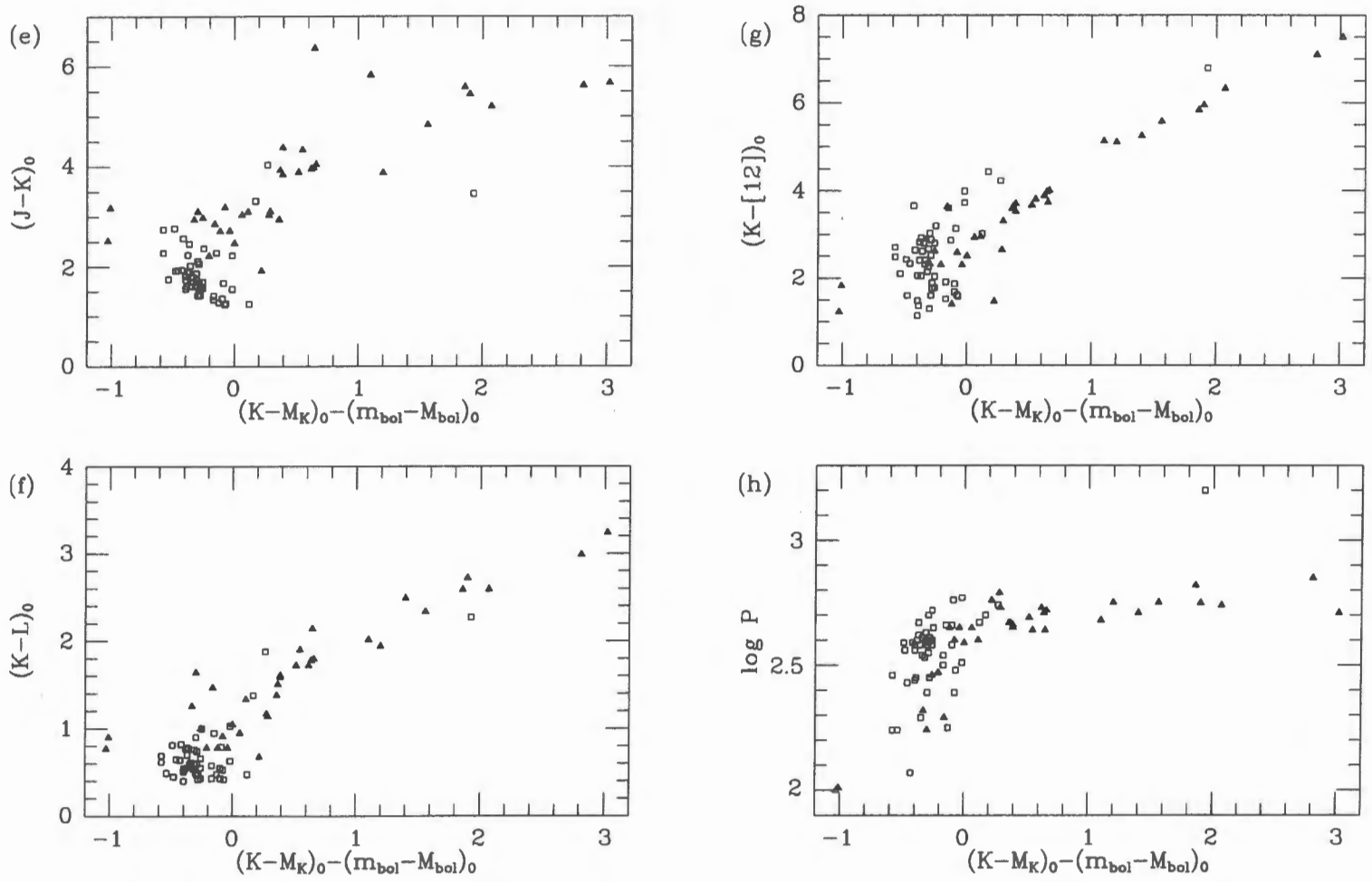

Figure 3.15: The colours and periods exhibited against the distance moduli derived from the $P-L$ relations at K and in the m_{bol} adopted in the present paper. Symbols are as in Figure 3.9

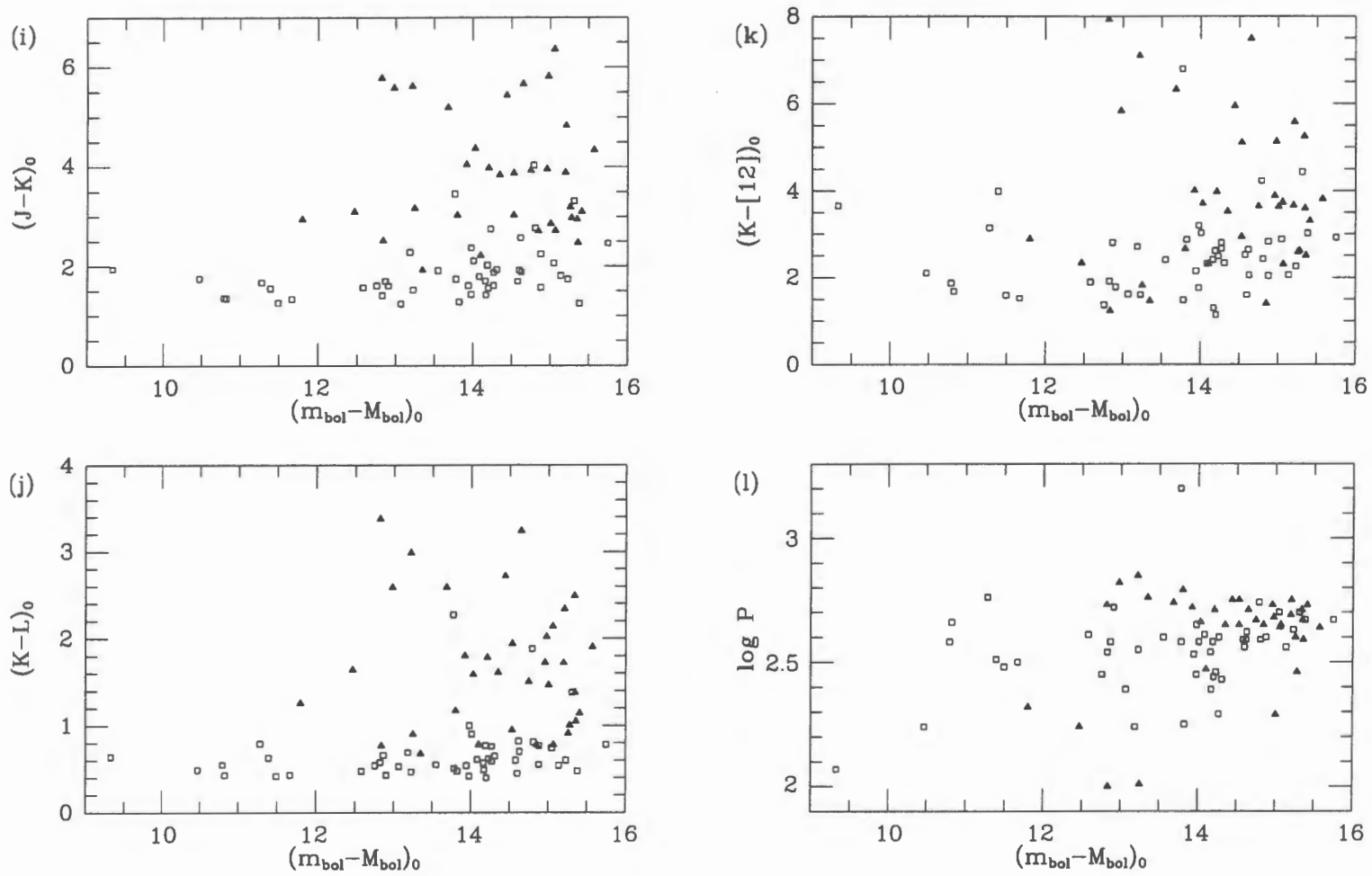

Figure 3.16: The colours and periods against the distance moduli adopted in this paper. Symbols are as in Figure 3.9.

3.4.1 The Z-Distance and Galactic Distributions

Figure 3.17 shows z, the distance from the galactic plane to the stars, plotted against periods and colours. As was noted for distances in Figure 3.16 (i) and (j), at any given z (with a few exceptions) in Figure 3.17 (b), the carbon-rich stars have redder colours than the oxygen-rich stars. However, the smaller zs are not populated primarily by oxygen-rich stars as was found at the shorter distances in Figure 3.16. In fact, the short period carbon-rich stars in the sample tend to be at small zs or very close to the galactic plane. There is no clear trend of period with z for the oxygen-rich Miras.

The work of Feast *et al.* (1972) indicates that the kinematics and hence the z-distance of Miras would be a function of pulsation period, at least for the oxygen-rich Miras. Whitelock *et al.* (1994) showed that z was correlated with period, in particular that the long period (> 500 days) Miras were only found close to the galactic plane. There is no such clear correlation in Figure 3.17 (a). If anything the shorter period stars are found close to the galactic plane and the longer period ones farther out. This is almost certainly a selection effect. The stars in the Whitelock *et al.* (1994) sample are at a high galactic latitude while those in the present sample are at a low galactic latitude. In the present sample, stars at high z-distance have to be at large r distance, and are therefore mostly bright Miras with large periods. In other words, a z to period correlation that is consistent with the work of Feast *et al.* (1972) and shown by Whitelock *et al.* (1994) cannot

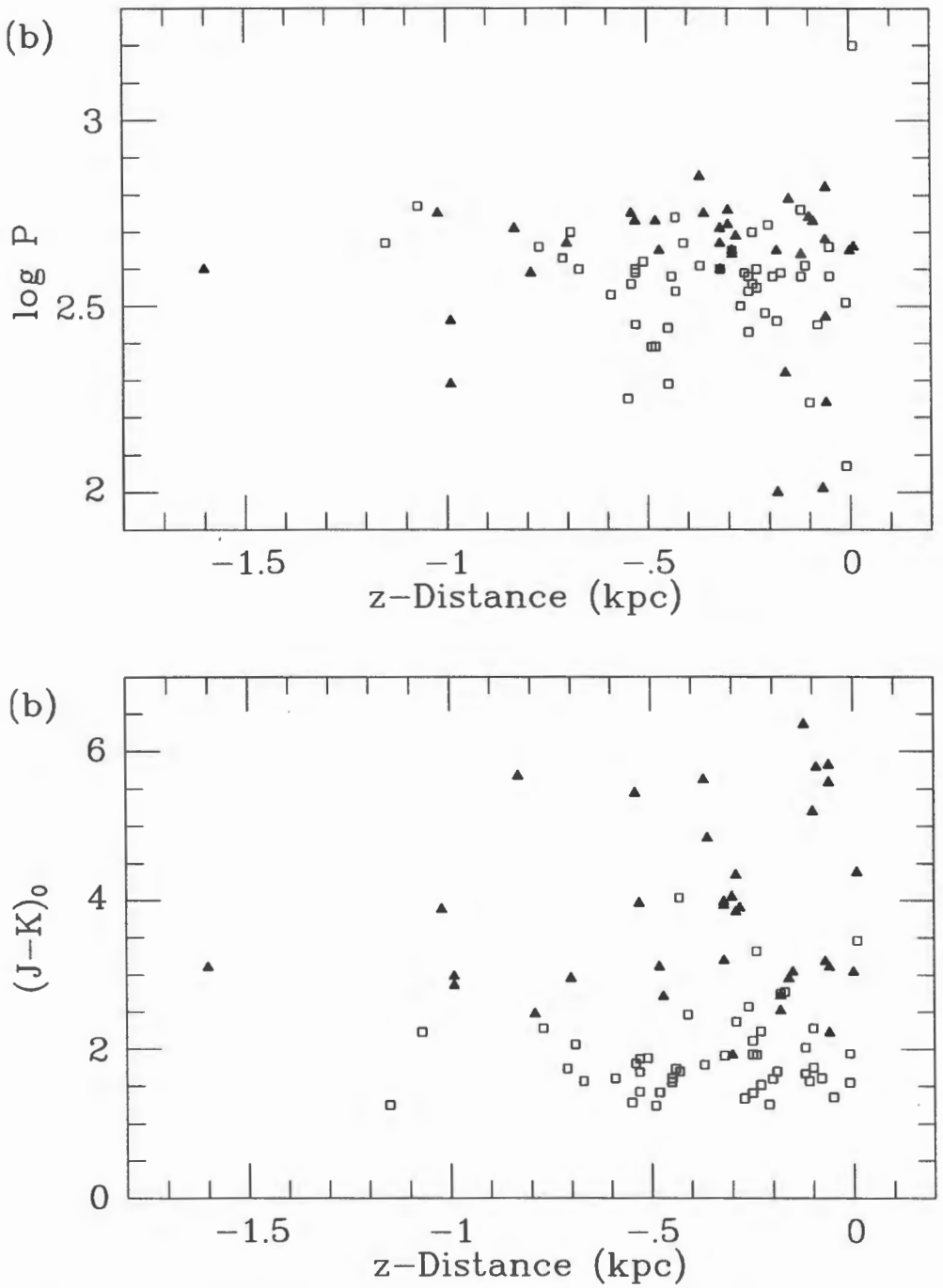

Figure 3.17: The distance above the galactic plane, z, is plotted against log-periods and colours for oxygen-rich (open squares) and carbon-rich (solid triangles) Miras. The negative z values indicate the distance below the galactic plane.

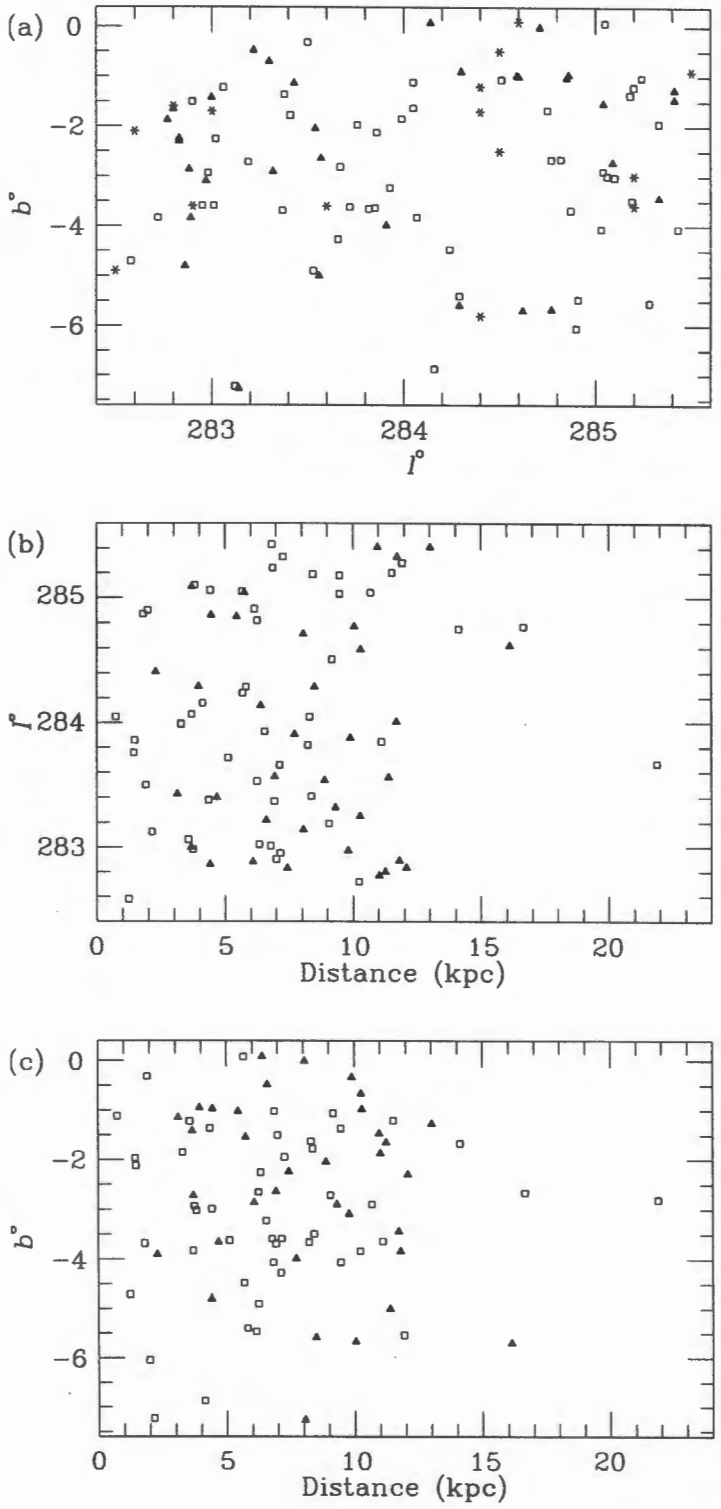

Figure 3.18: Galactic distributions of the O-rich (open squares) and C-rich (solid triangles) Miras in the sample. The asterisks in (a) represent the non-Miras.

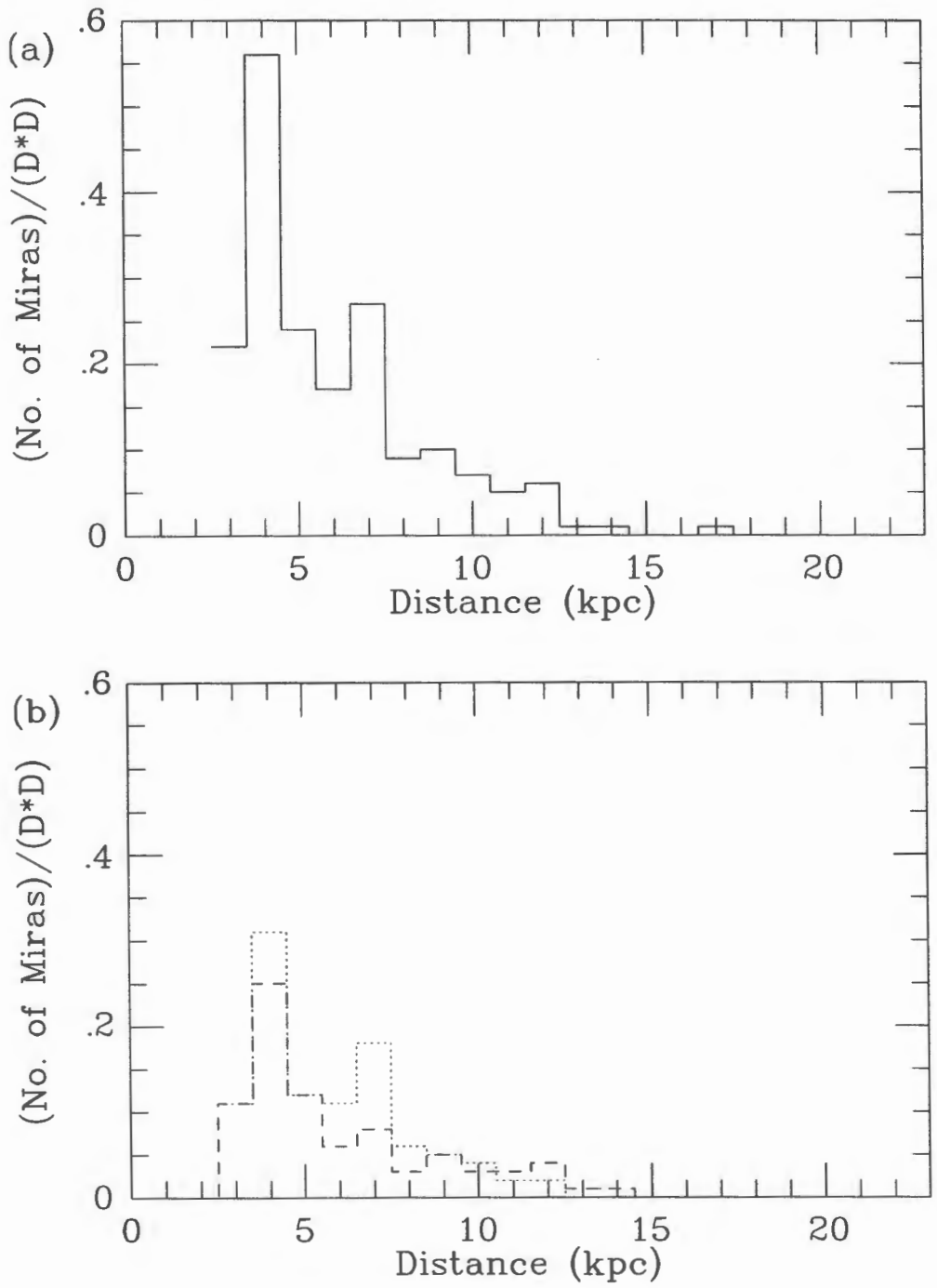

Figure 3.19: The solid-line histogram in (a) is for all Miras presented in the current paper. In (b) the dotted-line histogram is for O-rich Miras and the dashed-line histogram is for C-rich Miras. The parts of the histograms for distances below of 2 kpc are too large and off the diagrams.

be exhibited in the present sample because it is biased so that only the brighter stars with the longer periods can be seen at large z-distances. The only OH/IR star in the sample (*IRAS* 10287-5733) is at a z of about zero, or close to the galactic plane; searches of infrared counterparts of OH/IR sources by Engels *et al.* (1983) (at $2.2\mu m(K)$ and $3.7\mu m(L)$) resulted in discoveries of 17 infrared OH/IR stars, all at $b \leq 1°$.

In galactic co-ordinates, as illustrated in Figure 3.18, the oxygen-rich and carbon-rich Miras, as well as the non-Miras, in the current sample, are distributed in no obvious pattern. The galactic number-density distribution are illustrated in Figure 3.19 and provide insight into this. The number-density here is derived by taking the numbers of Miras at a radial distance, D, and then dividing that number by the square of the distance. Figure 3.19 (a) and (b) show the number-density decreasing with increasing distance. This is expected as the range of detectable absolute luminosities will decrease with increasing distance so that at far distances only objects with high absolute luminosities will be detected. In Figure 3.19 the number-densities at distances less than 2 kpc are very large and off the diagrams. For the present discussion the interesting point is illustrated in Figure 3.19 (b). The number-densities ratio of the oxygen-rich to the carbon-rich Miras is greater than 1 at shorter distances and less than 1 at larger distances. The high number of observed carbon-rich stars at the large distances is indicative of the infrared-bias of the sample: at large distances, the currently discussed *IRAS* sample is biased to have a relatively bigger representation of carbon-rich (the redder) than oxygen-rich (the bluer) Miras.

3.5 Summary of Results and Conclusions

Approximately 11 $JHKL$ photometry modules per star have been obtained for 101 $IRAS$ sources that lie close to the galactic plane and were expected to be Mira variables. It was estimated that the JHK magnitudes were, on average, accurate to 0.03 mag and the L magnitudes accurate to 0.05 mag.

From the photometry, the sample has been shown to comprise 85 Miras, 12 of which had published periods. New periods were determined for the 85 Miras at an accuracy of ± 15 days for periods less than 550 days and ± 25 for the longer periods.

The shapes of the phased K light curves vary from star to star and have been classified into symmetric, asymmetric and irregular types. The variation of the accuracies in periods and amplitudes from star to star was illustrated in the plots of the phased light curves. Due to the seasonal spacing of the observations, uncertainties in periods and amplitudes and the quality of the phased light curves of stars with periods of around a year are worse than those of other stars.

A fit marking the increase of amplitude with period has been estimated for stars for which these quantities were well determined. Miras with well determined peak-to-peak K amplitudes have a mean half-amplitude of 0.4 mag and their largest half-amplitude is 0.85 mag.

It has been shown that the *IRAS variability index* , $Var = 90$ is an effective way of selecting Miras. It has also been suggested that $Var = 80$ and 70 may also be effective ways of selecting Miras. However it has been

shown that it cannot be concluded that stars are not Miras merely because their Var is less than 70.

For all the 101 $IRAS$ sources, the $K-L$, $K-[12\mu m]$ and $[12\mu m]-[25\mu m]$ have been respectively studied for the temperature of the star, the thickness of the shell and the temperature of the shell. Sources for which good K phased light curves were obtained define fairly narrow sequences in the $J-H$ vs. $H-K$ and $J-K$ vs. $K-L$ two-colour diagrams. The sequence in the $J-H$ vs. $H-K$ diagram is narrower and bends at the redder colours.

Using the $K-L$ versus $[12\mu m]-[25\mu m]$ two-colour diagram the Miras in the sample were tentatively classified into oxygen-rich and carbon-rich stars. Inclusive of 21 stars that had published spectral classifications, the resultant classification tallies were 49 oxygen-rich and 36 carbon-rich Miras.

The two group of stars define the same sequence in the $J-H$ vs. $H-K$ and $J-K$ vs. $K-L$ diagrams, however the sequence is tighter for the oxygen-rich Miras. The $J-K$ and $K-L$ colours of the oxygen-rich stars are bluer than those of the carbon-rich stars suggesting that the optical thickness of the carbon-rich shells are greater.

The oxygen and carbon-rich Miras, respectively, have mean periods and pulsation half-amplitudes at K of 346 days (excluding star # 101 with P=1584 days) and 0.36 mag and 442 days and 0.46 mag. The minimum period for the groups is the same, about 100 days; while the maximum period is 600 days (again excluding # 101) for the oxygen-rich and 716 days for the carbon-rich Miras.

The period as well as $K-L$ and $K-[12\mu m]$ colours were shown to be

functions of amplitude. Separate oxygen-rich and carbon-rich correlations of $K - L$ with amplitude were presented, indicating that for stars with thin shells the two groups have different stellar temperatures at any given amplitude.

The Kolmogorov-Smirnov test showed that the probability that the period-distribution function of the oxygen-rich and carbon-rich Miras came from the same population was very small, *ie.* 0.00055.

Apparent bolometric magnitudes ($m_{bol}s$) were derived by integrating under spline fits to average $JHKL12, 25\mu m$ fluxes. Additional $m_{bol}s$ were determined by a Planck function fitting technique. It was shown that for the bluer stars, $m_{bol}s$ determined by the two techniques were similar, and that the difference in the two $m_{bol}s$ increased with increasing redness and shell thickness of the Miras. The behaviour is expected since the *IRAS* fluxes contribute significantly to the m_{bol}s of the redder stars.

Distances to the stars have been determined using absolute magnitude $P - L$ relations of oxygen-rich and carbon-rich Miras in the LMC, where the distance modulus from the LMC has been taken to be 18.57. It was shown that at every distance over the range studied, carbon-rich Miras had redder colours than the oxygen-rich Miras.

For the present sample the short period stars are found close to the galactic plane and the large period ones farther out, a correlation that is opposite to the z distance versus pulsation-period relation that is indicated in the kinematics studies of Feast *et al.* (1972) and shown by Whitelock *et al.* (1994). The reason for the opposite direction of the correlation is

because the stars in present sample are at low galactic latitudes and thus the sample is biased so that only the bright stars with long periods are seen at high z distances.

The oxygen-rich and carbon-rich Miras, and also the non-Miras, in the current sample, are distributed in no obvious pattern in galactic location. From number-density analysis, it was shown that a higher number of carbon-rich (redder) than oxygen-rich (bluer) stars were observed at large distances, indicative of the infrared-bias of the sample.

This work will contribute to the study of the Galactic structure.

Chapter 4

A Search for Miras in the Galactic Bulge

This chapter describes work that was done during a two-month studentship (April 03, to June 03, 1996) under the supervision of Dr. Shaun Hughes at the Royal Greenwich Observatory in Cambridge, England. A search for Mira candidates in the region of the Galactic Bulge with coordinates $-18.^\circ7 < l < -11.^\circ5$ and $-2.^\circ8 < b < 4.^\circ7$, a region referred to as the *Galactic Bulge South*, was undertaken using electronic data that were scanned and digitised from Schmidt plates by the Automatic Plate Measuring (APM) machine at Cambridge. Computer Reduction Programs adapted for the project were written by Dr. Hughes (RGO), originally for his search for Long Period Variables in the Large Magellanic Clouds (Hughes 1989).

4.1 Introduction

In a collaboration of astronomers from Australia, the United Kingdom, and South Africa, I band photographic plates were obtained from the Anglo-Australian Schmidt Telescope. The plates covered various fields in the Galactic Bulge and the Galactic Plane and were to be used to find Miras and to determine their pulsation periods. As Whitelock and Catchpole (1992) showed, such a study together with infrared photometry would allow distances and number density distributions to be derived and analysed, and thus provide insight into the structure of the Bulge and other regions of the Galaxy. In addition, the study would enable a comparison to be made of the properties of Miras in the Galactic Bulge and in the Plane (Whitelock 1995a).

Using I plates to search for Miras has the following advantages: (1) Miras, being red giants, are brightest in the infrared, hence on the I plate they stand out compared to other bluer stars; (2) there is less interstellar absorption at I; and (3) though amplitude of variability for Miras decreases with increasing wavelength, the uncertainty in Mira magnitudes on the photographic plates can be kept below the typical I amplitudes of variability for Miras. The search described below used seventeen plates or epochs obtained from 1990 to 1994 covering the *Galactic Bulge South.* A brief description of the methods used for discovery and period determination is given and the period distributions of the LPV candidates are presented. A spectral window for the observations is exhibited and the completeness of the sam-

ple discussed. In addition light curves and finding charts for the candidates are presented in Appendices B-I & B-II. Further detailed analysis of the results and associated projects are in progress and will be reported by Shaun Hughes, Patricia Whitelock and collaborators in due course.

4.2 The APM Machine and the Plate Scanning

The kernel of the APM machine is a fast laser microdensitometer with a dedicated microprocessor-based front end. The photographic plates are scanned and digitised into samples at $\sim 7.5\mu m$ spacing. (The Cambridge Astronomy WWW Home Page). In the mode of operation used during scans for the present paper, the following APM parameters for each of the identified images were produced: image shape, intensity and position. For each plate (epoch) scanned the APM produced a list of approximately 510 000 objects.

(a) Image Shape

The image shape is defined by the parameters a and b, respectively, for the image's semimajor and semiminor axes; and the ellipticity of the image is $\epsilon = 1 - b/a$. In uncrowded regions (ie. where blended LPV images are not expected) the non-circular images would be expected to be galaxies or plate defects and the circular images stars. In that case, an ellipticity limit can be set to select only images of stellar objects or would be LPV candidates. In addition to setting the ellipticity limit, the image shape parameters are used in defining the weighted centre of the image.

(b) Raw Magnitudes and Positions

Raw APM magnitudes are derived from APM pixel values, which are the local image maxima over a specified pixel grid minus an estimation of the sky background. Raw APM positions of the images are a weighted centre of the pixel positions and their intensities.

(a) Celestial Positions

About 15 standard stars from astrometric catalogues are identified on the plates and they are used to transform APM coordinates to celestial l and b. Positions accurate to $\sim 0.5''$ are then obtained.

4.2.1 The Digitised Data

The APM data were converted to a format suitable for Sun computers for further reduction. For efficient computation, these data were first partitioned into sixteen parts corresponding to sixteen sections (labelled Aa ... Ad, Ba, Bb ... Dd) of the Schmidt Plate scans. The common sections (eg. the Aa's) in the seventeen epochs were then reduced together.

Cross-identifying Stars in all Epochs

Transformations were applied to correct for *seeing*, plate position, and intensity zero-point differences from observation to observation. An initial coordinate transformation for each section was derived by cross-identifying the brightest isolated stars (ie. no neighbours within $5''$) in a *master* epoch with those in the remaining sixteen epochs. These transformations were

then refined by inter-comparing lists of all the stars. With the stars in different epochs correlated, a magnitude transformation was derived to put the raw magnitudes in each epoch in the same system as that of a *designated master* epoch.

4.2.2 Variability and Periodicity

The variability and periodicity searches were done by automated computer programs (Hughes 1989) and only the final checking and classification of selected phased light curves were done by eye. Automated searches are important not only for speed reduction but also in eliminating subjectivity.

Searching for Variability

The objects were culled based on the number of points in their light curves and their light variability, at first regardless of their periodicity. The culling factors were: (1) a minimum of 12 cross-identifications of the same object in the 17 epoch scanned (object may not appear in all epochs because of variations in the observing conditions or the star itself at different epochs); and (2) a maximum σ_{lim} for the scatter of the observations about their mean, where the scatter was estimated from the fourth-spread pseudo-sigma σ_F. For a sample of points taken from a Gaussian distribution with a standard deviation σ, $\sigma_F = \mathrm{F}/1.349$, where F is the spread, in magnitudes, of the middle 50% of the points that have been sorted in order of magnitude (Hughes 1989). The threshold σ_{lim}, for which the star was assumed to be variable, was scaled to the uncertainty associated with the photometry of each scan.

The precise level of σ_{lim} was set considering computing limitations and in comparison with studies by Hughes (1989). Objects whose light curves had more than 12 cross-identifications and a scatter $\sigma_F > \sigma_{lim}$ were selected and considered for periodic variability.

Searching for Periodicity

Periods were determined using the Phase Dispersion Minimisation (PDM) technique that was developed by Stellingwerf in 1978. In the PDM method, phase space is divided into equal compartments. The input data are put into bins according to a trial frequency. The periodicity is examined by finding the minimum of a parameter θ, which is the ratio of the σ of the binned observation and rms scatter of the observations about their mean. In this case σ is an estimation of the rms standard deviation, and not σ_F. The threshold for periodicity selection was $\theta \leq 0.6$.

The phased light curves of the selected objects were checked for a monotonic increase from minimum to maximum light. Before rejecting the objects whose phased light curves failed the above check, the phased data were fitted with sine curves and the objects were passed as periodic variables if the ratio of the rms scatter of the sine fit to the rms scatter about the mean of the observations (σ_F) was less than 0.7. The light curves of the periodic-variable candidates were then put through a final check and classification by eye.

4.2.3 Checking and Classification by Eye

Only the periodic-variable candidates with phased light curves of the following parameters were selected for the final periodicity check and classification by eye:

Theta	$\leq$	0.6
Amplitude	$>$	0.3
Min Period	$=$	100 days
Max Period	$=$	1000 days.

In the table above, theta is the same as defined in the previous section, and amplitude is peak-to-peak and of the phased light curves. The raw light curves of the candidates with one or two points off their phased curves were also examined by eye. Some discrepantly phased light curves were plotted at different periods or rejected. The periodic variable candidates that passed the final selection were classified and labelled **C** for Cepheids, **L** for Long Period Variables, **E** for Eclipsing Binaries, and **?** for Unidentifiable but Interesting Detections:

Phased Light Curve Classification Criteria

Class-type Label	Visual Shape of Light Curve	Period Restriction
C	saw-tooth	$<$ 100 days
L	sinuisodal	100 to 1000 days
E	constant with a spike	none
?	permutations of the above	none.

When there was doubt about the classification, a small letter was used for the respective labels.

4.2.4 Creating Finding Charts and Matching with Objects in Literature

The Galactic positions determined during the digitisation of the photographic data were converted from l and b to RA and Dec (1950). Finding charts (4x4 arcmin) were then created. The positions were further used to match the selected objects with objects published in literature, in particular the objects listed in Simbad data base of the *Observatoire de Strasbourg* in France.

4.3 The Mira Candidates

Out of some 500000 objects that were studied for variability, 140 candidates for long period variable stars have been found. They broke down in the following way: 43 **L**'s; 73 **l**'s; 1 **C**'s; 14 **c**'s; 0 **E**'s; 5 **e**'s; 4 **?**'s, where the labels are the same as described in section 4.2.2. In other words, 116 Mira candidates (**L** and **l**) and 24 related variable stars were discovered. It should be emphasised that only 43 are strong candidates (ie. of class-type **L**).

Out of the 140 variable star candidates discovered, 32 have been matched with stellar objects listed in Simbad. These matches include catalogued variable stars and all 16 published *IRAS* Miras in the field studied. In other words, 100% of the *IRAS* Miras in the field searched were found.

As a first approximation for the survey's completeness, a spectral window for the observation dates was computed. The spectral function is presented in Figure 4.1 and shows a strong secondary peak at the frequency of

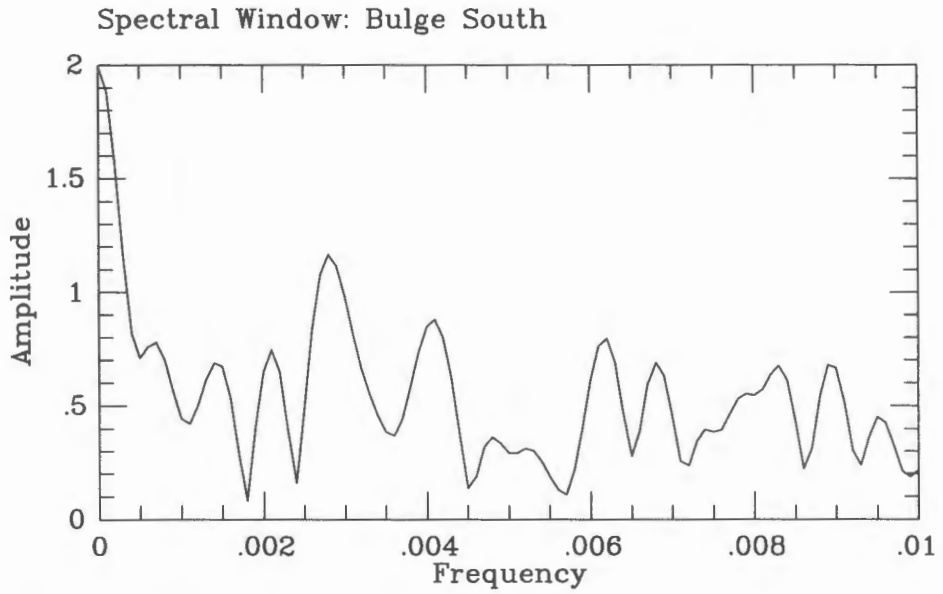

Figure 4.1: A Spectral-window illustrating the distribution of the Galactic South Bulge *I*-plate observations. Notice the peak at frequency is $\sim 0.0028/days$ or period is $\sim$ 359 days.

0.0028/days, *ie.* periods of 359 days or about a year. Evidentally, there will be a bias against detecting variables with periods corresponding to peaks in the spectral function. Unfortunately most Miras in the Galactic Bulge have a period of about a year (Whitelock 1995a) and their identification and the completeness of this survey will thus be undermined.

It has been noted that 100% of the *IRAS* Miras in the field searched for long period variable candidates have been found, *ie.* that the search is complete for the discovery of *IRAS* Miras. Though the sample of these *IRAS* sources contain only 16 stars, they provide a first test of the hypothesis about the completeness and possible bias of the survey that was deduced from analysizing the spectral window. Figure 4.2 is a presentation of a histogram of the period distribution and a plot of amplitude versus

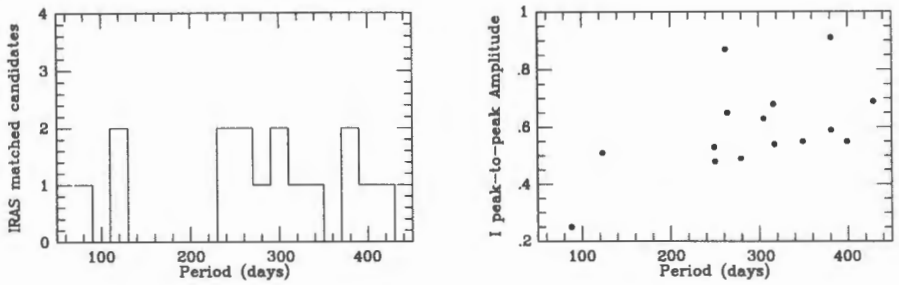

Figure 4.2: (a) A histogram of the period distribution in intervals of 20 days and (b) a plot of I amplitude versus period for the candidates that were matched with $IRAS$ Miras in the field searched.

period of the candidates that constitute this $IRAS$ sample. None of these Miras have periods within 10 days of the 359 day period that corresponds to the frequency of the secondary peak in the spectral function presented in Figure 4.1. However there are stars within ± 20 days (the error in the period determination) of this peak. Figure 4.2 (b) shows that the amplitudes of these stars were fairly large ($> 0.45 mag$) and clearly over the 0.3 mag amplitude cut-off that was set during the automated computer searches for periodicity. These large amplitudes may have made the stars' periodicities detectable even though the spectral function shown in Figure 4.1 suggests the search would be bias against discovery at these periods.

The period distributions of the candidates are presented in Figure 4.3. The mean period is 226 days for the 43 candidates of class-type **L** and 154 days for the 140 candidates of class-types **l** and **L**. At the low-period end, there are candidates of class-types **l** and **L**, while at the large-period end, there are only candidates of class-type **L**; infact, beyond the 300 days period, all but two of the candidates are of class-type **L**. Unlike the period

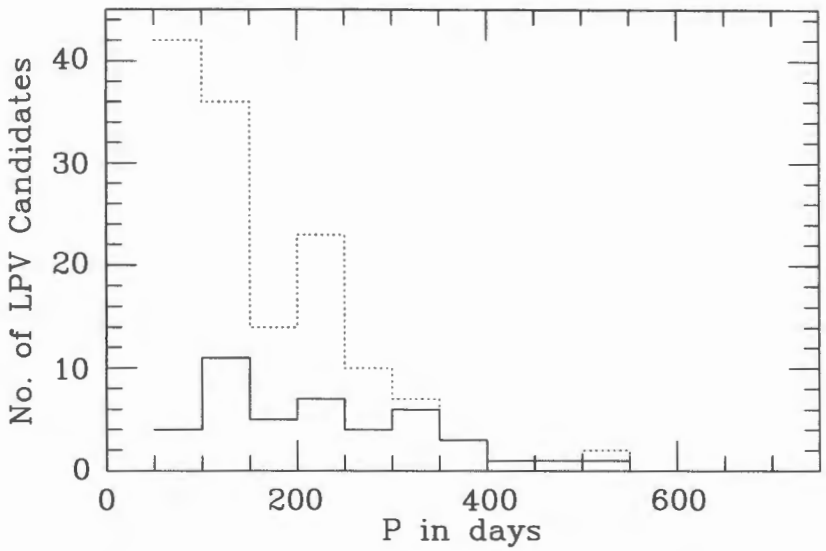

Figure 4.3: Histogram of the Galactic Bulge Mira Candidates. The solid-line histogram is for candidates of class-type **L**, and the dotted histogram is for class-types l and **L**.

distributions of Galactic Bulge Miras from Glass *et al.* (1995) for Sgr I, Lloyd Evans (1976) for NGC 6522 and from Whitelock *et al.* (1991) for $b \sim -7°$ (see a reproduction of these distributions in Figure 4.4) , the current period distribution (for class-type **L** candidates and more so for candidates of the other class-types) is shifted by about 100 days to the low period end. The selection of the Mira candidates presented here either has a period-bias as suggested above or Miras in the *Galactic Bulge South* have a unique period distribution; this will only be confirmed with further study of the candidates and the field.

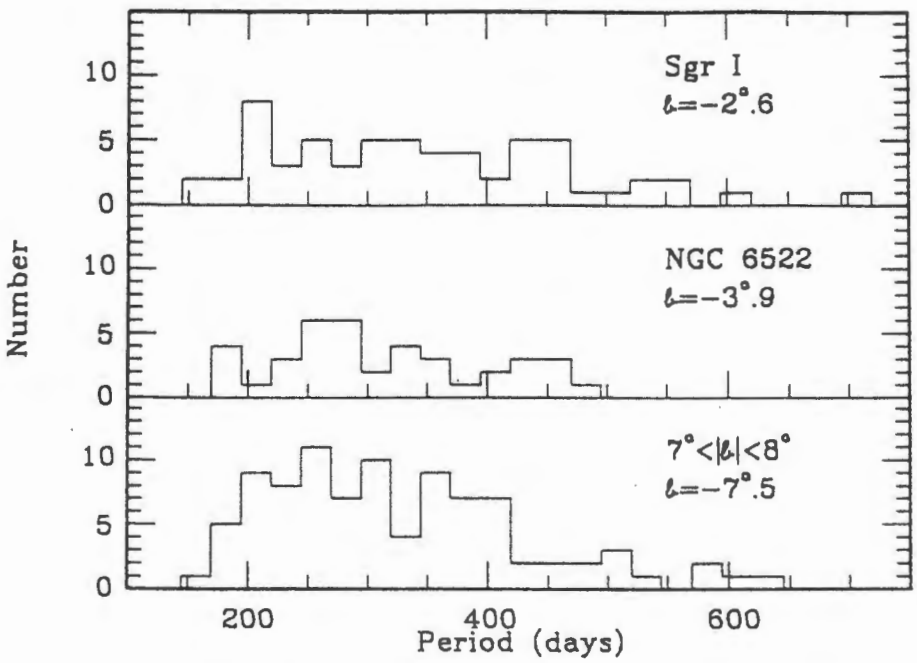

Figure 4.4: The period distribution of Miras in the Bulge. The periods for the Miras are from Glass *et al.* (1995) for Sgr I, Lloyd Evans (1976) for NGC 6522 and from Whitelock *et al.* (1991) for $b = -7°$. Reproduced from Whitelock (1992).

4.3.1 The Light Curves

Phased light curves for all the candidates are presented in Appendix B-I. One cycle of each is shown. The horizontal axis is period in days and the vertical is APM magnitudes as calibrated by APM standard stars. The label on the plot of each curve is made up of keys for the Candidate Class (see section 4.2.2), Schmidt Plate Section (see section 4.2.1), Object APM ID, and RA and Dec (1950) coordinates.

4.3.2 The Finding Charts

Finding charts for all candidates are presented in Appendix B-II. They are on a 4x4 arcmin grid, where the direction towards the North is up the East is to the left. The label on each charts is made up of the Candidate Class (see section 4.2.2) and the RA and Dec (1950) coordinates. The diameters of the images in the charts are proportional to the APM intensities of the scanned objects.

4.4 The Future

Near-infrared observations of the Mira candidates began in August 1996 (*ie.* shortly after the APM identification of these stars), using the SAAO 74-inch telescope in Sutherland. Searches of candidates in other Galactic Bulge fields are underway; and the Sutherland observations will include these candidate as they become available. Again, the study will be used to gain insights about the structure of the Galactic Bulge, and to compare the properties of

these Miras with those in the Galactic Plane.

Bibliography

1. Allen, C. W. 1973, *Astrophysical Quantities*, The Athlone Press, London.

2. Bidelman, W.P., MacConnel, D.J. 1982, *The Astronomical Journal*, **Vol. 87 No. 5** : 792-793.

3. Carter, B.S. 1990, *Monthly Notices of the Royal Astronomical Society*, **242**: 1-6.

4. Conover, W. J. 1971, *Practical Nonparametric Statistics*, John Wiley & Sons Inc., New York.

5. Danchi, W.C., Bester, M., Degiacomi, D.G., Greenhill, L.J., Townes, C.H. 1994, *The Astronomical Journal*, **107**: 1469-1513.

6. De Graauw, Th., *Infrared Astronomy*, IV Canary Islands Winter School of Astrophysics, ed. A. Mampaso, M. Prieto and F. Sanchez, Cambridge University Press, 379-415.

7. Elias, J. H. 1992, *The Astronomy and Astrophysics Encyclopaedia*, ed. by S. P. Maran, Van Nostrand Reinhold, New York, 747-749.

8. Engels, D., Kreysa, E., Schultz, G.V., Sherwood, W.A. *Astronomy and Astrophysics*, **124**: 123-138.

9. Epchtein, N., Le Bertre, T., Lepine, J.R.D., Marques dos Santos, P., Matsuura, O. T., Picazzio, E. 1987, *Astronomy and Astrophysics Supplement Series*, **71**: 39-55.

10. Feast, M.W. 1996, *Monthly Notices of the Royal Astronomical Society*, **278**: 11-21.

11. Feast, M.W. 1995, *Astrophysical Application of Stellar Pulsation*, ASP Conference Series Vol 85, ed. by R.S. Stobie and P.A. Whitelock, Astronomical Society of the Pacific, San Francisco, 209-218.

12. Feast, M.W. 1990, Whitelock, P.A., Carter, B.S. 1990, *Monthly Notices of the Royal Astronomical Society*, **247**: 227-236.

13. Feast, M.W., Glass, I.S., Whitelock, P.A., Catchpole, R.M. 1989, *Monthly Notices of the Royal Astronomical Society*, **241**: 375-392.

14. Feast, M.W. 1984, *Monthly Notices of the Royal Astronomical Society*, **211**: 51-55.

15. Feast, M.W. 1963, *Monthly Notices of the Royal Astronomical Society*, **125**: 367-415.

16. Fox, M.W., Woods P.R. 1982, *Astrophysical Journal*, **259**: 198-212.

17. Fueller, A.W. 1986, *The Study of Variable Stars Using Small Telescopes*, ed. by J.R. Percy, Cambridge University Press, 201-217.

18. Glass, I.S., Whitelock, P.A., Catchpole, R.M., Feast, M.W. 1995, *Monthly Notices of the Royal Astronomical Society* , **273**: 383-400.

19. Guglielmo, F., Epchtein, N., Le Bertre, T., Fouque, P., Hron, J., Kerschbaum F. and Lepine, J.R.D, *Astronomy and Astrophysics Supplement Series.*, **99**: 31-69.

20. Hughes 1989, S.M.G., *The Astronomical Journal* , **97**: 1634-1687.

21. Iben, I., *Jr.*, Renzini, A. 1983, *Annual Review of Astronomy and Astrophysics*, **21**: 271-342.

22. *IRAS* Science Team 1988, IRAS *Point Source Catalog - Version 2*, NASA Scientific and Technical Information Division, Washington, DC.

23. *IRAS* Science Team 1988, IRAS *Point Source Catalog – Explanatory Supplement* , NASA Scientific and Technical Information Division, Washington, DC., Vol 1.

24. Jashek, C., Jashek, M. 1987, *The Classification of Stars*, The Cambridge University Press, Cambridge.

25. Kholopov, P. N. 1985, *General Catalogue of Variable Stars*, Nauka Publishing House, Moscow, Vols. 1-3.

26. Kukarkin, B. V. *et al.* 1982, *New Catalogue of Suspected Variable Stars*, Nauka Publishing House, Moscow.

27. Lambert, D.L. 1990, *Evolution of Peculiar Red Giant Stars*, I.A.U. Colloquium 106, ed. by H.R. Johnson and B. Zuckerman, Cambridge

University Press, 101-130.

28. Le Berte, T., Epchtein, N., Guglielmo, F., Le Sidaner, P. 1994, *Astrophysics and Space Science*, **217**: 105-116.

29. Le Berte, T. 1993, Astronomy and Astrophyics Supplement Series, **97**: 729-754.

30. Lloyd Evans, T. 1976, *Monthly Notices of the Royal Astronomical Society*, **174**: 169- .

31. McLean, I. S 1993, *Infrared Astronomy*, IV Canary Islands Winter School of Astrophysics, ed. A. Mampaso, M. Prieto and F. Sanchez, Cambridge University Press, 335-378.

32. Merrill, P.W. 1960, *Stellar Atmospheres*, ed. by Jesse L. Greenstein, The University of Chicago Press, Chicago, 509-529.

33. Menzies, J. W., Whitelock, P. A., *Monthly Notices of the Royal Astronomical Society*, **212** : 783-797.

34. Neckel, Th., Klare, G. 1980, *Astronomy and Astrophysics Supplement Series*, **42**: 251-281.

35. Olnon, F.M., Raimond, E., IRAS Science Team 1986, *Astronomy and Astrophysics Supplement Series*, **65** : 607-1065.

36. Shu, R.H. 1980, *The Physical Universe*, University Science Books, Mill Valley, California.

37. Stephenson, C.B. 1989, *A General Catalogue of Cool Galactic Carbon Stars, Second Edition*, Warner and Swasey Publications, Cleveland, Vol. 3 No. 2.

38. Stephenson, C.B. 1984, *A General Catalogue of Galactic* S *Stars, Second Edition* , Warner and Swasey Publications, Cleveland, Vol. 3. No. 1.

39. Stephenson, C.B. 1973, *A General Catalogue of Cool Carbon Stars*, Warner and Swasey Publications, Cleveland, Vol. 1. No. 4.

40. te Lintel Hekkert, P., Caswell, J.L., Habing, H.J., Haynes, R.E., Norris, R.P. 1991, *Astronomy and Astrophysics Supplement Series*, **90** : 327-353.

41. Vardya, M.S. 1992, *The Astronomy and Astrophysics Encyclopaedia*, ed. by S. P. Maran, Van Nostrand Reinhold, New York, 747-749.

42. Weinberg, M.D. 1992, *Astrophysical Journal*, **384**: 81- .

43. Whitelock, P.A. 1996, *Light Curves of Variable Stars*, ed. by C. Jashek and C. Sterken, Cambridge University Press.

44. Whitelock, P.A. 1996b, *The Carbon Star Phenomenon*, IAU Symposium 177, ed. by R. Wing, Antalya.

45. Whitelock, P.A. 1995a, *Astrophysics and Space Science.*

46. Whitelock, P.A. 1995b, *Astrophysical Application of Stellar Pulsation*, ASP Conference Series: Vol 85, ed. by R.S. Stobie and P.A. Whitelock,

Astronomical Society of the Pacific, San Francisco, 209-218.

47. Whitelock, P. A., Menzies, J., Feast, M. W., Catchpole, R., Marang, F., Carter, B. 1995, Monthly Notices of the Royal Astronomical Society , **276** : 219-254.

48. Whitelock, P.A., Menzies, J., Feast, M.W., Marang, F., Carter, B., Roberts, G., Catchpole, R., Chapman, J. 1994, *Monthly Notices of the Royal Astronomical Society*, **267**: 711-742.

49. Whitelock, P.A., Catchpole, R.M. 1992, *The Center, Bulge and Disk of the Milky Way*, ed. by L. Blitz, Kluwer Academic Publishers, Netherlands.

50. Whitelock, P.A. 1992, *Galactic Bulges*, IAU Symposium 153, ed. by H. Dejonghe and H.J. Habing, Kluwer Academic Publishers, Netherlands, 39-54.

51. Whitelock, P.A., Feast, M.W., Catchpole, R. 1991, *Monthly Notices of the Royal Astronomical Society*, **248**: 276-312.

52. Williams, D.A. 1992, *The Astronomy and Astrophysics Encyclopaedia*, ed. by S. P. Maran, Van Nostrand Reinhold, New York, 747-749.

53. Wilson, W.J., Schwartz, P.R., Neugebauer, G., Harvey, P.M., Becklin, E. E. 1973, *The Astrophysical Journal*, **177**: 523-540.

54. Winters, J.M., Fleischer, A.J., Gauger, A., Sedlmayr, E. 1995, *Astronomy and Astrophysics*, **302**: 483-496.

Appendix A

The following is a presentation of the results of **mean J and K magnitudes** derived from (1) the averages of the minimum and maximum, (2) Fourier fitting, and (3) the averages of the observations for each star. The results show that the mean magnitude derived from averages of the minimum and maximum observations and that from averages of all the observations for each star agree well with the mean from Fourier fitting. Eight phased light curves of different shapes, periods and amplitudes were tested. The observations are of stars classified as Miras in the present paper.

Results of Mean Magnitudes by Different Techniques

Star	O- or C-rich	(Per,ΔK) (day,K mag)	(J,K) Mean Magnitudes by Ave. of Min/Max	Fourier Fit	Ave. of all Obs.
2	Cy	567,0.61	11.10,7.11	11.03,7.08	11.25,7.14
8	Oz	284,0.12	7.70,6.16	7.73,6.16	7.73,6.15
12	Cx	510,0.87	14.99,9.21	-,9.21	14.90,9.21
13	Oyy	177,0.14	8.25,6.86	8.22,6.86	8.23,6.81
29	Cx	565,0.82	13.28,7.73	13.16,7.69	13.08,7.61
53	Cyy	210,0.29	7.34,4.28	7.26,4.27	7.35,4.33
54	Oyy	281,0.29	6.56,4.84	6.55,4.86	6.54,4.84
70	Cx	468,0.48	10.43,7.37	10.58,7.40	10.52,7.36

The running numbers of the stars are the same as in previous sections of this paper. The letters **x, y, yy, z** in the 'O- or C- rich' column of the table are for the shapes of the light curves, where **x** indicates symmetric, **y** and **yy** asymetric, and **z** irregular, in the same way as these letters were used in Figure 3.1.

The means derived from the Fourier fitting compared to the results of the averages of maximum and minimum as follows: $\sigma = 0.067 \pm 0.004, s^2 =$

0.025 and to the results of the averages of all the observations as follows: $\sigma = 0.067 \pm 0.006, s^2 = 0.025$. The difference of the mean J magnitudes by the presented techniques were generally larger than those of the mean K magnitudes. The difference from star to star were not correlated to period, amplitudes or shapes of the phased light curves. All said, it has been shown that for near-infrared observations of Mira variables in the present sample, averages of maximum and minimum magnitudes of the raw light curve give a good estimate of the mean magnitudes derived from Fourier fitting.

Appendices B-I & B-II

The following pages are a presentation of phased light curves (Appendix **B-I**) and finding charts (Appendix **B-II**) as described in section 4.3.1 and 4.3.2, respectively, and as they were generated from computer programs by Shaun Hughes of the Royal Greenwich Observatory.

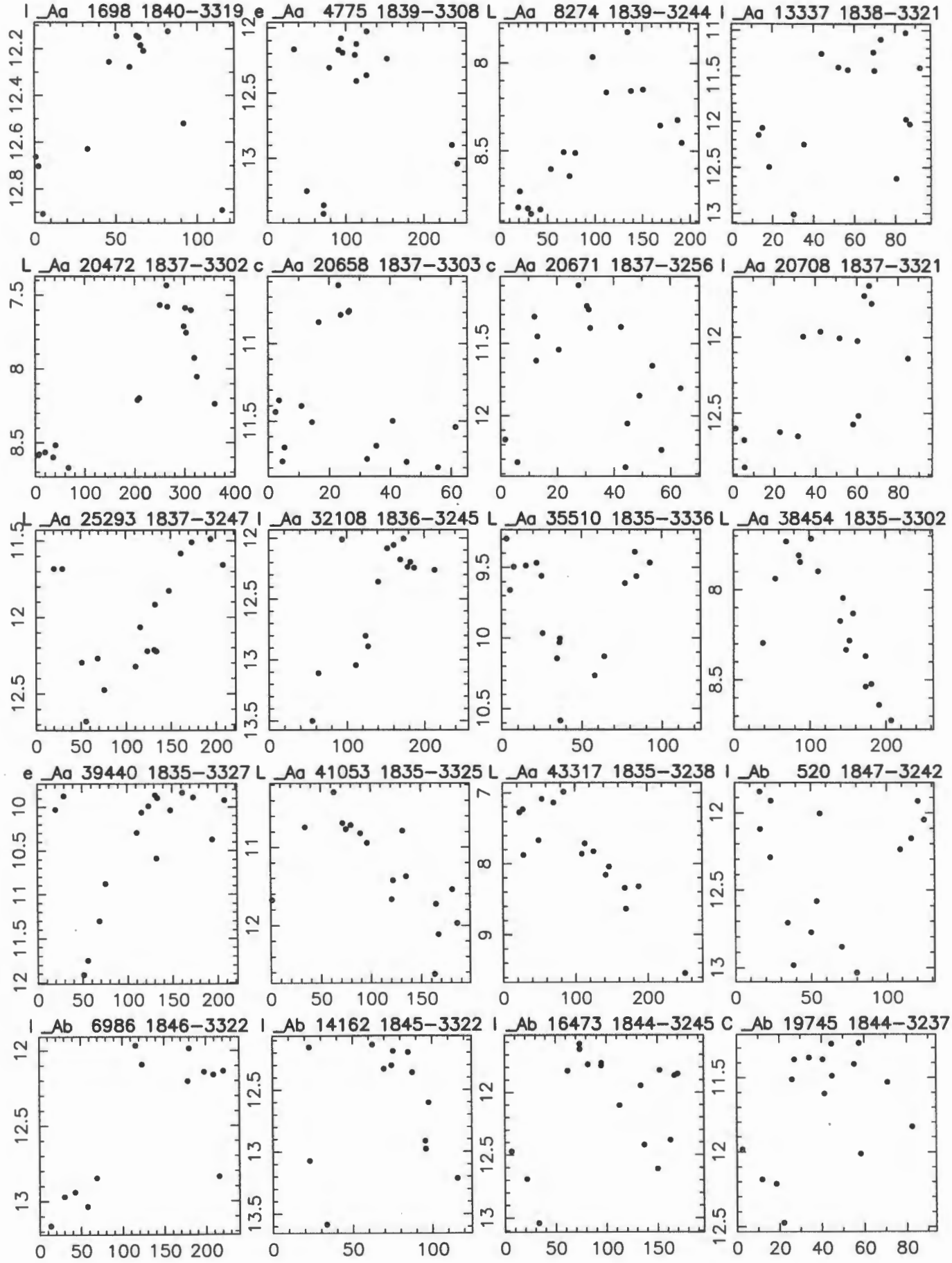
I _Aa 1698 1840−3319
e _Aa 4775 1839−3308
L _Aa 8274 1839−3244
I _Aa 13337 1838−3321
L _Aa 20472 1837−3302
c _Aa 20658 1837−3303
c _Aa 20671 1837−3256
I _Aa 20708 1837−3321
L _Aa 25293 1837−3247
I _Aa 32108 1836−3245
L _Aa 35510 1835−3336
L _Aa 38454 1835−3302
e _Aa 39440 1835−3327
L _Aa 41053 1835−3325
L _Aa 43317 1835−3238
I _Ab 520 1847−3242
I _Ab 6986 1846−3322
I _Ab 14162 1845−3322
I _Ab 16473 1844−3245
C _Ab 19745 1844−3237

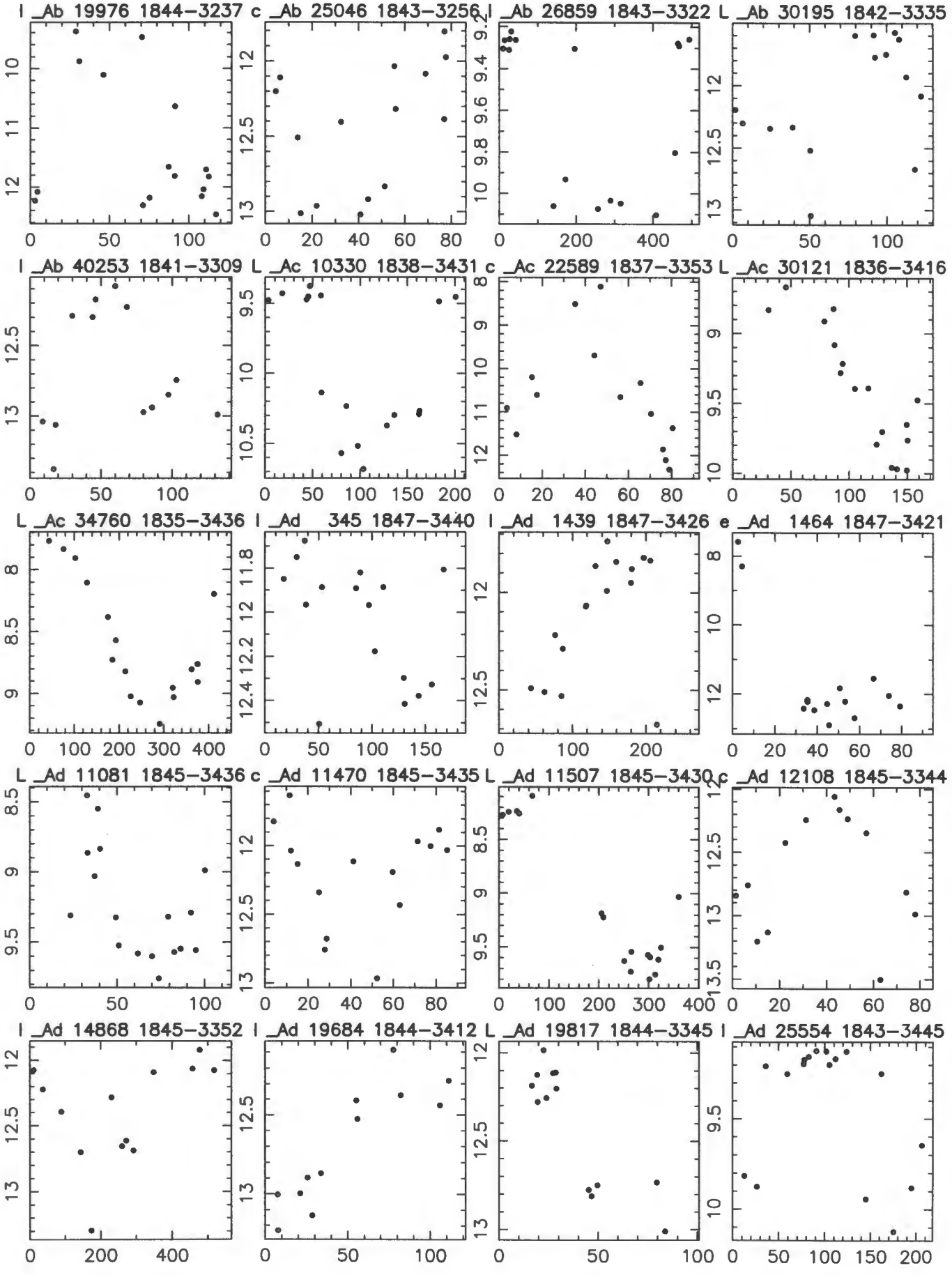
I _Ab 19976 1844−3237
c _Ab 25046 1843−3256
I _Ab 26859 1843−3322
L _Ab 30195 1842−3335
I _Ab 40253 1841−3309
L _Ac 10330 1838−3431
c _Ac 22589 1837−3353
L _Ac 30121 1836−3416
L _Ac 34760 1835−3436
I _Ad 345 1847−3440
I _Ad 1439 1847−3426
e _Ad 1464 1847−3421
L _Ad 11081 1845−3436
c _Ad 11470 1845−3435
L _Ad 11507 1845−3430
c _Ad 12108 1845−3344
I _Ad 14868 1845−3352
I _Ad 19684 1844−3412
L _Ad 19817 1844−3345
I _Ad 25554 1843−3445

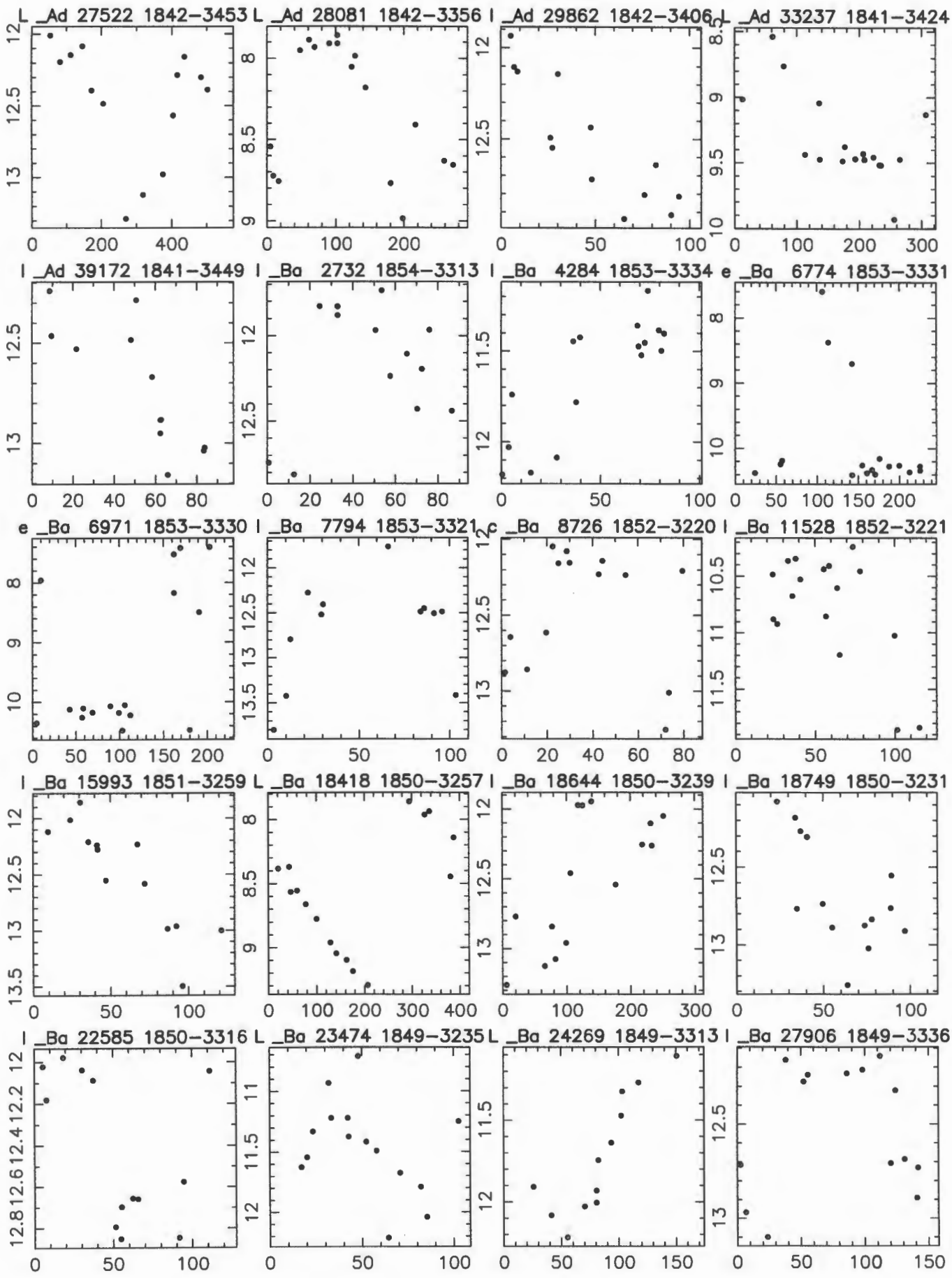
L _Ad 27522 1842-3453
L _Ad 28081 1842-3356
I _Ad 29862 1842-3406
L _Ad 33237 1841-3424
I _Ad 39172 1841-3449
I _Ba 2732 1854-3313
I _Ba 4284 1853-3334
e _Ba 6774 1853-3331
e _Ba 6971 1853-3330
I _Ba 7794 1853-3321
c _Ba 8726 1852-3220
I _Ba 11528 1852-3221
I _Ba 15993 1851-3259
L _Ba 18418 1850-3257
I _Ba 18644 1850-3239
I _Ba 18749 1850-3231
I _Ba 22585 1850-3316
L _Ba 23474 1849-3235
L _Ba 24269 1849-3313
I _Ba 27906 1849-3336

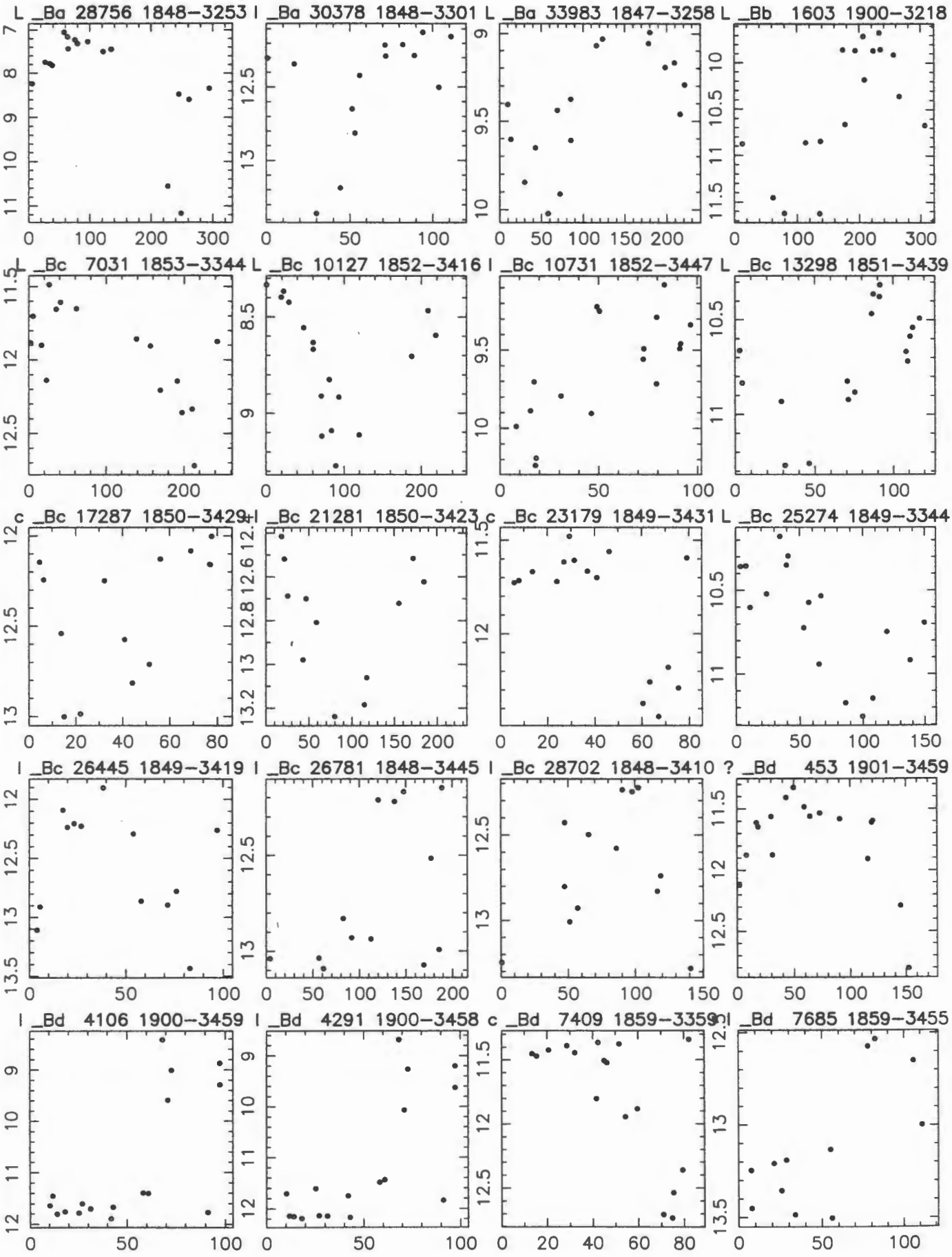
L _Ba 28756 1848−3253
I _Ba 30378 1848−3301
L _Ba 33983 1847−3258
L _Bb 1603 1900−3218
L _Bc 7031 1853−3344
L _Bc 10127 1852−3416
I _Bc 10731 1852−3447
L _Bc 13298 1851−3439
c _Bc 17287 1850−3429
I _Bc 21281 1850−3423
c _Bc 23179 1849−3431
L _Bc 25274 1849−3344
I _Bc 26445 1849−3419
I _Bc 26781 1848−3445
I _Bc 28702 1848−3410
? _Bd 453 1901−3459
I _Bd 4106 1900−3459
I _Bd 4291 1900−3458
c _Bd 7409 1859−3359
I _Bd 7685 1859−3455

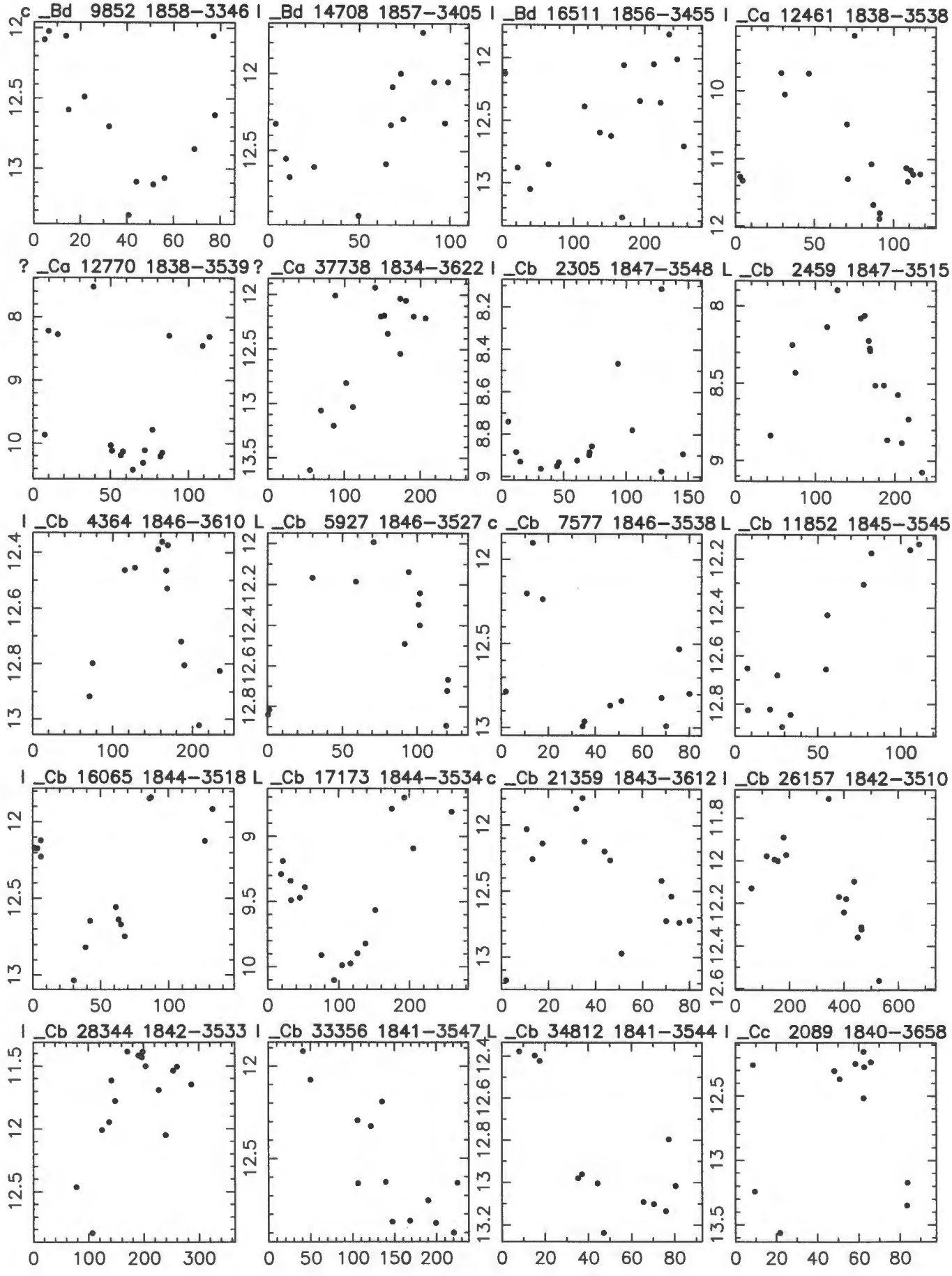
c _Bd 9852 1858−3346
I _Bd 14708 1857−3405
I _Bd 16511 1856−3455
I _Ca 12461 1838−3538
? _Ca 12770 1838−3539
? _Ca 37738 1834−3622
I _Cb 2305 1847−3548
L _Cb 2459 1847−3515
I _Cb 4364 1846−3610
L _Cb 5927 1846−3527
c _Cb 7577 1846−3538
L _Cb 11852 1845−3545
I _Cb 16065 1844−3518
L _Cb 17173 1844−3534
c _Cb 21359 1843−3612
I _Cb 26157 1842−3510
I _Cb 28344 1842−3533
I _Cb 33356 1841−3547
L _Cb 34812 1841−3544
I _Cc 2089 1840−3658

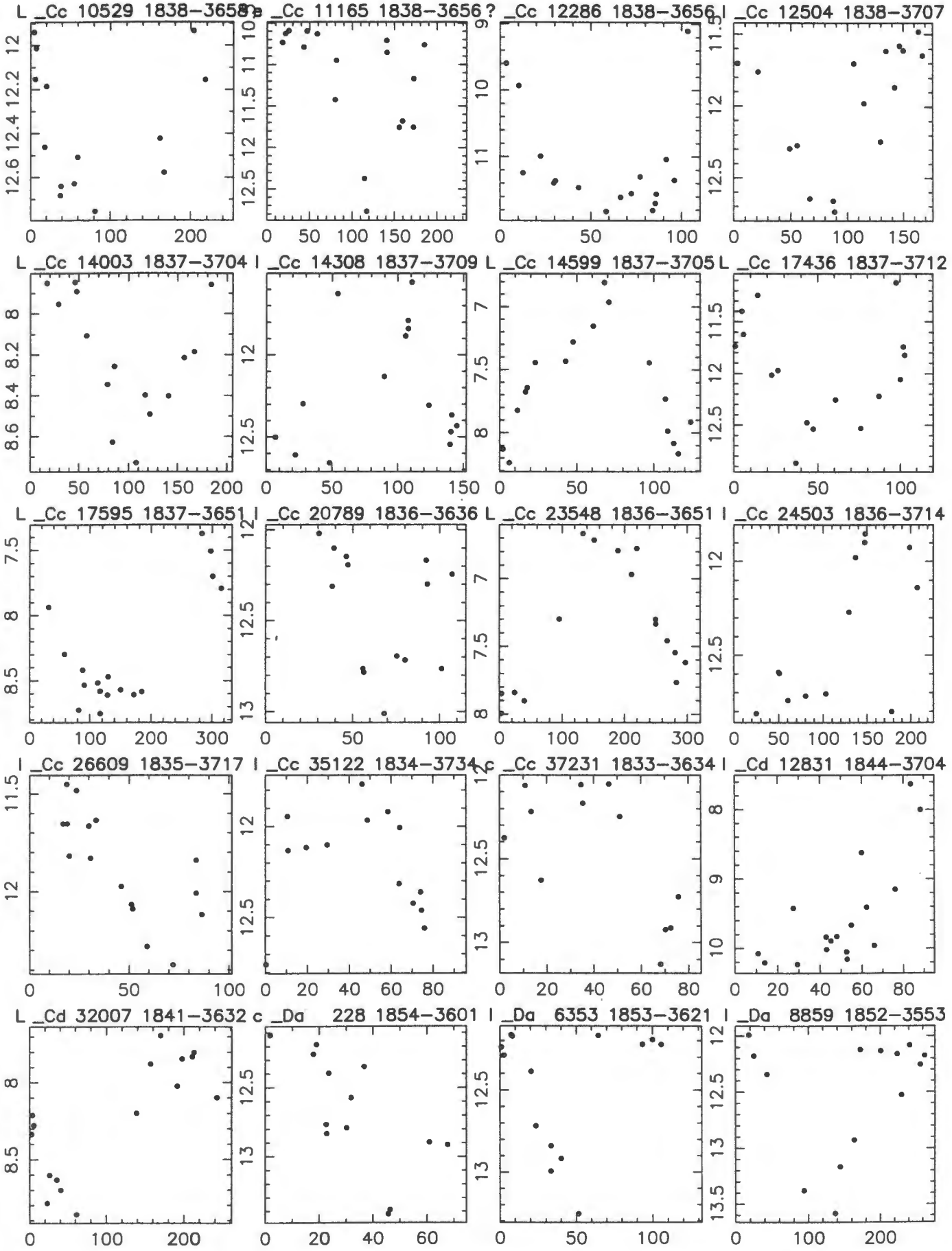
L _Cc 10529 1838−3658
_Cc 11165 1838−3656 ?
_Cc 12286 1838−3656 I
_Cc 12504 1838−3707
L _Cc 14003 1837−3704 I
_Cc 14308 1837−3709 L
_Cc 14599 1837−3705 L
_Cc 17436 1837−3712
L _Cc 17595 1837−3651 I
_Cc 20789 1836−3636 L
_Cc 23548 1836−3651 I
_Cc 24503 1836−3714
I _Cc 26609 1835−3717 I
_Cc 35122 1834−3734 c
_Cc 37231 1833−3634 I
_Cd 12831 1844−3704
L _Cd 32007 1841−3632 c
_Da 228 1854−3601 I
_Da 6353 1853−3621 I
_Da 8859 1852−3553

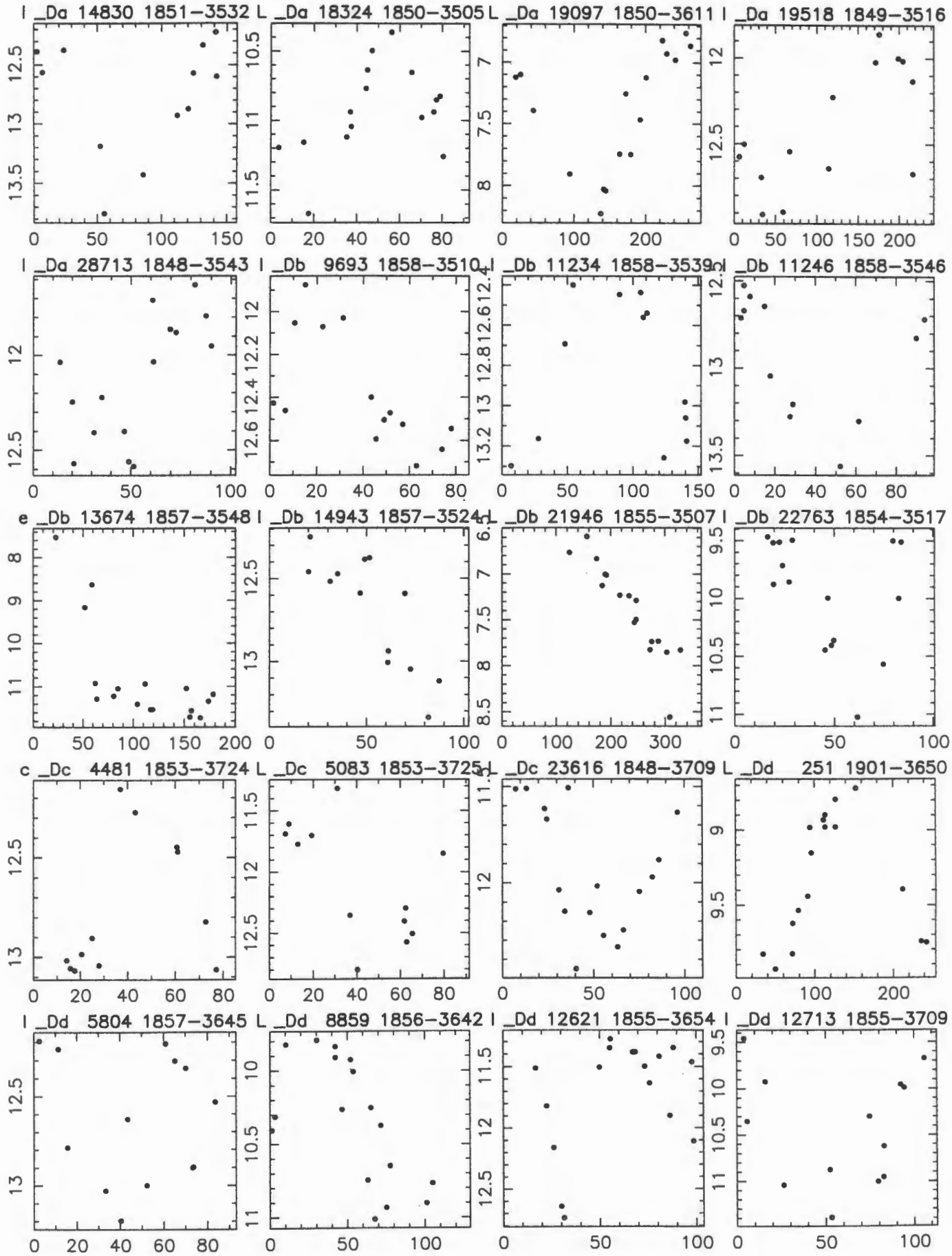
I _Da 14830 1851−3532
L _Da 18324 1850−3505
L _Da 19097 1850−3611
I _Da 19518 1849−3516
I _Da 28713 1848−3543
I _Db 9693 1858−3510
I _Db 11234 1858−3539
I _Db 11246 1858−3546
e _Db 13674 1857−3548
I _Db 14943 1857−3524
L _Db 21946 1855−3507
I _Db 22763 1854−3517
c _Dc 4481 1853−3724
L _Dc 5083 1853−3725
L _Dc 23616 1848−3709
L _Dd 251 1901−3650
I _Dd 5804 1857−3645
L _Dd 8859 1856−3642
I _Dd 12621 1855−3654
I _Dd 12713 1855−3709

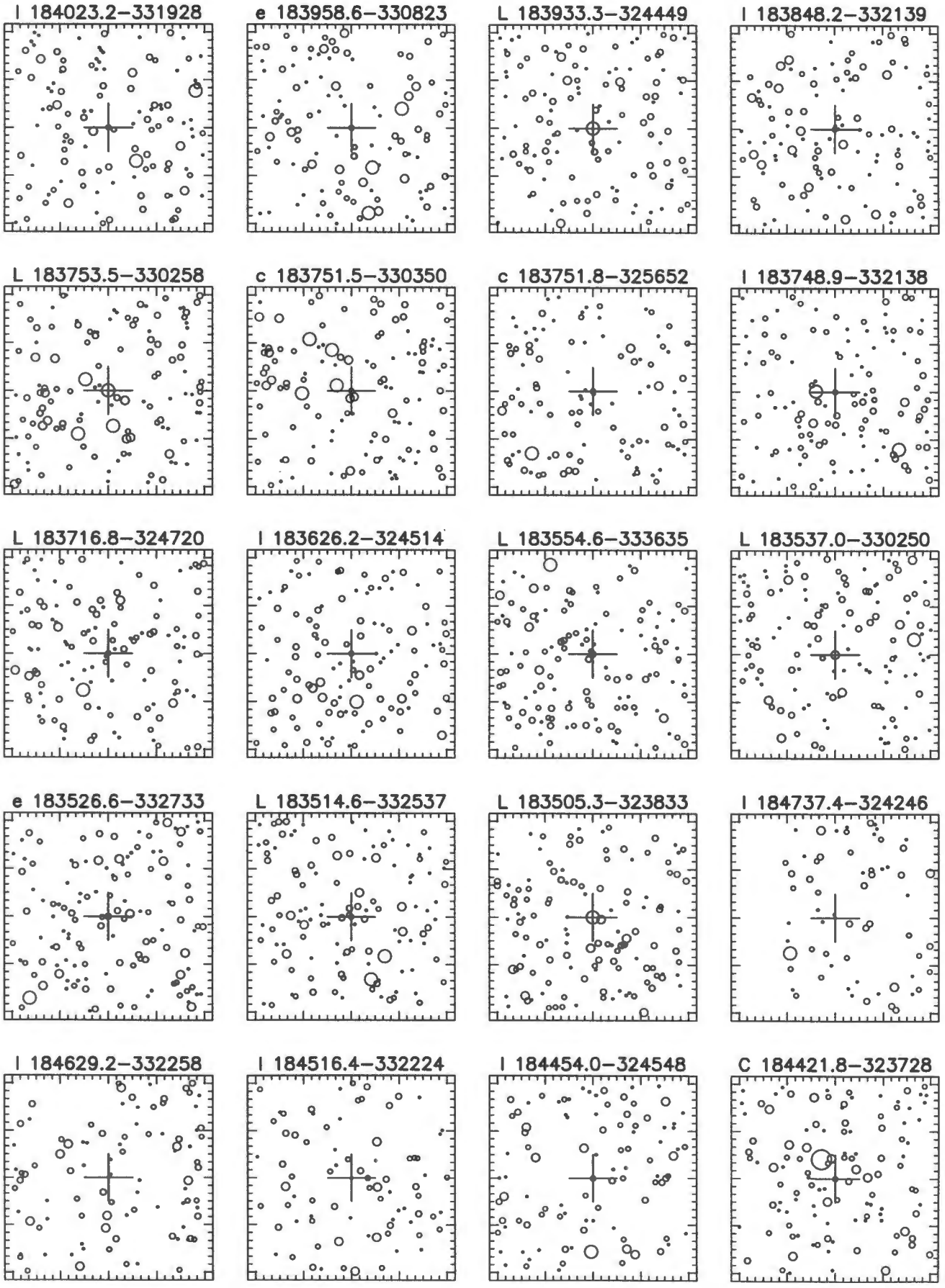
I 184023.2−331928
e 183958.6−330823
L 183933.3−324449
I 183848.2−332139
L 183753.5−330258
c 183751.5−330350
c 183751.8−325652
I 183748.9−332138
L 183716.8−324720
I 183626.2−324514
L 183554.6−333635
L 183537.0−330250
e 183526.6−332733
L 183514.6−332537
L 183505.3−323833
I 184737.4−324246
I 184629.2−332258
I 184516.4−332224
I 184454.0−324548
C 184421.8−323728

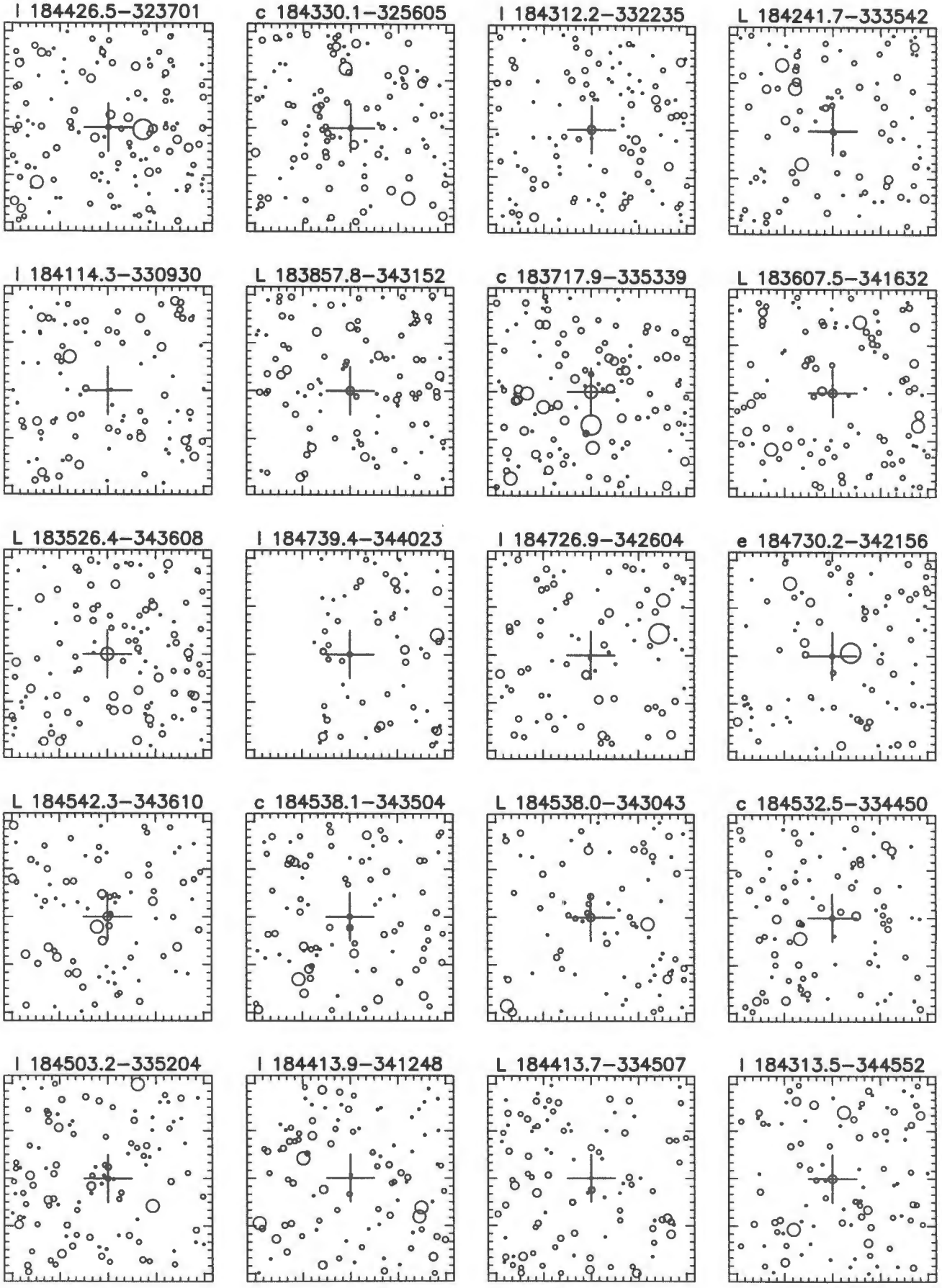
I 184426.5−323701
c 184330.1−325605
I 184312.2−332235
L 184241.7−333542
I 184114.3−330930
L 183857.8−343152
c 183717.9−335339
L 183607.5−341632
L 183526.4−343608
I 184739.4−344023
I 184726.9−342604
e 184730.2−342156
L 184542.3−343610
c 184538.1−343504
L 184538.0−343043
c 184532.5−334450
I 184503.2−335204
I 184413.9−341248
L 184413.7−334507
I 184313.5−344552

L 184252.9−345314

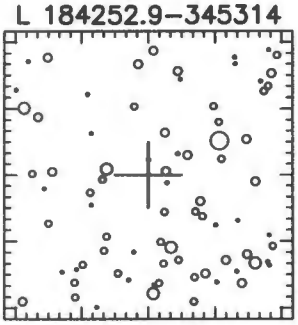

L 184250.5−335611

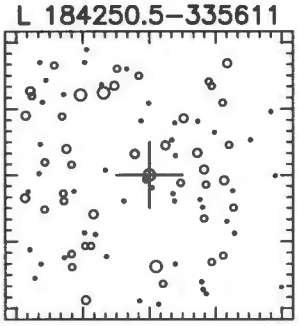

I 184232.8−340621

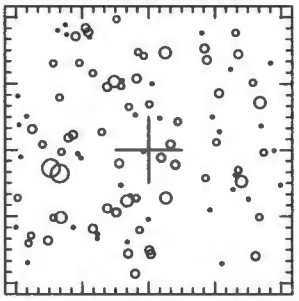

L 184159.5−342457

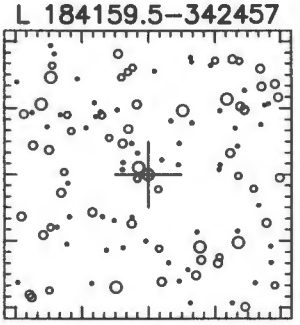

I 184100.6−344916

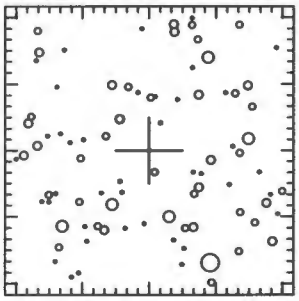

I 185412.7−331343

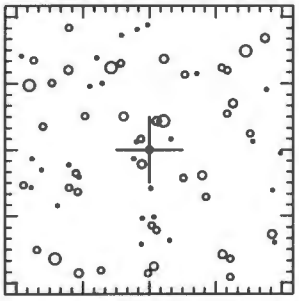

I 185354.6−333440

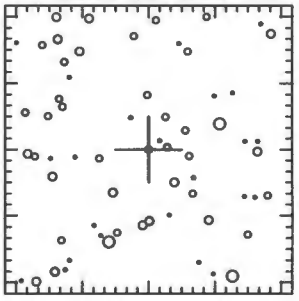

e 185321.9−333127

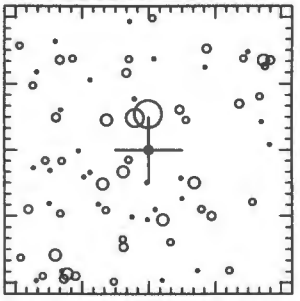

e 185319.7−333051

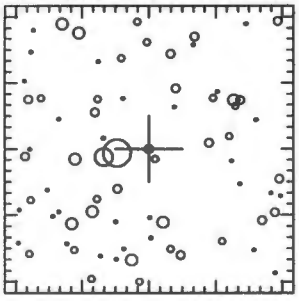

I 185308.5−332149

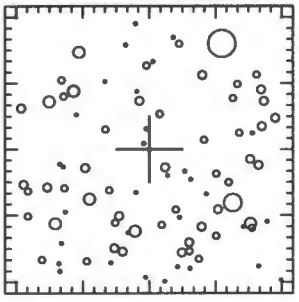

c 185252.3−322037

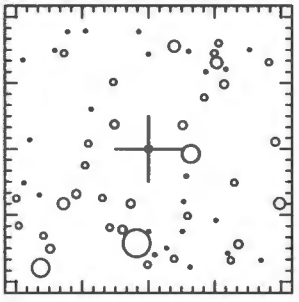

I 185218.6−322153

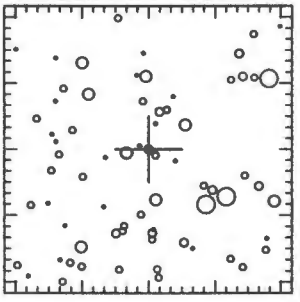

I 185125.3−325941

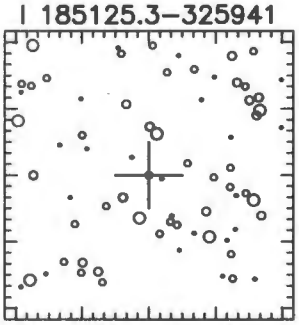

L 185056.0−325714

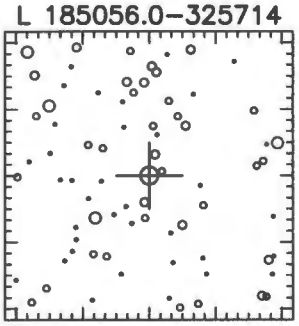

I 185052.1−323938

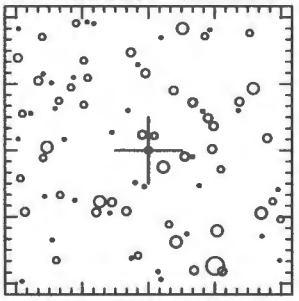

I 185050.3−323157

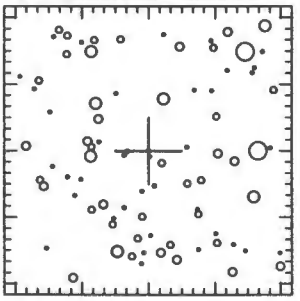

I 185006.7−331604

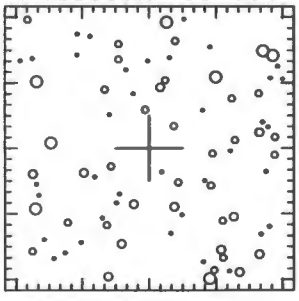

L 184955.0−323508

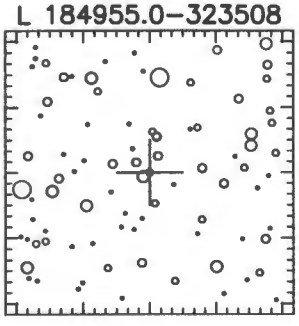

L 184947.4−331353

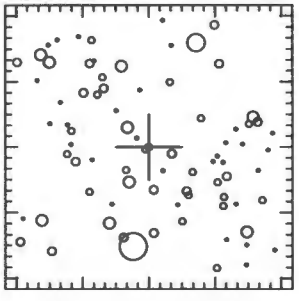

I 184905.6−333635

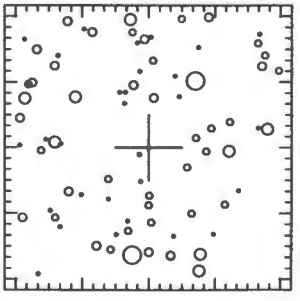

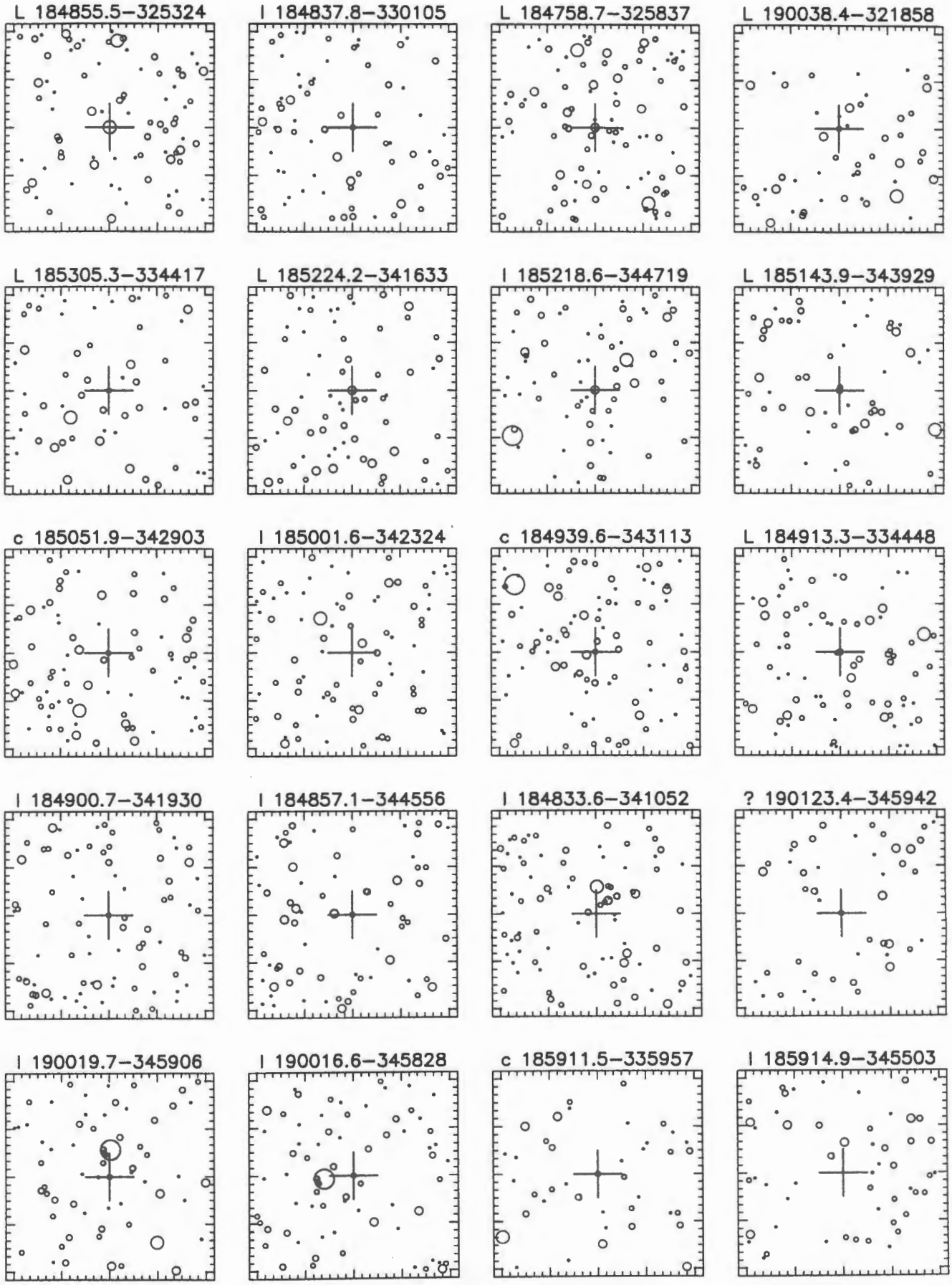
L 184855.5−325324
I 184837.8−330105
L 184758.7−325837
L 190038.4−321858
L 185305.3−334417
L 185224.2−341633
I 185218.6−344719
L 185143.9−343929
c 185051.9−342903
I 185001.6−342324
c 184939.6−343113
L 184913.3−334448
I 184900.7−341930
I 184857.1−344556
I 184833.6−341052
? 190123.4−345942
I 190019.7−345906
I 190016.6−345828
c 185911.5−335957
I 185914.9−345503

c 185828.6−334613

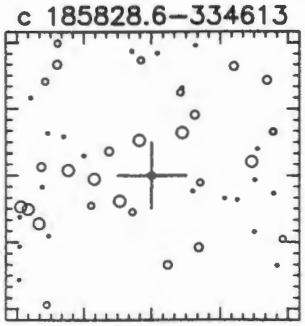

I 185711.2−340532

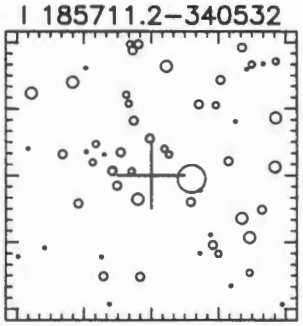

I 185647.6−345507

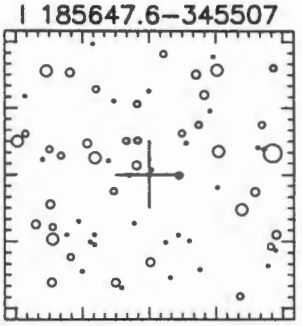

I 183834.2−353817

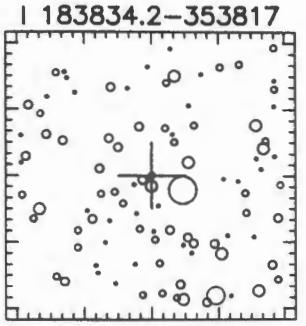

? 183831.6−353912

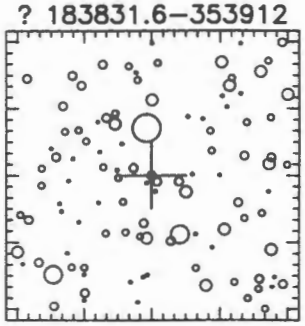

? 183425.3−362209

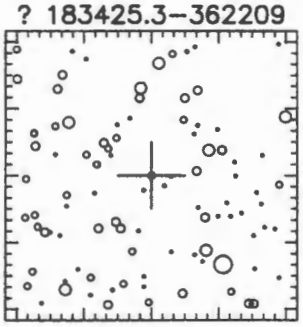

I 184715.6−354817

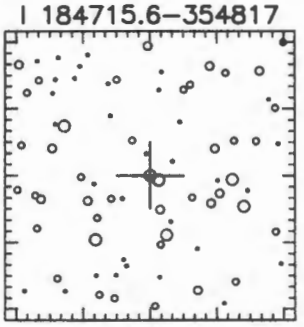

L 184713.0−351543

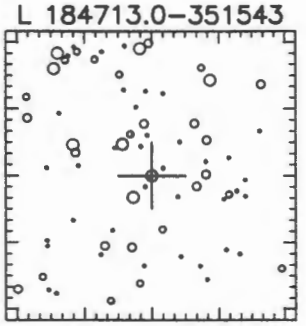

I 184648.4−361026

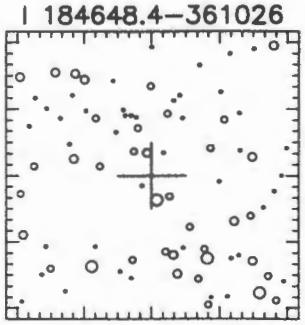

L 184629.1−352700

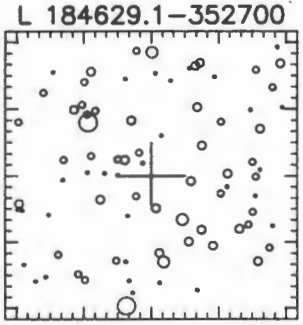

c 184609.3−353828

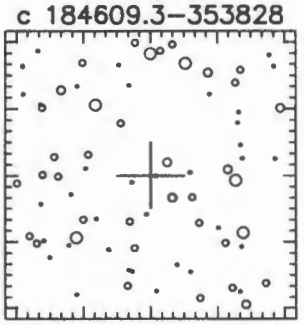

L 184517.7−354509

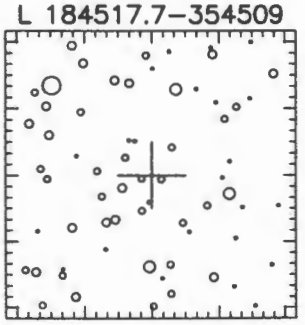

I 184430.8−351833

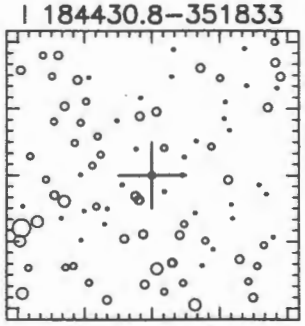

L 184418.8−353437

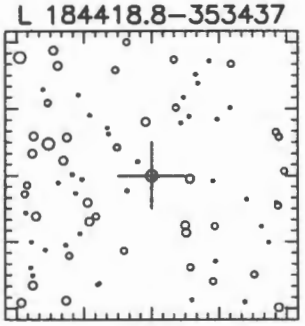

c 184330.0−361205

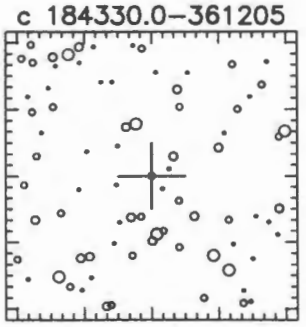

I 184240.1−351013

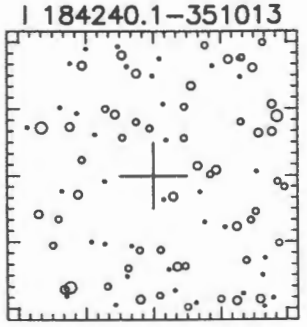

I 184215.9−353302

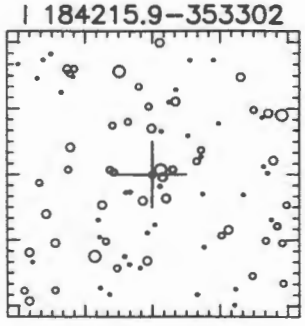

I 184121.5−354721

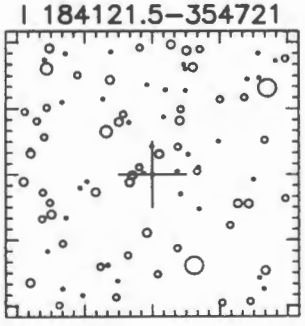

L 184106.9−354411

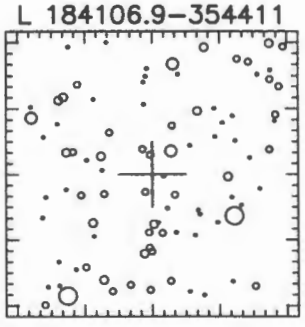

I 184016.1−365807

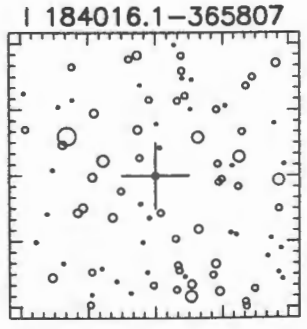

L 183837.1−365855

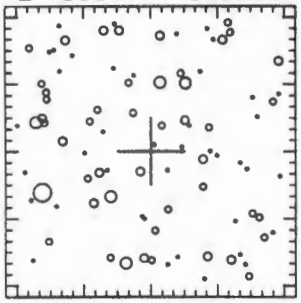

e 183830.2−365623

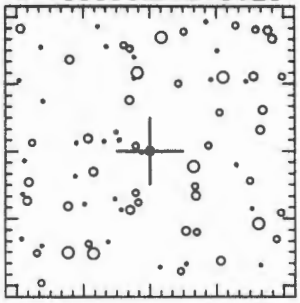

? 183817.2−365639

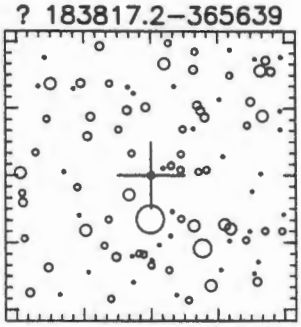

I 183813.6−370709

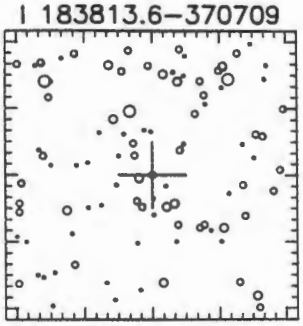

L 183758.4−370454

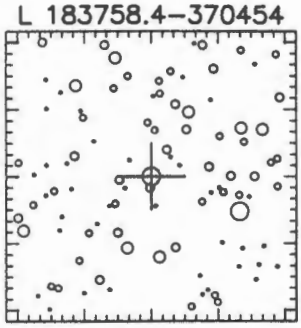

I 183753.0−370945

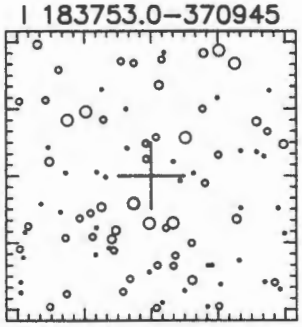

L 183751.7−370525

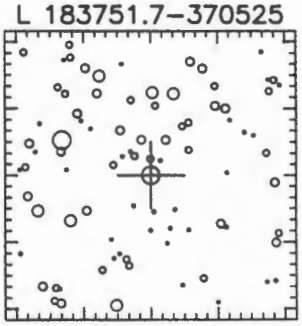

L 183718.8−371246

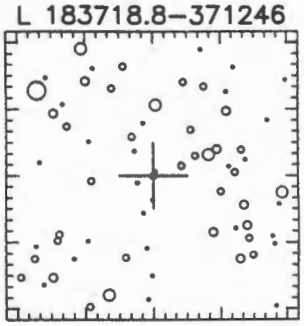

L 183720.8−365130

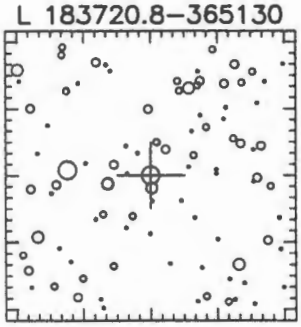

I 183647.5−363646

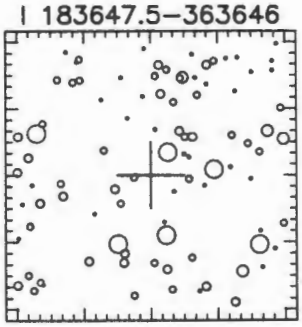

L 183617.9−365126

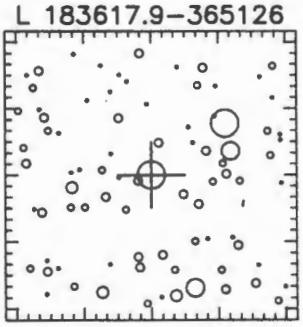

I 183602.1−371418

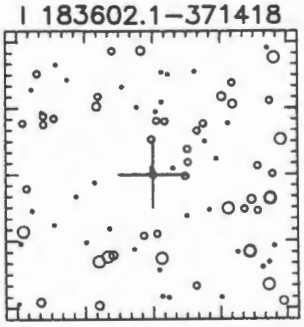

I 183539.1−371752

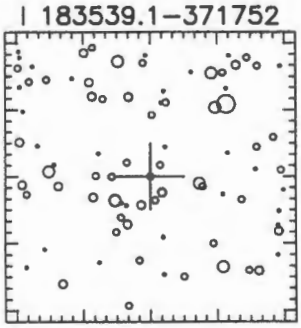

I 183404.0−373415

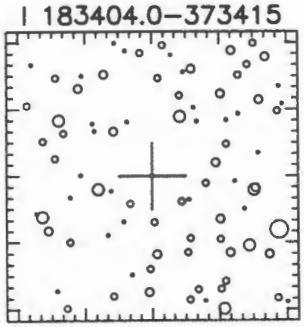

c 183352.1−363444

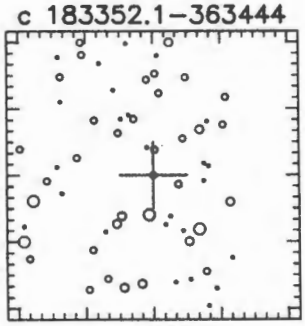

I 184458.6−370447

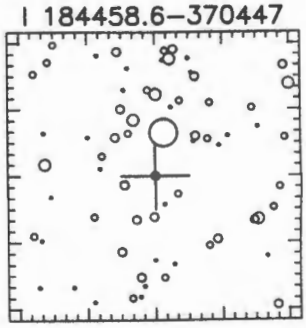

L 184107.5−363227

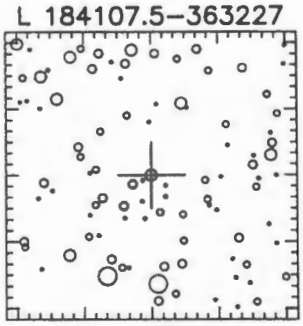

c 185445.4−360146

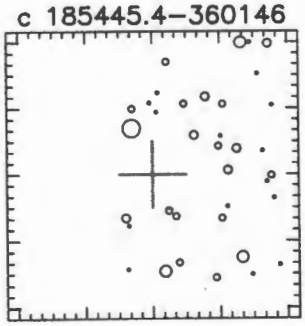

I 185313.8−362126

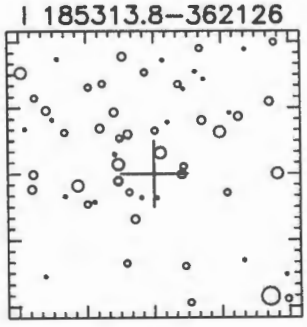

I 185234.9−355309

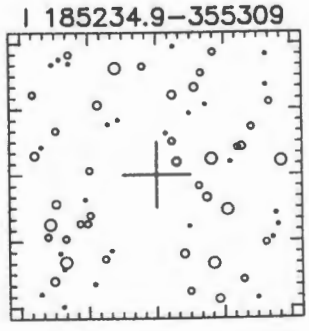

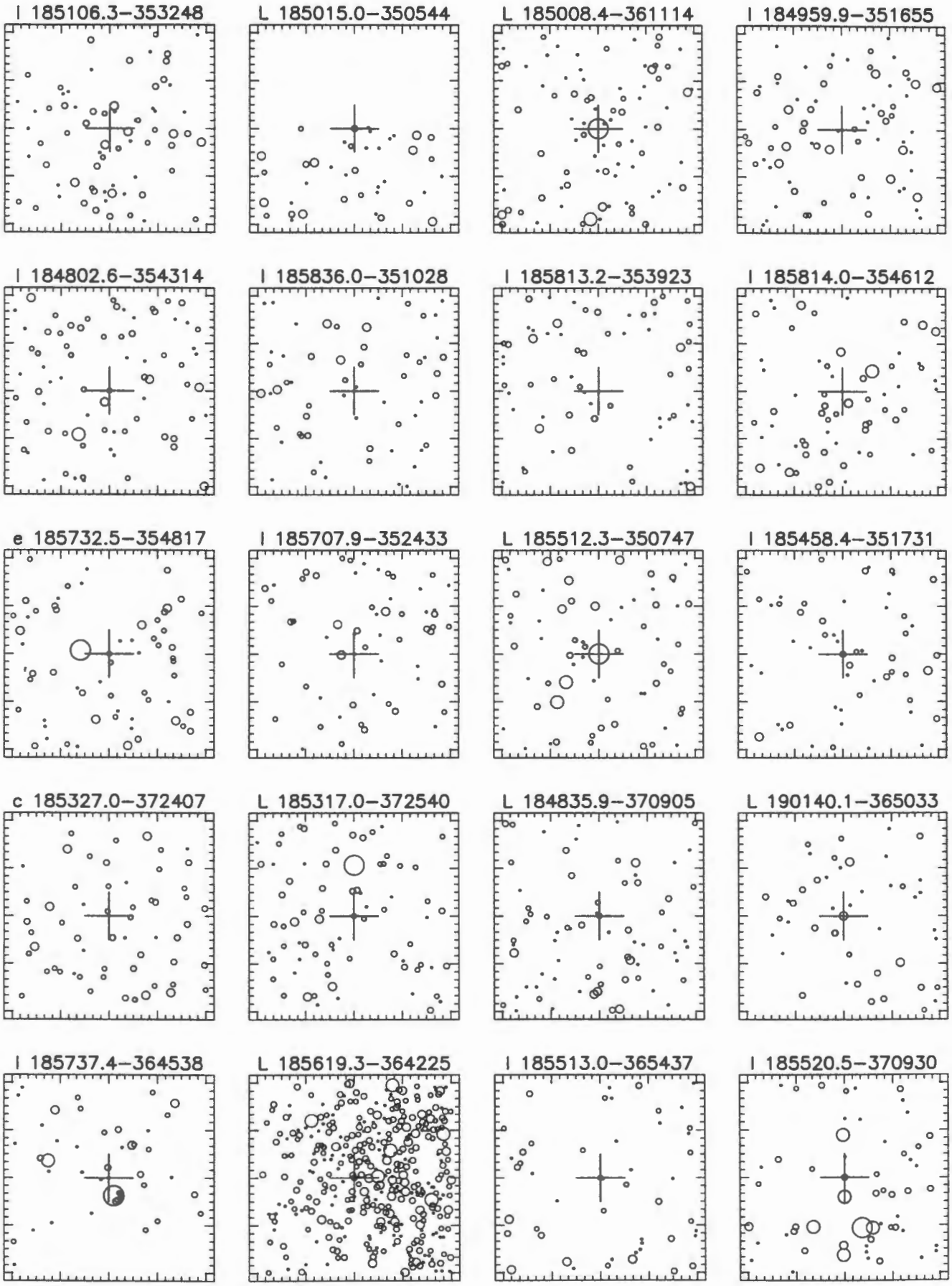
I 185106.3−353248
L 185015.0−350544
L 185008.4−361114
I 184959.9−351655
I 184802.6−354314
I 185836.0−351028
I 185813.2−353923
I 185814.0−354612
e 185732.5−354817
I 185707.9−352433
L 185512.3−350747
I 185458.4−351731
c 185327.0−372407
L 185317.0−372540
L 184835.9−370905
L 190140.1−365033
I 185737.4−364538
L 185619.3−364225
I 185513.0−365437
I 185520.5−370930